

Holin-dependent secretion of a large clostridial cytotoxin by *C. perfringens*

Nathaniel Hinton Flynn

Thesis submitted to the faculty of the Virginia Polytechnic Institute and State University in
fulfillment of the requirements for the degree of

Master of Science

In

Biological Sciences

Stephen Melville, Chair

David Popham

Florian Schubot

May 8th, 2025

Blacksburg, VA

Holin-dependent secretion of a large clostridial toxin by *C. perfringens*

Nathaniel Hinton Flynn

Academic Abstract

The clostridia are gram-positive, spore-forming, anaerobic pathogens capable of causing various diseases in both humans and animals. To do so, clostridial pathogens secrete a number of lethal toxins each associated with specific diseases. One family of proteins secreted by the clostridia are the large clostridial toxins (LCTs). These LCTs include TcdA and TcdB in *C. difficile*, TcsL and TcsH in *P. sordellii*, and TpeL in *C. perfringens*. LCTs bind and inactivate small GTPases in host mammalian cells, shutting down cell-signaling and eventually leading to cell death. Intriguingly, LCTs all lack any conventional signal peptide, rendering them incapable of being translocated by the Sec- or Tat-secretion system. However, according to recent publications, each LCT has been shown to be dependent on a cognate holin located in their pathogenicity loci. The holins for *C. difficile* and *P. sordellii* share similar membrane topologies to that of the phage lambda holin. However, TpeE in *C. perfringens* shares a similar membrane topology to TatA, a key protein in the Twin Arginine Transport (Tat) secretion system. This thesis tests two models, a pore-forming model and a membrane destabilization model that may explain the mechanism behind TpeE-dependent secretion of TpeL in *C. perfringens*. The pore-forming model was tested using FAST fluorescence technology and cell-surface biotinylation to determine if the amphipathic helix of TpeE changes its orientation in the presence of TpeL. Using FAST fluorescence, the mean pixel intensity for each frame did not change between TpeE-FAST and TpeE-FAST TpeL cultures, using a membrane impermeable dye. This suggested that

the amphipathic helix does not flip into the cell-membrane in the presence of the toxin.

Unfortunately, the cell-surface biotinylation was unable to support this as it yielded inconclusive results due to unforeseen errors within the experimental design. However, attention shifted to a proposed membrane destabilization model for TatA which places the focus of the mechanism on the length of the transmembrane helix of TpeE. To test this, anti-His₆ western blotting is being conducted to observe a difference in secretion efficiency of lengthened and shortened TpeE to the wild type. We believe that this system may utilize a membrane destabilization model that represents a novel and ubiquitous secretion method that shares aspects of both holin-dependent and Tat-secretion systems.

Holin-dependent secretion of a large clostridial toxin by *C. perfringens*

Nathaniel Hinton Flynn

General Abstract

The clostridia are pathogens capable of causing various diseases in both humans and animals. To do so, clostridial pathogens secrete a number of lethal toxins each associated with specific diseases. One family of proteins secreted by the clostridia are the large clostridial toxins (LCTs). LCTs bind and inactivate proteins in host mammalian cells, eventually leading to cell death. Intriguingly, LCTs are incapable of being translocated by common secretion pathways. However, each LCT has been shown to require a cognate holin-like protein to facilitate secretion. In *C. perfringens*, the LCT is known as TpeL and its cognate holin is known as TpeE. This thesis tests two models that may explain the process behind TpeE-dependent secretion of TpeL, a pore-forming model and a membrane destabilization model. The pore-forming model was tested using fluorescence protein technology and cell-surface labeling to determine if TpeE changes its orientation in the presence of TpeL. Using FAST fluorescence, the fluorescent signal for each frame did not change between TpeE-FAST and TpeE-FAST TpeL cultures, using a dye that is incapable of passing through the cell membrane. This suggested that TpeE does not change its orientation in the presence of the toxin. Cell-surface labeling was unable to support this as it yielded inconclusive results due to unforeseen errors within the experimental design. However, attention shifted to a proposed membrane destabilization model which places more of a focus on the length of TpeE. To test this, secretion efficiencies of cultures expressing lengthened and shortened versions of TpeE were compared to its original size. Due to the previous results and

preliminary data, it is believed that this system may utilize a membrane destabilization model that represents a novel and ubiquitous secretion method.

Table of Contents

	Page Number
List of Figures.....	ii
List of Table.....	iv
I. General Overview.....	1
a. <i>Clostridium perfringens</i>	2
b. Toxin types and Associated Diseases.....	2
c. Protein Secretion Systems.....	4
d. <i>Clostridium perfringens</i> membrane.....	8
e. Large Clostridial Toxins.....	9
f. TpeE-Dependent Secretion.....	10
II. Testing the pore-forming model for TpeE-dependent secretion of a large clostridial toxin (TpeL).....	16
a. Abstract.....	17
b. Introduction.....	19
c. Methods.....	23
d. Results.....	31
e. Discussion.....	48
III. Testing the membrane-destabilization model for TpeE-dependent secretion of a large clostridial toxin (TpeL).....	54
a. Abstract.....	55
b. Introduction.....	57
c. Methods.....	61
d. Results.....	67
e. Discussion.....	79
IV. Conclusions.....	82
Acknowledgments.....	87
References.....	88

List of Figures

	Page Number
1. Proposed Tat secretion components and Process	6
2. Gene synteny, membrane topology, and sequence homology of LCTs and their holin-like protein.....	10
3. TpeL secretion is TpeE dependent in <i>C. perfringens</i>	12
4. TpeE localizes to the membrane in <i>C. perfringens</i>	12
5. Western blots of TpeL insertion and TpeE-FLAG crosslinking	14
6. Potential Mechanism of TpeE-dependent secretion of TpeL.....	15
7. FAST Fluorescence Experimental Design.....	21
8. Biotinylation Experimental Design.....	22
9. Controls for Coral and Amber-NP dyes.....	28
10. HN13 growth during expression of <i>tpeE</i> -FAST.....	32
11. TpeE-FAST secretion of TpeL in HN13.....	34
12. TpeE-FAST Densitometry in HN13 and Strain 13.....	35
13. TpeE-FAST Coral Fluorescence: HN13.....	36
14. TpeE-FAST AmberNP Fluorescence: HN13.....	37
15. TpeE-FAST Live Dead Fluorescence: HN13.....	38
16. Growth of Strain 13 during expression of <i>tpeE</i> -FAST.....	39
17. TpeE-FAST Secretion in Strain 13.....	40
18. TpeE-FAST Coral Fluorescence: Strain 13.....	41
19. TpeE-FAST AmberNP Fluorescence: Strain 13.....	42
20. Fluorescence of Mixed culture: TpeE and TpeE-FAST Strain 13.....	42
21. Lysine Biotinylation and Anti-His ₆ Western blot.....	43
22. Growth of HN13 during expression of mutant <i>cys tpeE</i> : Holin alone.....	44
23. Growth of HN13 during expression of mutant <i>cys tpeE</i> : Holin Toxin.....	45
24. Mutant Cys TpeE secretion in HN13 western blot.....	46
25. Mutant Cys TpeE secretion in HN13 densitometry.....	46
26. Cysteine Biotinylation Whole-cell extracts.....	47
27. Cysteine Biotinylation Membrane Fractions.....	48
28. TatA and <i>E. coli</i> lipid lengths.....	58
29. Molecular Dynamics of manipulated lengths of TatA.....	59
30. Membrane Destabilization model for TpeE-dependent secretion.....	60
31. TpeE Membrane Topology.....	61
32. Holin Transmembrane Helix Deletions: HN13 Growth.....	67
33. Holin Toxin Transmembrane Helix Deletions: HN13 Growth.....	68
34. Holin Transmembrane Helix Insertions: HN13 Growth.....	69
35. Holin Toxin Transmembrane Helix Insertions: HN13 Growth.....	69
36. ProSA Results of AlphaFold3 Models.....	71

37. AlphaFold3 Model 1.....	71
38. AlphaFold3 Model 2.....	72
39. AlphaFold3 Model 3.....	72
40. AlphaFold3 Model 4.....	73
41. AlphaFold3 Model 5.....	73
42. ProSA Results of Robetta Models.....	74
43. Robetta Model 1.....	74
44. Robetta Model 2.....	75
45. Robetta Model 3.....	75
46. Robetta Model 4.....	76
47. Robetta Model 5.....	76
48. Shortened TpeE Secretion in HN13.....	77
49. Shortened Mutant TpeE Secretion Densitometry.....	78
50. Lengthened TpeE Secretion in HN13.....	78
51. Lengthened Mutant TpeE Secretion Densitometry.....	79

List of Tables

Page Number

1. List of primers used for the cell-surface biotinylation experiment.....25
2. List of plasmids used in the FAST fluorescence and cell-surface biotinylation experiments.....25
3. List of primers used in the membrane destabilization experiments.....63
4. List of plasmids used in the membrane destabilization experiments.....64

Chapter I

Literature Review

Clostridium perfringens

Clostridium perfringens is a Gram-positive, spore forming, rod-shaped bacterium commonly found in soil, food, sewage, and the normal gut microbiota [1, 2]. It is responsible for approximately 1 million cases of food poisoning in the United States each year, involving symptoms like stomach cramps and diarrhea [3]. Along with the ability to cause food poisoning, *C. perfringens* is also the common culprit for gas gangrene, a condition characterized by toxin-mediated tissue necrosis [4]. Despite being an obligate anaerobe that lacks the ability to utilize an electron transport chain, *C. perfringens* is quite aerotolerant and is one of the fastest growing organisms with a less than 10-minute division rate in ideal conditions [5]. Its fast division rate and its ability to secrete ~20 toxins allow this bacterium to cause numerous lethal diseases in humans and animals [6].

Toxinotypes and Associated Diseases

Clostridial pathogenicity is dependent on the secretion of a plethora of toxins, each capable of causing disease in most mammals. There are currently 7 toxin types (A-G) to which *C. perfringens* can be classified, each associated with a specific disease [7]. In this section, toxin types A-D will be covered.

Type A strains, which cause food poisoning, myonecrosis, and necrotic enteritis in humans and animals, produce alpha toxin (CPA) [5]. CPA, a key toxin in the development of gas gangrene, is a zinc containing phospholipase C that can bind and break down the host membrane [5, 6]. CPA is ubiquitous in all toxin types of *C. perfringens*; however, type A seems to secrete CPA more readily than others [8].

Type B strains are associated with enterotoxemia and necrotic enteritis in animals as they are CPA, beta (CPB), and epsilon (ETX) positive [5]. CPB, a pro-toxin, is a β -pore-forming toxin that binds to host cell membranes and disturbs their homeostasis, leading to a variety of symptoms [6]. ETX increases intestinal permeability and facilitates its own absorption into other organs, leading to enterotoxemia [9]. Once bound to epithelial cells, ETX will cause host cells to become swollen, leaky, and necrotic, causing edema [9].

Type C strains are CPA, CPB, and *C. perfringens* enterotoxin (CPE) positive and are commonly associated with myonecrosis, necrotic enteritis, and gastrointestinal symptoms [5, 6, 10]. CPE is characterized as an enterotoxin and is the common culprit of the gastrointestinal symptoms experienced during *C. perfringens* food poisoning infections [10]. CPE is produced during the sporulation of *C. perfringens* in the gut, where CPE binds to claudin receptors and oligomerize to form a prepore on the surface of the host membrane [10]. CPE has also been seen in some strains of types A and G *C. perfringens* [6].

Type D strains are both CPA and CPE positive and are associated with gas gangrene in animals and gastrointestinal symptoms [5, 6]. Type E strains are CPA and iota (ITX) positive and are associated with dermonecrotic disease and enterotoxemia in animals [6]. ITX consists of two components: an enzyme component (Ia) and a binding subunit (Ib) [11]. The alpha subunit of iota toxin ADP-ribosylates skeletal muscle α -actin and non-muscle β/γ -actin which will then be transferred to a set of target proteins eventually resulting in cell death [11].

Each type is equipped with their own associated toxins that can cause various lethal diseases in humans and animals. However, in order for these toxins to cause disease, they require a secretion system to facilitate translocation from the cytoplasm to the environment.

Protein Secretion Systems in Gram-positive Bacteria

Protein secretion systems are an essential aspect of survival for all organisms [12]. Specifically, for clostridial pathogens, the secretion of toxins is key to their pathogenesis in many of their hosts [13-15]. This section will cover the protein secretion systems commonly found in most Gram-positive bacteria, starting with the general secretion system.

The general secretion system (Sec). This is an essential and ubiquitous secretion system found in both Gram-negative and Gram-positive bacteria [12, 16-18]. This system is capable of the incorporation of proteins in the cell membrane as well as their translocation through it [12, 16]. Proteins that require the Sec system are commonly synthesized as preproteins with a cleavable and recognizable peptide sequence, referred to as the signal peptide [12, 16]. Signal peptide sequences are not homologous and encode 20-30 residues, containing core regions such as a positively charged N-terminus, a hydrophobic core region, and a polar C-terminus that includes a signal peptidase recognition site [12]. Initiation of secretion begins when chaperones, most notably SecB (*E. coli*) and SecB-like proteins (Gram-positives), bind newly synthesized proteins to keep them unfolded and guide them to another core Sec protein, SecA [12, 16]. SecA will transport the preprotein to the Sec translocase, SecYEG, which spans the cytoplasmic membrane [12, 19]. This interaction and the utilization of ATP initiates the step-by-step translocation of the preprotein through SecYEG [12, 19]. The dissociation of SecA from SecYEG further promotes the translocation process [12]. The signal peptide is cleaved by a membrane-embedded signal peptidase either during or after the translocation process [12]. The final product following translocation can include a membrane-embedded or free-floating folded protein [12, 16].

The twin-arginine transport secretion system (Tat). This is a system found in both bacteria and archaea [17, 18, 20]. The Tat system has been shown to be a key aspect of bacterial metabolism, cell wall synthesis, nitrogen fixation, and pathogenesis [20]. A special characteristic of the Tat system is its ability to transport fully folded proteins across the cytoplasmic membrane [12, 21-25]. Most proteins that require the Tat system contain a cleavable and recognizable signal peptide sequence that is similar to the Sec system signal peptide [12]. However, a Tat signal peptide includes a twin-arginine motif present in the N-terminus region separates it from the Sec signal peptide [12, 18, 23, 25, 26]. The components of the Tat system commonly include TatA, TatB, and TatC (Figure 1) [22, 27]. TatA and TatB are quite similar and contain both a transmembrane helix and an amphipathic helix whereas TatC is comprised of approximately 6 predicted transmembrane helices [12]. The components of the Tat system vary between organisms where some do not include TatB in their genome while some contain multiple copies of each component [21]. These components interact with each other to form two major complexes: the docking complex, containing a TatA-like protein and TatC, and the translocation complex, containing multiple TatA-like proteins and TatC (Figure 1). The Tat system initiates when the docking complex recognizes the signal peptide on the Tat-dependent protein, triggering the recruitment and oligomerization of TatA [12, 22]. This oligomerization of TatA, which interacts with the docking complex, forms the active Tat translocase [12, 22]. However, the mechanism of which the protein crosses the membrane has not yet been confirmed [22].

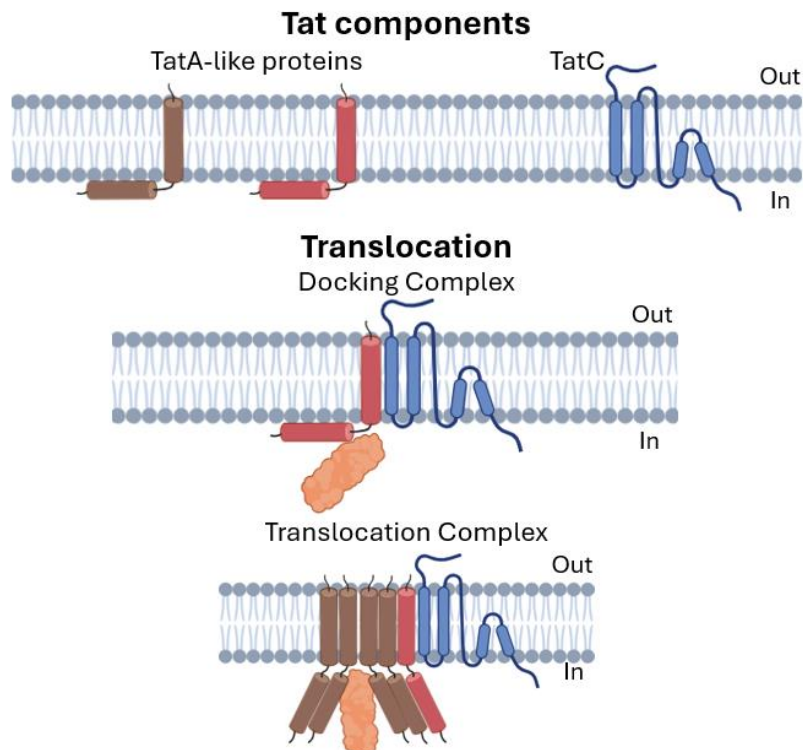


Figure 1. Proposed Tat secretion components and Process [22]. This illustration depicts the key proteins utilized in the Twin-arginine transport system, TatA-like and TatC. This process involves the interaction between the target protein (Orange) and the docking complex which consists of a TatA-like protein (Red) and TatC (Blue). This interaction signals the recruitment of multiple TatA-like proteins (Brown) to form a complex known as the translocation complex. The recruitment of TatA will then facilitate secretion of the target protein.

There are currently two popular models that seek to explain the translocation process, a pore model and a membrane-destabilization model. The pore model suggests that the oligomerization of TatA or TatA-like proteins form a pore around the target protein, utilizing either a trap-door or twisting mechanism for transportation [22]. The membrane-destabilization model suggests that the oligomerization of TatA or TatA-like proteins form aggregates that destabilize a region of the membrane to facilitate the translocation of the target protein [22]. While both models have a substantial amount of supporting evidence, however, there does not appear to be a consensus [22].

Type IV secretion systems (T4SSs). These carry out some key functions in both Gram-negative and Gram-positive bacteria which include type 4 pilus formation, protein secretion, gene transfer, and biofilm production [12, 28, 29]. Specifically in *Brucella*, VirB, a T4SS protein, is a key virulence factor that mediates *Brucella's* intracellular survival [30]. T4SSs are separated by 3 major functions: 1) the transfer of ssDNA and one or more proteins across the bacterial membrane into a target cell via conjugation; 2) the transfer of effectors to target through direct contact with eukaryotic cells; and 3) the release of cell contents to the extracellular space [12, 29, 31]. Gram-positive bacteria possess a minimized version of the T4SSs which consists of 6 core subunits and is commonly used as a conjugative system [31, 32].

Type VII secretion systems (T7SSs). These are a recently discovered systems originally found in mycobacteria but have been discovered in a wide range of Gram-positive bacteria, specifically in both *Bacillus* and *Staphylococcus* species [12, 33-35]. The T7SSs are comprised of 5 secretion systems that secrete 3 families of T7SS substrates which have been shown to play roles in many bacterial processes including sporulation, conjugation, and cell wall stabilization [12, 33]. The components in mycobacteria arrange themselves in a hexameric complex that include EccB, EccC, EccD, and EccE [33]. At the center of this complex, EccC, a multidomain ATPase, has been shown to recognize its substrate through C-terminal signal peptides [33]. Members of the T7SS substrate families are secreted as folded heterodimers [36].

Holin-dependent secretion systems. This system is thought to originate from phages, now found in Gram-positive and Gram-negative bacteria, and facilitates the translocation of endolysins across the cytoplasmic membrane [37]. There are currently several superfamilies of holins which are commonly divided into two groups: 1) canonical holins, commonly found in bacteria, directly transfer their target protein and 2) pinholins which depolarize the membrane,

which allows the release of the transported protein [37]. Until recently, holin secretion systems were thought to only cause lesions in the cell membrane, causing the cells to lyse [37, 38]. However, non-lytic versions of holin-dependent protein secretion have been characterized in both Gram-negative and Gram-positive bacteria [37]. Although similar to the Tat secretion system, these holin systems have been shown to carry out secretion in two steps to transport fully folded proteins and have been linked to the secretion of virulence factors in certain pathogens [13, 37, 39, 40]. Regardless of the type of secretion system being utilized, it is important to understand how these proteins interact in the cell-membrane of specific organisms as it can help characterize each mechanism.

***C. perfringens* Membrane**

Information on the lipid structure and composition of the *C. perfringens* cell-membrane is limited; however, a few groups have conducted comparative analysis of lipidomic data across a majority of the Clostridial species. The overall lipid structure and composition within Clostridial membranes is incredibly diverse. According to lipidomic analysis of species in *Clostridium sensu stricto*, phosphatidylglycerol (PG), phosphatidylethanolamine (PE), and cardiolipin (CL) are the only three phospholipids that are commonly found across all species [41]. Another commonality across these species is the presence of glycosyldiradylglycerols, however the concentration of these varies widely [41]. In *C. perfringens*, the cell membrane consists of aminoacyl-PG, in the form of ala-PG, which is hypothesized to be a defense mechanism from host immune cells present in damaged tissue [41-43]. PE and PG (very little of each are in the plasmalogen form) make up the great majority of the cell membrane, although exact percentages of the PG and PE have yet to be determined. However, the primary fatty acids present are

dodecanoic acid (12:0, 29%), tetradecanoic acid (14:0, 21%), tetradecenoic acid (14:1, 14%), hexadecanoic acid (16:0, 8%), and octadecanoic acid (18:0, 8%), with some strains characteristically having high levels of dodecanoic and tetradecanoic acid [43, 44]. Currently, the known molecular species within each PE and ala-PG are 14:0,14:0 (26.3%, 33.6%), 12:0,14:0 (19%, 18.7%), 14:0,16:0 (22.4%, 26.3%), and 16:0,16:0 (17.6%, 15.2%), respectively [43]. Although these percentages are a good start, more information would be useful in determining membrane-protein interactions and the dynamics of certain secretion systems within *C. perfringens*, especially the secretion of lethal toxins.

Large Clostridial Cytotoxins

Large clostridial toxins (LCTs) are a family of bacterial toxin that includes TpeL from *C. perfringens*, TcdA and TcdB in *Clostridioides difficile*, as well TcsL and TcsH in *Paeniclostridium sordellii* [13, 39, 40]. Each of these toxins have been directly linked to virulence in both animal models and humans [45-48]. Specifically for *C. perfringens*, TpeL has been shown to play a role in necrotic enteritis in poultry but has yet to be linked to virulence in humans [49-51]. To cause infection, these toxins inactivate host GTPases via glycosylation, which generally leads to the disruption of the actin cytoskeleton, causing cells to lose their shape and undergo apoptosis [52]. Almost all LCTs consist of a biologically active domain, a pore-forming and delivery domain, a cysteine protease domain, and a CROPs domain (C-terminal receptor binding domain contain repetitive oligopeptides) [2, 53-55]. However, TpeL lacks the CROPs domain, consisting only of a glycotransferase domain, autocatalytic domain, and a transmembrane domain [2, 55]. Due to the lack of a signal peptide, these toxins cannot be transported by general secretion pathways such as the Sec- or Tat- secretion systems [13]. However, the pathogenicity locus for each toxin

encodes a small holin-like protein directly adjacent to each toxin gene (Figure 2) [13]. Previous studies on TcdA, TcdB, TcsL, and TcsH have shown that these LCTs require their cognate holins to facilitate translocation through the membrane [13, 39, 40]. Until recently, the relationship between TpeL and its cognate holin, TpeE, had not yet been characterized [13].

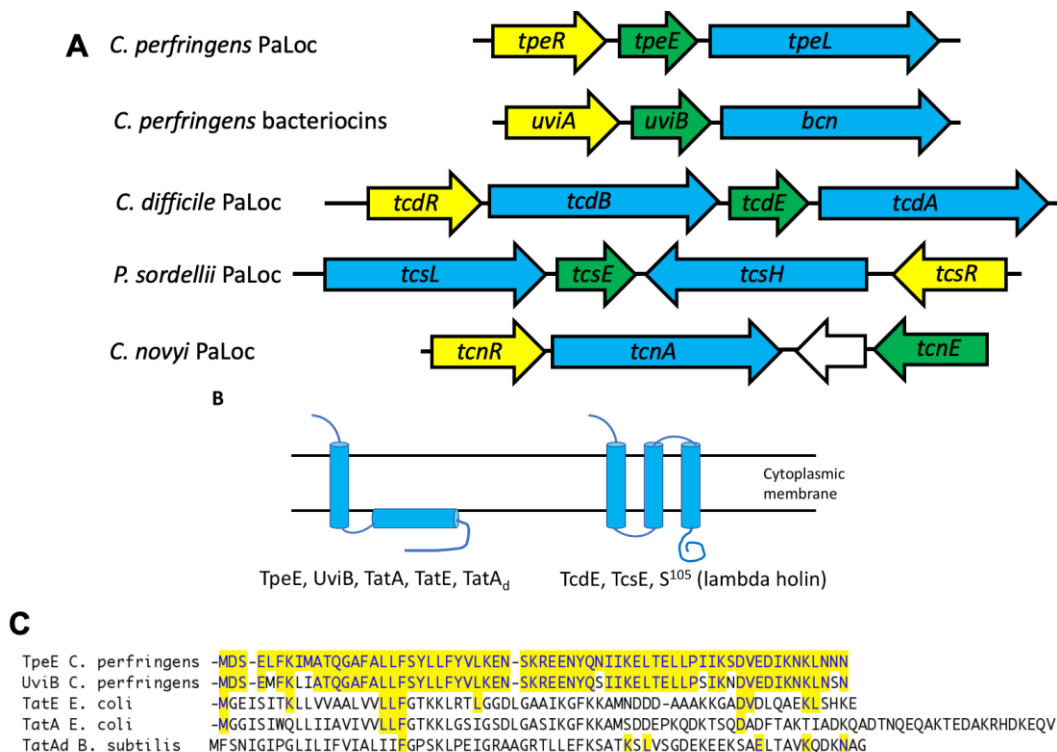


Figure 2. Gene synteny, membrane topology, and sequence homology of LCTs and their holin-like protein. (A) Gene organization of LCT pathogenicity loci and a bacteriocin-containing operon. LCTs, light blue; holin-like proteins, green; sigma factors, yellow. **(B)** Proposed membrane topology for holins and holin-like proteins from panel A and TatA/TatAd from the twin-arginine secretion system. **(C)** ClustalW sequence alignment of the holin-like proteins. Matching residues are highlighted in yellow [13].

TpeE-dependent secretion of TpeL

TpeE is part of the Bh1A protein family. Through conserved domain analysis, TpeE is classified within the Bh1A holin family (superfamily VI) [13, 56-58]. This family of proteins, primarily found in Firmicutes, represents a wide array of putative holin-like proteins [57-60]. It

is unclear if these holins facilitate translocation of endolysins through cell-lysis, leakage, or secretion and may depend on the specific holin-substrate interactions [58]. Holins within this family commonly consist of a singular transmembrane helix domain with a weakly hydrophobic amphipathic helix domain [57]. Unlike other bacterial holin-like proteins, such as TcdE and TcsE which share a similar membrane topology to the phage lambda holin, the membrane topology of TpeE is consistent with other BhlA proteins, involving a transmembrane helix (TMH) and an amphipathic helix (APH), which happens to be similar to the proposed membrane topology of TatA, a key protein in the Tat-secretion system [13]. Due to this similarity, it was hypothesized that TpeE may be required for TpeL secretion, representing a novel and ubiquitous secretion system that shares aspects of Tat-secretion as well as holin-dependent secretion [13].

TpeE is required for TpeL secretion: A recent publication focused on determining if TpeE is required for TpeL secretion [13]. Cloning of *tpeE* and *tpeL* was conducted using chromosomal genes from a C type *C. perfringens* JGS 1495 cloned into HN13, a laboratory strain of *C. perfringens*, using a lactose-inducible expression plasmid, pKRAH1 [13]. To test for secretion, western blots were conducted using an antibody specific to a His₆-tag on the C-terminus of TpeL [13]. When comparing the supernatants of each strain, it was found that TpeL is only found in the supernatant of strains expressing both TpeE and TpeL (Figure 3, [13]). Whole-cell lysates were compared to corresponding supernatants to ensure that TpeL was being expressed (Figure 3, [13]). To ensure that results were not due to lysis of the cells before sample collection, BCP, a naturally biotinylated and known cytoplasmic protein, was probed with fluorescently labeled streptavidin [13].

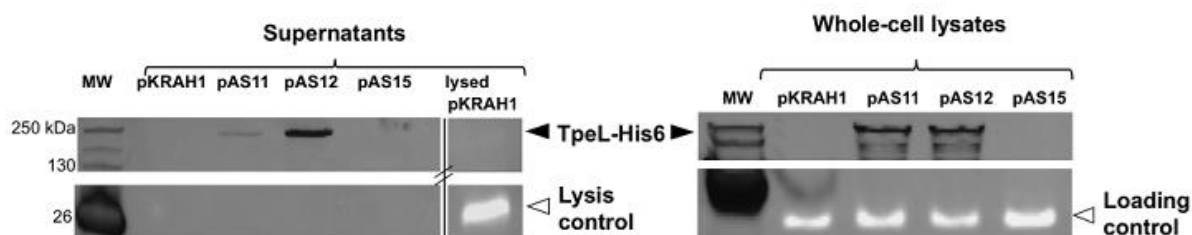


Figure 3. TpeL secretion is TpeE dependent in *C. perfringens*. Western Blot using antibody directed against His₆-tag on TpeL. pKRAH1, empty vector; pAS11, expressing TpeL alone; pAS12, expressing both TpeE and TpeL; pAS15, expressing TpeE alone. Lysis control and loading controls, BCP identified by fluorescently labeled streptavidin [13].

TpeE localizes to the membrane. After determining that TpeE is required for TpeL secretion, the lab was interested in determining where TpeE localizes within *C. perfringens*. To detect TpeE in a western blot, TpeE was tagged on the C-terminus with a FLAG tag [13]. After expression, cytoplasmic and membrane fractions were prepped alongside untagged TpeE [13]. It was found that TpeE was detected only in the membrane fractions of cells containing the FLAG tagged TpeE (Figure 4, [13]). To ensure the results were not due to cell lysis, BCP was again probed with fluorescently labeled streptavidin [13].

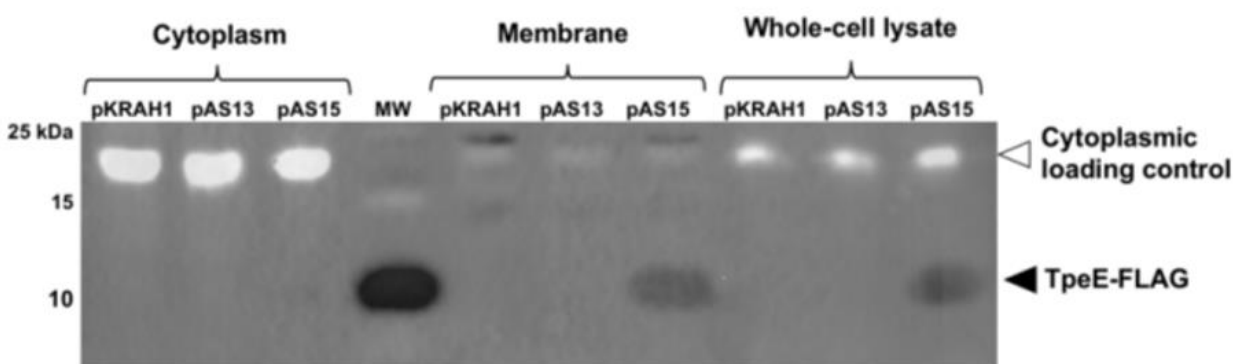


Figure 4. TpeE localizes to the membrane in *C. perfringens*. Western blot using anti-FLAG antibodies to detect the location of TpeE. pKRAH1, vector control; pAS13, *tpeE*; pAS15, *tpeE*-FLAG. The cytoplasmic loading control consisted of a fluorescent streptavidin conjugate to detect the cytoplasmic BCP protein of *C. perfringens*. MW signifies the molecular weight ladder. The band present in this lane is the 10 kDa marker [13].

TpeL localization. After determining the localization of TpeE, they began to determine where TpeL localizes as well. Localization was conducted via western blots using anti-His₆ antibodies to detect the location of TpeL by Angela Saadat. It was found that, regardless of TpeE expression, TpeL was consistently found in the membrane of *C. perfringens* (Figure 5). This suggests that TpeL will insert itself into the membrane even in the absence of TpeE. In addition to TpeL localization, the lab was interested in determining the role that TpeL may play in the oligomerization of TpeE. To detect oligomerization, a formaldehyde crosslinking experiment was applied, conducted by Stephen Melville. Cells expressing TpeE in the presence or absence of the toxin were exposed to formaldehyde which will establish covalent bonds between possible oligomers, resulting in larger band sizes depending on the size of the oligomer. Using western blots with anti-FLAG antibodies, it was found that TpeE is predominantly present in the monomer form in a TpeE only culture. However, larger multimers of TpeE are detected when TpeL is co-expressed (Figure 5).

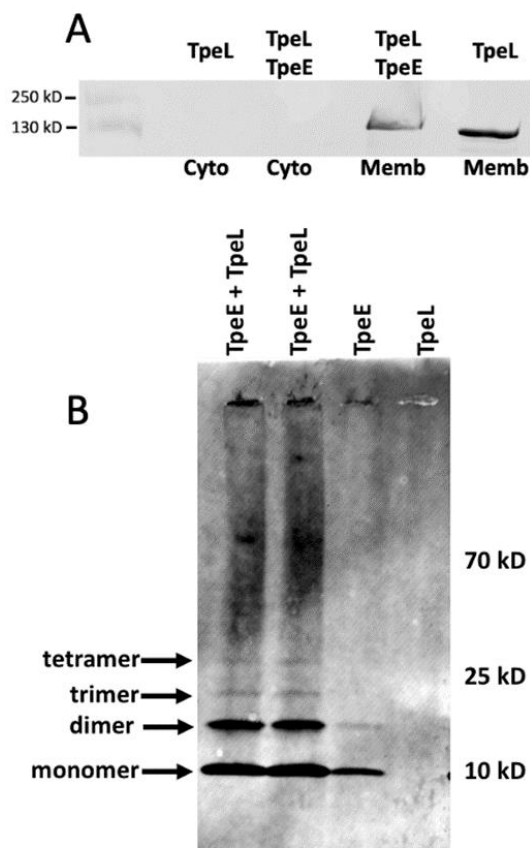


Figure 5. Western blots of TpeL insertion and TpeE-FLAG crosslinking. (A) Western blot showing detection of His6-tagged TpeL in the membrane regardless of TpeE presence. Cyto, cytoplasm; Memb, membrane. (B) Crosslinking of TpeE-FLAG only in the presence of TpeL. Proteins were cross-linked with 2% paraformaldehyde. Experiments were conducted by Angela Saadat and Stephen Melville.

Using these results, a preliminary secretion model was created that suggested a potential mechanism for TpeE-dependent secretion of TpeL (Figure 6, [13]). The model suggests that TpeL and TpeE localize and interact in the membrane of the cell. This interaction will facilitate the secretion of TpeL by signaling the oligomerization of TpeE, forming a pore around TpeL.

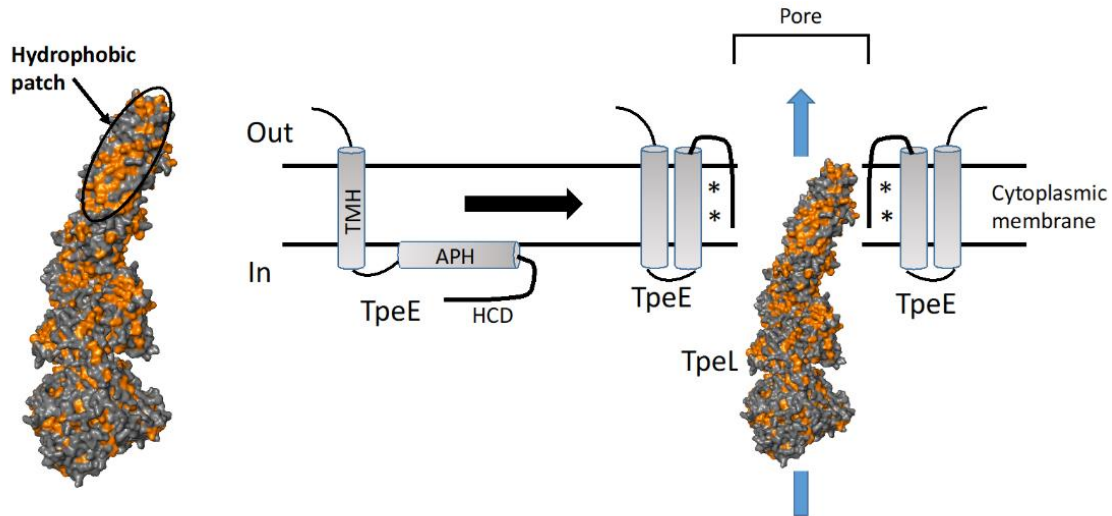


Figure 6. Potential Mechanism of TpeE-dependent secretion of TpeL. TpeE localizes in the membrane of the cells and consists of a trans-membrane helix (TMH), an amphipathic helix (APH), and a high charge density domain (HCD). Using a hydrophobic patch, TpeL inserts itself into the membrane, signaling the oligomerization of TpeE. TpeE will then form a pore in the membrane, allowing TpeL to be secreted.

About a year later after this publication, Brüser and Mehner-Bretfield [37], who primarily study the Tat secretion system, reviewed the potential holin-dependent secretion model. Their model for holin-mediated transport agrees with most of the steps of the secretion model in *C. perfringens*. The key difference is the mechanism by which the transported protein exits the membrane. Brüser and Mehner-Bretfield believe that the oligomerization of the holin affects the stability of the membrane which allows the hinge-like motion to occur, combining aspects of both the pore-forming and membrane destabilization models of the Tat-secretion system.

Chapter II

TpeE-Dependent Secretion of TpeL: Pore-Forming Model

Abstract:

The Clostridia are anaerobic Gram-positive pathogens which cause numerous lethal diseases in humans and animals. All Clostridial pathogens secrete toxins as an essential aspect of their pathogenesis. One family of toxins are the large clostridial cytotoxins (LCT), which include TpeL from *C. perfringens* and TcdA/B from *C. difficile*. All LCTs lack a signal peptide for Sec-dependent secretion. However, the pathogenicity locus encoding each toxin gene also encodes a phage holin-like protein, TpeE for *C. perfringens*. Each toxin has been shown to be dependent on their cognate holin for secretion. However, TpeE shares a similar membrane topology with the TatA protein, a key component of the Twin-Arginine Transport (Tat) secretion system while others are like lambda holin. It is hypothesized that TpeE represents a novel and ubiquitous class of secretion proteins with features from both Tat and holin-like protein secretion systems. A recent publication showing that TpeE is required for the secretion of TpeL in *C. perfringens* supports this hypothesis. A comprehensive model for the mechanisms underlying holin-dependent secretion was developed in which TpeL inserts into the cytoplasmic membrane using a hydrophobic patch on its surface which catalyzes the oligomerization of the holin, TpeE, and formation of a pore through which the toxin is secreted. To test if the amphipathic helix of TpeE folds into the cell-membrane to facilitate the formation of a pore, FAST fluorescence technology and cell-surface biotinylation were applied. TpeE was tagged on the C-terminus of the amphipathic helix with a FAST protein which will bind to a set of permeable and impermeable dye. The theory behind this experiment was that if amphipathic helix of TpeE flips in the presence of TpeL, then the C-terminal FAST tag would be exposed to the outside of the cell and bind to the impermeable dye. However, experimental results did not support this major step. When using a membrane impermeable dye, the mean pixel intensity of each frame experienced

no change throughout the induction of TpeE-FAST in the presence of the toxin. This suggests that TpeE-dependent secretion of TpeL does not involve the flipping of the amphipathic helix of TpeE into the cell-membrane when forming a pore. Cell-surface biotinylation was unable to support these results due to unforeseen errors within the experimental design.

Introduction:

Clostridial pathogens are Gram-positive, anaerobic, spore forming bacteria capable of causing numerous diseases in both humans and animals [61-65]. It is a common characteristic across all clostridial pathogens to secrete lethal toxins to bring about these diseases [13, 66-68]. More specifically, *C. perfringens* is the causative agent of ~1,000,000 cases of food poisoning in the United States each year as well as being the most frequent cause of gas gangrene [3, 69]. This organism is capable of causing these diseases in various hosts as it is armed with approximately 20 toxins that vary amongst different strains [1]. One family of these toxins is the large clostridial toxins (LCTs) capable of shutting down host cell signaling through the inactivation of host Rho family GTPases via glycosylation [13, 70]. This family includes toxins such as TcdA and TcdB from *C. difficile*, TcsH and TcsL from *P. sordellii*, TcnA from *C. novyi*, and TpeL from *C. perfringens*, each associated with virulence in different hosts [13, 71-73]. Each LCT encoding gene is located within a pathogenicity locus that also includes a holin-like protein-encoding and a sigma factor-encoding gene (Figure 2A) [13]. A characteristic shared amongst all LCTs is that they cannot be translocated through conventional secretion systems, such as the general secretion system and Tat-secretion, as they all lack a signal peptide [13]. However, recent publications have determined that almost all of these particular LCTs require their cognate holin for secretion [13, 39, 74].

LCT holins seem to come in two separate membrane topologies, where TcdE and TcsE share similar membrane topologies to the phage lambda holin and TpeE shares a similar membrane topology to TatA, a key protein in the Tat-secretion system [13]. Specifically for TcdE and TcsE, these holins consist of three transmembrane helix domains and a cytoplasmic C-terminal domain [13]. Whereas TpeE and TatA have a predicted membrane topology that

involves a singular transmembrane helix domain alongside a amphipathic helix domain [13].

Due to this similarity, it was hypothesized that TpeE may represent a novel secretion system that combines aspects of holin-dependent secretion with the Tat-secretion system [13].

There are currently two supported models for Tat-secretion: a Pore-forming model and a Membrane Destabilization model [75]. Aspects of the pore-forming model will be the subject of this chapter. According to the pore-forming model, the Tat-secretion system consists of two complexes: the docking complex, which consists of TatA-like/TatB and TatC, and a translocase complex, which involves the recruitment and oligomerization of TatA to the docking complex [12, 22, 76, 77]. It was thought that when TatA oligomerizes, it forms a pore that is big enough to facilitate translocation due to the presence of multiple channel-like structures within TatA extractions [76].

Applying this mechanism to holin-mediated LCT secretion in *C. perfringens*, it was thought that TpeL would insert into the cell-membrane where it will then interact with TpeE, catalyzing its oligomerization where the amphipathic helix will flip into the cell-membrane to form a pore [13]. This study tried to determine if the amphipathic helix of TpeE does in fact change its orientation in the presence of the toxin (TpeL). To do so, FAST Fluorescence and Biotinylation technologies were applied.

A fluorescence absorption shifting tag (FAST) from the Twinkle Factory is a protein that acts a target for a specific set of fluorophores to bind and fluoresce [78]. This particular protein requires no molecular oxygen to become fluorescently active, perfect for imaging proteins under anaerobic conditions [78]. Along with the FAST tag, a set of cell-permeant and impermeant dyes are sold to conduct cell-surface fluorescent labeling [78]. This study utilizes these functions to help characterize the mechanism of TpeE-dependent secretion of TpeL in *C. perfringens*. To do

so, a FAST tag was fused to the C-terminus of TpeE where it was then exposed to a permeable (Coral) dye and an impermeable (AmberNP) dye in the presence and absence of TpeL. Live-cell movies were imaged using an Olympus IX71 with Cool SNAP HQ² Photometrics and analyzed using a new segmentation and image analysis software called SuperSegger-omnipose from the Wiggins Laboratory at the University of Washington [79]. It was hypothesized that in the presence of TpeL, the amphipathic helix of TpeE will flip into the cell-membrane which will expose the FAST to the outside of the cell, allowing both the Coral and AmberNP dye to bind and fluoresce (Figure 8). Whereas, in the absence of the TpeL, the amphipathic helix of TpeE will not flip, allowing only the Coral dye to bind and fluoresce (Figure 7).

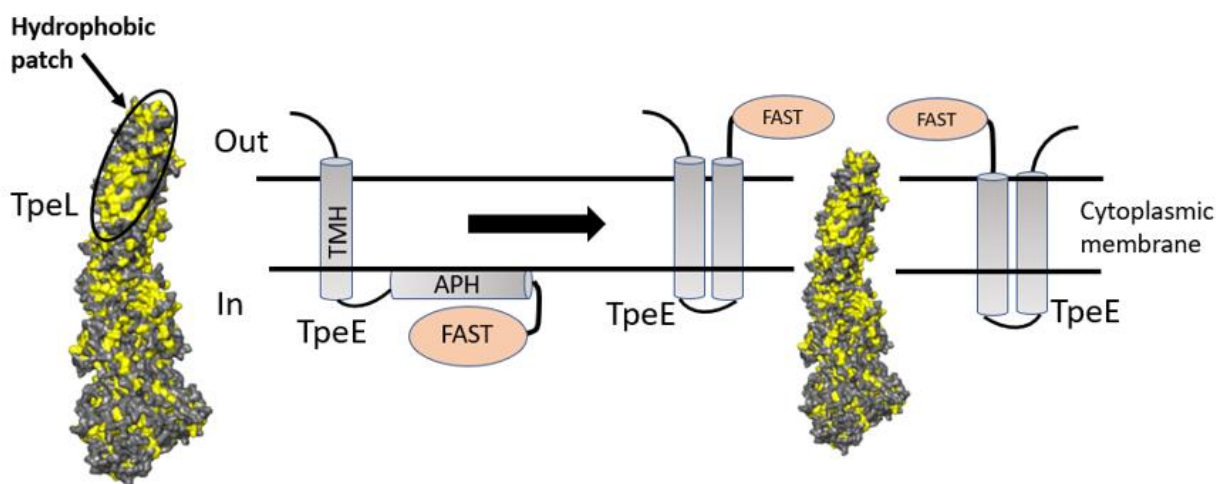


Figure 7. FAST fluorescence experimental design. This states that in the absence of the toxin (TpeL), the holin (TpeE) will not oligomerize and change its orientation, leaving the FAST tag within the cell. However, in the presence of the toxin, the holin will oligomerize as well as flip the amphipathic helix inside the cell-membrane, exposing the FAST to the outside of the cell.

As an alternative experiment, Biotinylation technology was pursued. There are many different reactive species of biotinylating reagents, such as amine, sulfhydryl, carboxyl, and carbonyl specific [80]. These reagents preferentially bind to a specific reactive group, labelling it with a molecule called biotin [80]. Biotin has an incredibly high affinity to avidin and is

consistently used to help purify and visualize labelled proteins [81]. The specific biotinylating reagents used in this study were Sulfo-NHS-LC-LC-Biotin (amine reactive) and Maleimide-Peg2-Biotin (sulfhydryl reactive). Sulfo-NHS-LC-LC-Biotin was used as a control to detect the amount of cell-surface exposed proteins in the cell-membrane of *C. perfringens*. To test the hypothesis that the amphipathic helix flips into the cell-membrane, TpeE was mutated via substitution of cysteine residues in the N- and C-terminus. It was hypothesized that if the amphipathic helix flips in the presence of the toxin, then C-terminal cysteine residues will be biotinylated and detected via mass spectrometry and western blotting using fluorescently labelled streptavidin (Figure 8).

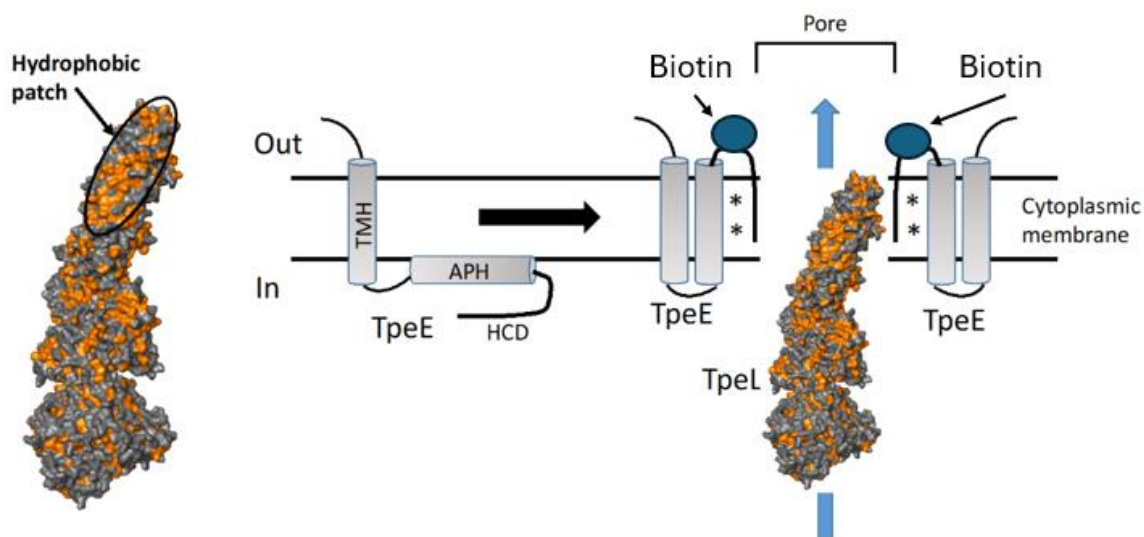


Figure 8. Biotinylation experimental design. This states that in the absence of the toxin (TpeL), the holin (TpeE) will not oligomerize and change its orientation, leaving C-terminal cysteine residues inside the cell. Whereas in the presence of the toxin, the holin will oligomerize and flip the amphipathic helix into the cell-membrane, exposing C-terminal cysteine mutations to the outside of the cell.

The goal of this study is to determine the changes that TpeE may undergo in the presence of the toxin. This will in turn give the community a deeper understanding of holin-dependent secretion as well as the underlying mechanism of the Tat-secretion system.

Methods:

Bacterial Strains and Culture Conditions

C. perfringens strain HN13 and strain 13 were cultured in an anaerobic chamber at 37 °C in PGY medium (3% proteose #3 peptone, 2% glucose, 1% yeast extract, and 0.1% sodium thioglycolate) or TY medium (3% tryptone, 2% yeast extract, 0.1% sodium thioglycolate). DH10B *E. coli* strain was grown at 37 °C on Luria-Bertani (LB) broth (1% salt and tryptone and 0.5% yeast extract). For HN13 or Strain 13 cultures containing pKRAH-erm, 30 µg/µL of erythromycin was added to PGY or TY media, whereas for cultures with pKRAH1, 20 µg/µL of chloramphenicol was added to PGY or TY media. For DH10B cultures containing the pCRBluntII TOPO vector, kanamycin (100 µg/µL) was added to LB media.

Cloning of TpeE-FAST into HN13 and Strain 13

To obtain cultures that contain TpeE-FAST, TpeL, or both, the plasmids for each were constructed and electroporated into an HN13 strain or Strain13 of *C. perfringens*. For the creation of *tpeE*-FAST plasmids, our laboratory sent a sequence to be synthesized that contained *tpeE*, a linker region, and the sequence for FAST. The synthesized template was received within a pBluescript II plasmid, which contained SacII and Sall restriction sites that flank the 5' and 3' ends respectively. The template and a vector (pKRAH-erm) were cut with SacII and Sall and ligated to assemble the construct. The constructs were electroporated into a prepped overnight culture of HN13 or Strain 13 grown in 3 ml of PGY media. The cells were prepped by performing 3 washes with sucrose electroporation buffer (SEB), centrifuged (3,500 rpms for 5 minutes), and resuspended in SEB with half the volume grown overnight. The electroporation parameters are as such: peak voltage set at 2,500 V, resistance set at 125 Ω, and the capacitance

set at 50 μ F. After the electroporation, the cells were incubated at 37°C anaerobically in PGY media for 3 hours to ensure phenotypic expression. The cells were then centrifuged, concentrated, and plated on PGY-erm30. The plates were incubated overnight at 37°C, anaerobically. Colonies were checked for the insertion of the *tpeE*-FAST through polymerase chain reaction (PCR). For creation of the TpeE-FAST and TpeL 2 plasmid culture, the same plasmid described above was electroporated into a TpeL-His₆ culture using the previously described electroporation methods. However, to maintain both plasmids, the incubation for phenotypic expression contained chloramphenicol to ensure that the *tpeL*-His₆ plasmid was not lost during the 3 hours. After phenotypic expression, the cells were plated and grown overnight at 37°C on PGY cm20 erm30 agar. Isolated colonies were screened for *tpeE*-FAST using PCR.

Cloning of Mutant TpeE into HN13 for Biotinylation

To minimize any effect on the function of TpeE, it was decided that it was best substitute amino acids amino acids closer to the N- and C- terminus. Sites of the substitutions included S3, K59, N60, and N65. Substitutions were made through overlapping PCR using a *C. perfringens* Type C JGS 1495 chromosomal prep. Primer sets used for S3C, N65C, N60C, and K59C were ONF 15 and 16, ONF 17 and 21, ONF 17 and 20, and ONF 17 and 18, respectively. Each mutant PCR product was then ligated to pCRBluntII TOPO via blunt-end ligation and transformed into *DH10B E. coli* by electroporation (2,450V, 125 Ω , and 50 μ F). Mutant *tpeE* was then cut from pCRBluntII TOPO using 5' SacII and 3' BamHI restriction sites and ligated to pKRAH-erm. pKRAH-erm plasmids were then transformed into *C. perfringens* strain HN13 via electroporation (2,500V, 125 Ω , and 50 μ F). Cultures were then checked using OAS28 and OAS31. Sequences were checked using Sanger Sequencing at the Fralin Life Science Institute Genomic Sequencing Center.

Table 1. List of primers used for the cell-surface biotinylation experiment.

Name	Description	Sequence
ONF15	Forward: Used to make the N-terminal substitution for S3C	5'- CCGCGGATTTATAGGAGGTTAATTGTG GATTGTGAACTGTTTAAAATTATG-3'
ONF16	Reverse primer for S3C	5'- GGATCCTATAAATTTTTCTAATTATTATTC AATTATTTTTTATGTCTTCAACATC -3'
ONF17	Forward primer for N65C, N60C, K59C	5'- CCGCGGATTTATAGGAGGTTAATTGTGGA TTCAGAACTGTTTAAAATT-3'
ONF18	Reverse: Used to make C-terminal substitution for N65C	5'- GGATCCTATAAATTTTTCTAACAATTATT CAATTATTTTTTATGTCTTCAAC-3'
ONF19	Reverse: Used to make C-terminal substitution for N60C	5'- GGATCCTATAAATTTTTCTAATTATTATTC AATTACATTTTTATGTCTTCAACATC-3'
ONF20	Reverse: Used to make C-terminal substitution for K59C	5'- GGATCCAAATTTTTCTAATTATTATTCAA TTTATTACATATGTCTTCAACATCACT-3'

Table 2. List of Plasmids used in the FAST fluorescence and cell-surface biotinylation experiments.

Name	Description	Resistance
pKRAH1	Lactose-inducible vector	cm ^r
pKRAH-erm	Lactose-inducible vector	erm ^r
pCRBluntIITOPO	Cloning vector	kan ^r
pNF 1	<i>tpeEFAST</i> -pKRAH	erm ^r
pNF 2	<i>tpeEFAST-tpeL</i> -pKRAH	erm ^r
pNF 3	<i>tpeE-S3C</i> -CRBluntIITOPO	kan ^r
pNF 4	<i>tpeE-N65C</i> -CRBluntIITOPO	kan ^r
pNF 5	<i>tpeE-N60C</i> -CRBluntIITOPO	kan ^r
pNF 6	<i>tpeE-K59C</i> -CRBluntIITOPO	kan ^r
pNF 7	<i>tpeE-S3C</i> -pKRAH	erm ^r
pNF 8	<i>tpeE-N65C</i> -pKRAH	erm ^r
pNF 9	<i>tpeE-N60C</i> -pKRAH	erm ^r
pNF 10	<i>tpeE-K59C</i> -pKRAH	erm ^r
pNF 31	<i>tpeE-His</i> -pKRAH	erm ^r
pAS45	<i>tpeL-His</i> -pKRAH1	cm ²

Growth Curves

Growth curves were conducted on each clone created to ensure its overall health. Each strain was cultured anaerobically in 1ml of PGY media overnight at 37°C. Overnight cultures were used to inoculate 2 ml of PGY media, containing a 20 mM lactose concentration. This was then aliquoted into a 96 well plate, 6 wells per culture. The optical density 600 (OD) of each well was taken every 3 minutes for 24 hours. The mean OD at each timepoint was graphed in Prism 9 (GraphPad) to visualize and calculate the growth rate and bacterial yield.

TpeL Secretion

Secretion was determined by conducting western blots using anti-His₆ antibodies to detect and measure the amount of TpeL secreted. *C. perfringens* cultures were incubated anaerobically in PGY media overnight at 37°C. The overnight cultures were diluted (1:50) in 5mls of PGY and grown at 37°C. The cultures were induced with lactose (20 mM) every hour for 5-6 hours and then centrifuged to separate the pellet and the supernatant (3,500 rpm for 5 minutes). The supernatant fractions for each were filtered and concentrated using trichloroacetic acid precipitation and washed with acetone. The pellet fractions were collected by resuspending the pellet in Dulbecco's phosphate-buffer saline and lysed through a series of bead beating steps using zircon beads. The fractions were then suspended in 4x SDS-PAGE buffer with 100 mM dithiothreitol and heated at 95°C for 15 minutes. Proteins were separated via SDS-PAGE and immunoblotted with anti-His₆ antibodies. After separation, proteins were transferred to a polyvinylidene membrane and blocked for 5 minutes with 20mls of Every Blot Blocking Buffer (BioRad). The primary antibody was added to the membrane and incubated at room temperature for 1 hour or kept overnight in a 4°C fridge. The membranes were washed 5 times for 5 minutes with Tris-buffered saline-1% Tween 20 (TBS-T). The secondary antibody was diluted in 20 ml of Every Blot Blocking Buffer, added to the membrane, and incubated for 1 hour in the dark at

room temperature. The membrane was washed with TBS-T 6 times for 5 minutes and then submerged in methanol and dried for imaging. Membranes were imaged with the StainFree and Starbright filters on the Bio-Rad ChemiDoc MP imaging system. Densitometry was conducted using ImageJ by creating a region of interest around each band to graph the pixel intensities. The area underneath the peaks in the graph corresponds to the amount of TpeL secreted.

FAST Fluorescence microscopy

Cultures containing *tpeE*-FAST only and *tpeE*-FAST *tpeL* were grown in 1ml of PGY overnight at 37°C. The overnight cultures were diluted (1:50) and grown for 1 hour at 37°C. A Rose chamber, which is used for anaerobic live-cell imaging, was constructed using 2 metal slips, 2 coverslips, a 1% TY agarose pad, and 2 rubber gaskets. One metal slide with a coverslip was placed on the bottom with a rubber gasket on top. Molten 1% TY agarose (1ml), containing a specific dye, was pipetted into the center of the slide and cooled. For this project, the membrane permeable dye (Coral) and impermeable dye (AmberNP) were used. The agarose pad was inoculated with 1µl of the culture and dried. A coverslip was placed on top of the cells, followed by a rubber gasket and another metal slide. The metal slides were screwed together to maintain an anaerobic environment during the imaging process.

Imaging was conducted using a phase contrast microscope (Olympus IX71 with Cool SNAP HQ² Photometrics) equipped with fluorescent filters. Each culture was imaged with both dyes: Coral and AmberNP. For images taken with the Coral dye, the cells were excited with a 516 nm light for 0.5 seconds which will then be emitted in 600nm. For images taken with the AmberNP dye, the cells were excited with a 505nm light for 1 second which will then be emitted in 559nm. The difference for the excitation time is due to the 2-fold difference in the quantum yield between the two dyes. To ensure the dyes work as advertised, the FAST tag was attached

to PilT, a known cytoplasmic protein, and exposed to both dyes. The permeable dye (Coral) was able to pass through the cell membrane and bind to PilT-FAST (Figure 9). However, the impermeable dye (AmberNP) was unable to do so (Figure 9).

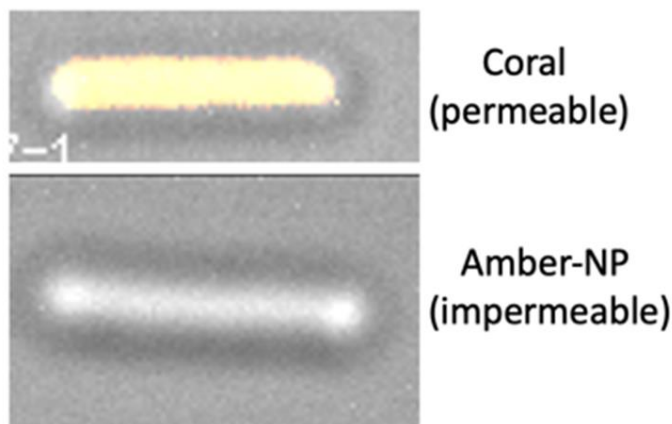


Figure 9. Controls for Coral and Amber-NP dyes. A FAST protein was fused to PilT, a known cytoplasmic protein, and exposed to the two dyes. The permeable coral dye passed through the membrane and bound to the FAST protein, shown by fluorescent signal. The impermeable amber-NP dye did not pass through the membrane and could not bind to FAST.

Image analysis was conducted using a program called superSegger-omnipose.

superSegger-omnipose conducts accurate cell segmentation and extracts the mean pixel intensity (MPI) for each cell within a frame. The background for each image was collected by selecting regions of known background and measuring its MPI. Each frames cell values were subtracted by the corresponding background MPI. Data was analyzed and graphed using a program called Prism9 GraphPad.

If membranes are leaky, the AmberNP dye can enter the cell and bind to the FAST protein. To determine the number of cells that are super fluorescent due to having a compromised membrane, both cultures were imaged with a live-dead stain. Cells were imaged using the same rose chamber method as described above. However, instead of incorporating AmberNP or coral dye, a mixture of propidium iodide and SYTO 9 nucleic acid stain were added

to the molten 1% TY agarose pad. The SYTO 9 nucleic acid stain stained living cells green since it is membrane permeable. The propidium iodide stained dead cells red since it cannot pass through the cell-membrane to bind to nucleic acids unless the membrane is compromised. Cells were imaged every minute for 1 hour. The excitation/emission for the SYTO 9 and propidium iodide strains are 488nm/515nm and 570nm/602nm.

Inclusion of TpeE-FAST and TpeL into pKRAH erm

To determine if it is necessary for *tpeE* and *tpeL* to be adjacent in the construct, a new construct was made to include both *tpeE* and *tpeL* in pKRAH erm. To do so, a ClonExpress Ultra One Step Cloning Kit from VAzyme was used, which uses a Gibson assembly like mechanism. Using VAzyme's primer design tool, primers were designed to flank the 5' and 3' ends of *tpeE*-FAST and *tpeL*-His₆. Another set of primers corresponds to the desired cloning region of the vector. Along with targeting each fragment, each primer contained an overhang that will be complimentary to the overhang of another. The primers will bind as such: the reverse primer of the vector is complimentary to the forward primer of *tpeE*-FAST, the reverse primer of *tpeE*-FAST is complimentary to the forward primer of *tpeL*, and the reverse primer of *tpeL* is complimentary to the forward primer of the vector.

The DNA templates for *tpeE*-FAST, *tpeL*, and pKRAH-erm underwent a polymerase chain reaction (PCR) using the primers stated previously and the 2x Phanta Flash master mix contained in the VAzyme cloning kit. The PCR parameters are as such: initial denaturation was at 98°C for 30 seconds, denaturation was 98°C for 10 seconds, annealing was at 45°C for 5 seconds, extension will be at 72°C for 5 seconds/kb, and the final extension will be at 72°C for 1 minute. Fragments were identified by size as such: *tpeE*-FAST is ~700 bp, *tpeL* is ~6,000 bp,

and pKRAH erm is ~8,900 bp. The fragments were purified using Thermo Scientific's GeneJET gel extraction kit.

The purified fragments underwent a Gibson-like homologous recombination for assembly of the circularized plasmid. For multi-fragment homologous recombination, each fragment was added to 2x ClonExpress mix and water. The concentrations of each fragment added followed a 1:1:1 ratio (*tpeE*-FAST: TpeL: pKRAH erm) to decrease efficiency and receive a countable number of colonies after electroporation. The mixture was incubated at 50°C for 15 minutes and immediately iced. After recombination, the mixture was transformed via electroporation and screened for insertions using the previously described electroporation method.

Biotinylation of Cell-Surface Proteins

The biotinylation of cell-surface proteins was used as an alternative method to determine if the holin undergoes a hinge-like motion in the presence of the toxin. The method used in this chapter was derived from a previous publication on the enrichment of cell-surface proteins in *Bacillus subtilis* [81]. This study used two cell-impermeant biotin labeling reagents: Sulfo-NHS-LC-LC-Biotin (amine reactive) and Maleimide-Peg2-Biotin (sulfhydryl reactive). To conduct the biotinylation, cultures that expressed TpeE and/or TpeL were induced with lactose as previously described in the secretion methods. The optical density of each was measured to ensure that cell concentrations were similar. The cultures were then centrifuged to separate the pellet and the supernatant (3,500 rpm for 5 minutes). Cell pellets were then washed with DPBS and then resuspended in 1ml of DPBS. To add the biotin labeling reagent, 1mg of either the sulfhydryl reactive or the amine reactive reagent was dissolved in 100µl of DPS and added to each sample. The cells were then continuously inverted at 4°C for 1 hour. The cells were then

washed 3 times in DPBS/500mM glycine (amine reactive) or 6 times with DPBS (sulfhydryl reactive) to ensure that all excess biotin had been removed. Cells were then lysed and prepped for SDS-page electrophoresis as described previously in the secretion methods. After separation, proteins were transferred to a polyvinylidene membrane and blocked for 5 minutes with 20mls of Every Blot Blocking Buffer (BioRad). To visualize biotinylated proteins, streptavidin was diluted in the same 20ml Every Blot Blocking Buffer and added to the membrane for 1 hour at room temperature. Samples were imaged with the StainFree and IR800 filters on the Bio-Rad ChemiDoc MP imaging system. Membrane fractions were separated via ultracentrifugation (45,000 rpms, 4° C, 1 hr) and imaged using the same method.

Sequencing

Each culture was checked to ensure the cloned fragments are in the correct reading frame via Sanger sequencing. Each fragment underwent PCR using primers that target specific regions of the genes. PCR products were checked for their size by gel electrophoresis and purified, using ddH₂O for the final elution. Purified PCR products were diluted to the proper concentrations (ng/μl) based on the length of the fragment. Primers were diluted to 3.2 pm/μl and then added to 10μl of the prepped DNA template for a total volume of 13 μl. Samples were sent to Virginia Tech's Genomic Sequencing center for sequencing. Sequences were viewed using SnapGene. The open reading frames of each sample were analyzed using an ORF finder application.

Results:

Growth of HN13 with TpeE-FAST

Three growth curves each were conducted on strain HN13, a TpeE, a TpeE-FAST, and a TpeE-FAST and TpeL-His₆ culture. As expected from previous growth curves, the HN13 and

TpeE cultures exhibited normal growth rates and similar bacterial yields (Figure 10). However, both cultures that contained the TpeE-FAST, although similar to each other, exhibited much slower growth rates and lower bacterial yields when compared to the HN13 and TpeE cultures (Figure 10). This suggests that attaching the FAST to TpeE may cause the holin to perform an interaction that it does not commonly do. We currently have not tested the exact reason as to why the FAST would affect the function of TpeE. However, we believe that the FAST tag may be causing TpeE to aggregate in the cell-membrane, which may cause the cells to become leaky.

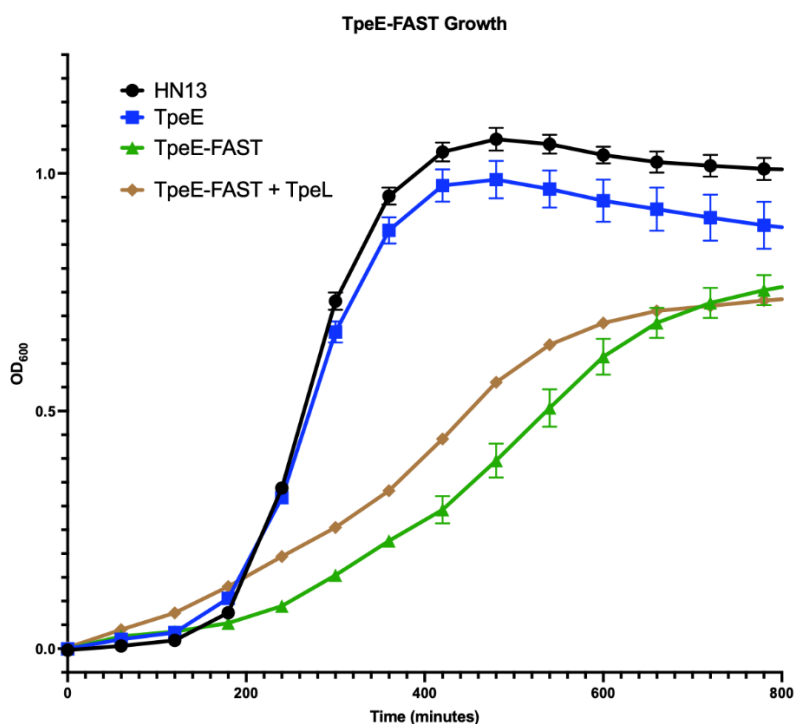


Figure 10. Expression of *tpeE-FAST* in *C. perfringens* strain HN13 negatively affects its growth rate. HN13 (control) in black; TpeE in blue; TpeFAST in brown; TpeEFAST-TpeL in green. Each strain was induced with lactose (20mM). Measurements were taken every 3 minutes for 24 hours. Mean and SEM were calculated from 6 replicates for each timepoint.

Secretion

Strains containing TpeE-FAST and TpeL were tested for secretion via western blotting. Along with the TpeE-FAST and TpeL strain, a cultures containing TpeL-alone, a TpeE-alone, and a wildtype culture containing TpeE and TpeL were used as controls. For both the TpeE only and TpeL control, TpeE and TpeL were detected only within the whole-cell lysate at approximately 15 kD and 250 kD, respectively (Figure 11). For the wildtype, TpeL was detected in both the whole-cell lysate and the supernatant (Figure 11). These results were as expected since a previous paper demonstrated that TpeL requires TpeE for secretion [13]. For the TpeE-FAST and TpeL culture, TpeL-His₆ was detected in both the whole-cell lysate and supernatant fractions, suggesting that attaching the FAST to TpeE does not inhibit the secretion of TpeL (Figure 11). Densitometry to compare pellet and supernatant fractions was conducted on three replicates (Figure 12).

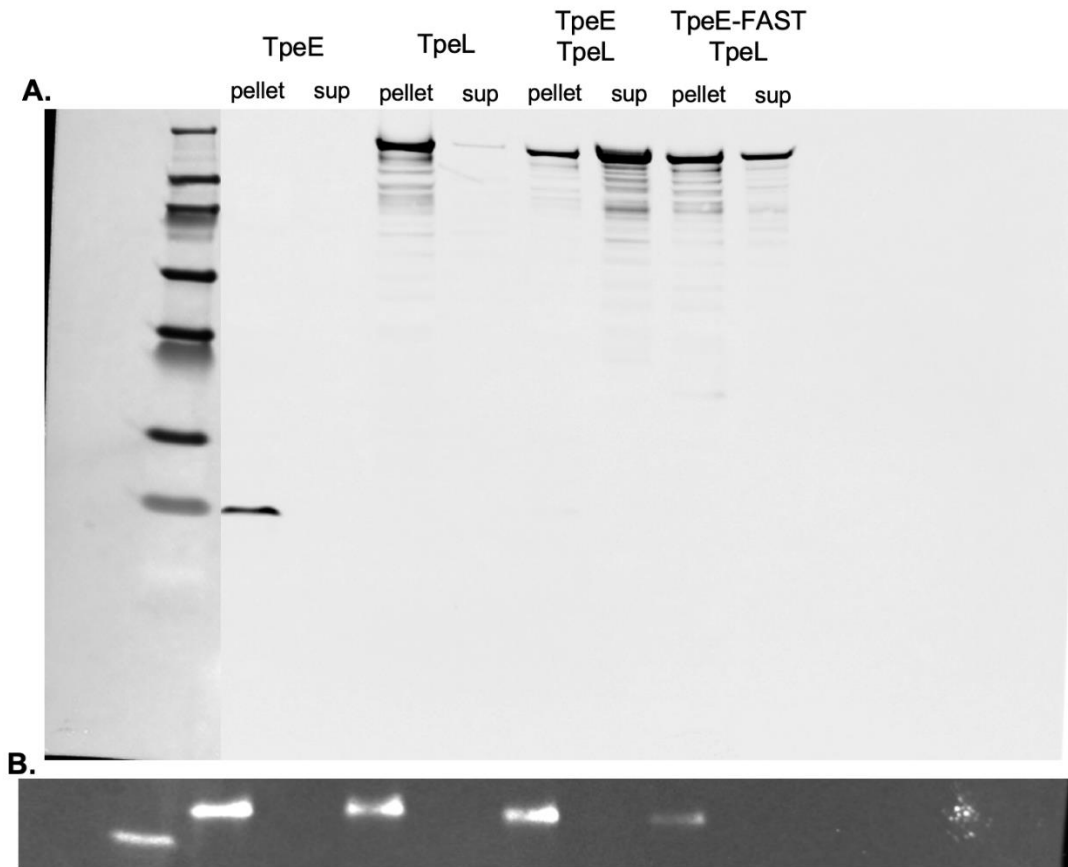


Figure 11. (A)Western blot showing detection of His6-tagged TpeE and TpeL. Lane 2-3: TpeE pellet and supernatant; Lane 4-5: TpeL pellet and supernatant; Lane 6-7: TpeE-TpeL pellet and supernatant; Lane 8-9: TpeEFAST-TpeL pellet and supernatant. Cultures were grown for 5-6 hours and induced with 20mM lactose for the first 2 hours. **(B)**Each sample was checked for lysis using streptavidin which will bind to BCP, a known cytoplasmic protein in *C. perfringens*.

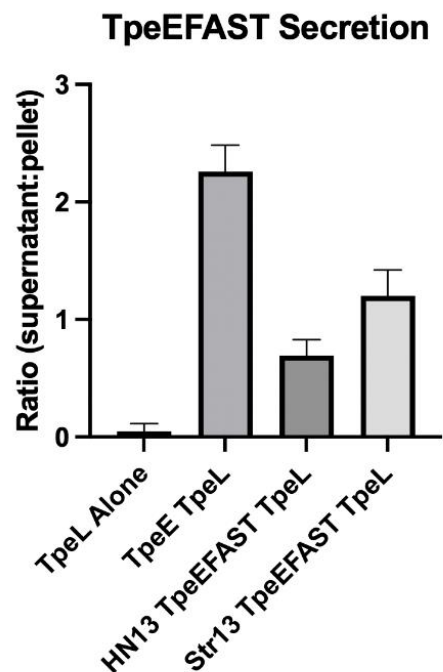


Figure 12. TpeE-FAST Secretion Densitometry. This graph depicts the secretion efficiency of TpeL only (HN13), TpeE TpeL WT (HN13), TpeE-FAST TpeL (HN13), and TpeE-FAST TpeL (Strain 13). Secretion efficiency was calculated by mapping out the mean pixel intensity for both the supernatant and whole-cell pellet fractions, calculating the area underneath intensity peaks, and comparing supernatant:pellet. This suggests that the FAST tag effects secretion efficiency but does not completely inhibit secretion of TpeL.

Fluorescence Microscopy

To test the hinge-like motion depicted in our secretion model, TpeE-FAST cultures in both the presence and absence of the toxin were imaged with either a membrane permeable dye (Coral) or an impermeable dye (AmberNP). For both TpeEFAST only and TpeEFAST-TpeL cultures, the Coral dye was able to pass through the cell-membrane and bind to FAST. This resulted in an overall increase of mean pixel intensity (MPI) over time during induction (Figure 13). The results shown are an accumulation of several movies for each condition (Figure 13).

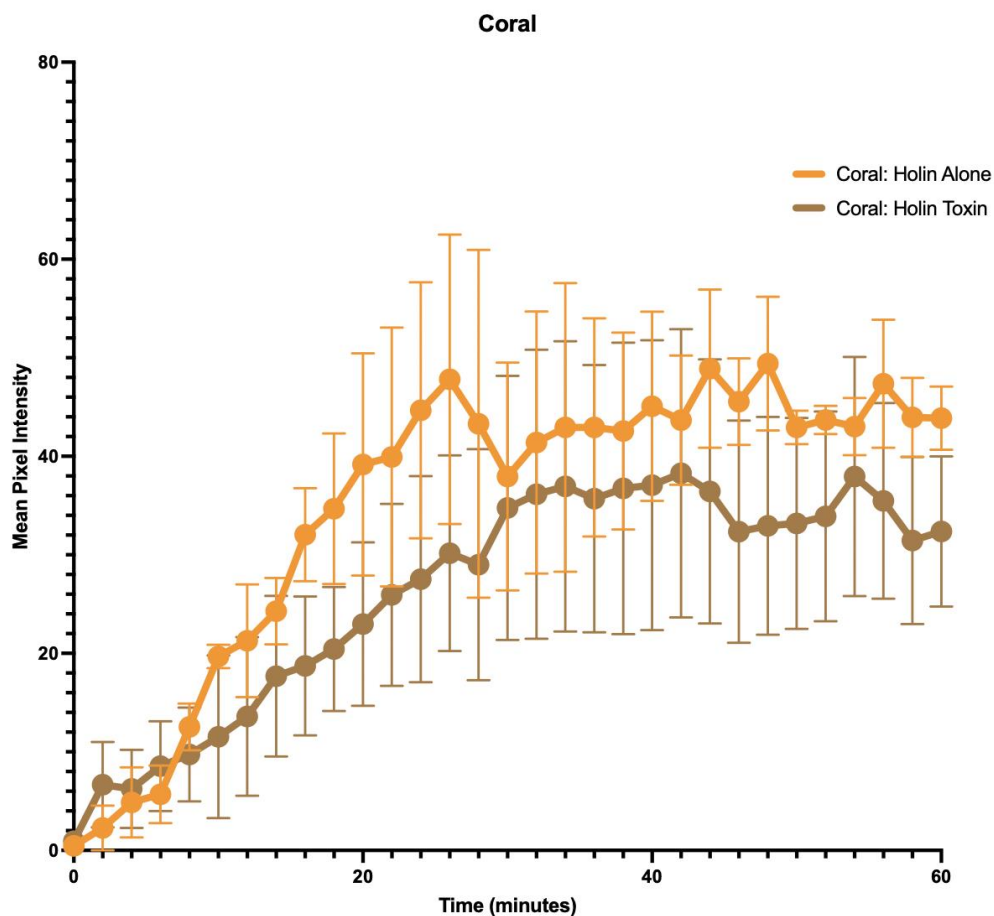


Figure 13. Fluorescence of TpeE-FAST using the coral dye. Cells were imaged every 30 seconds to create a 1-hour movie. Excitation: 516nm light for 0.5 seconds every frame; Emission: 600nm. As expected, the coral dye is capable of binding to FAST in the absence of TpeL. Both strains resulted in a relatively high signal when compared to the amberNP dye. There is an interesting trend for the TpeEFAST and TpeL co-expression strain where the mean pixel intensity (MPI) increases over time. However, in the TpeEFAST only strain, MPI seems to fluctuate along a flat line.

For the TpeE-FAST only culture, the average AmberNP fluorescent signal was close to zero (Figure 14). For the culture that contained TpeE-FAST and TpeL, the average AmberNP fluorescent signal was slightly higher than the holin alone culture. Although, the results do not indicate an overall increase in MPI over time (Figure 14).

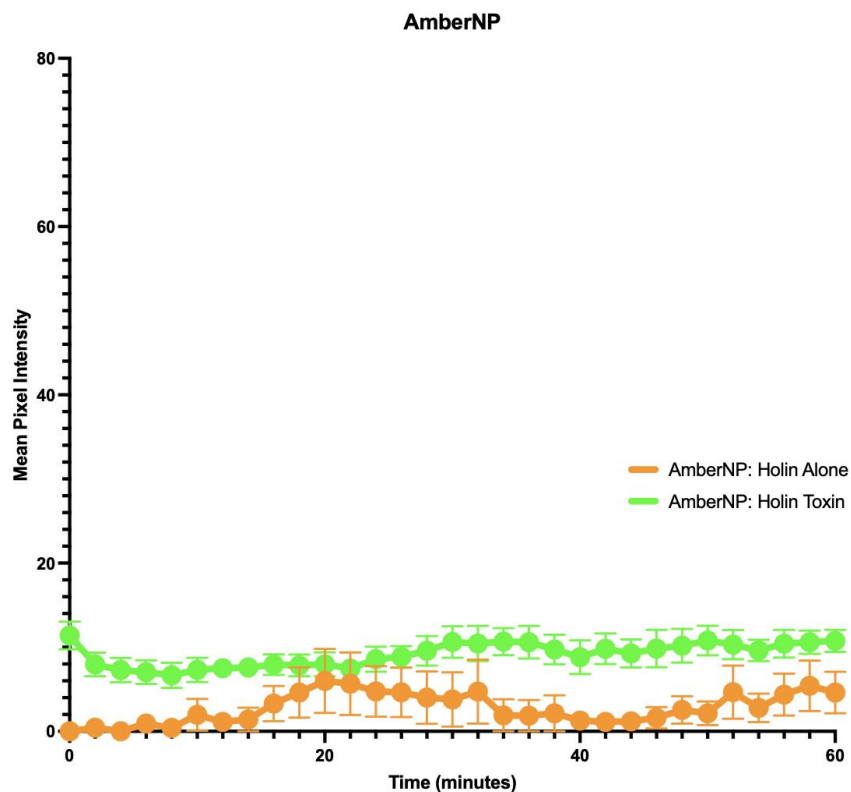


Figure 14. Fluorescence of TpeE-FAST using the amberNP dye. Cells were imaged every 30 seconds to create a 1-hour movie. Excitation: 505nm light for 1 second every frame; Emission: 559nm. The amberNP dye resulted in a very low signal in both the TpeE-FAST only strain and the TpeE-FAST+TpeL co-expression strain. This may be due to the amount of FAST that is exposed to the outside of the cell.

Live Dead Cell Imaging of HN13 with TpeE-FAST

To visualize if the expression of TpeE-FAST compromises the integrity of the cell-membrane in HN13, SYTO 9 and propidium iodide dyes were used to stain live and dead cells for a culture containing *tpeE*-FAST in the presence/absence of the inducing agent, lactose (Figure 15). Live cells will fluoresce green due to the membrane permeable SYTO 9 dye, whereas dead cells, with their membrane being compromised, will fluoresce red due to the membrane impermeable propidium iodide dye. For cultures in the absence of the inducing agent, there were no major qualitative differences between timepoints (Figure 15A). For cultures in the

presence of the inducing agent, there were no major qualitative difference observed between timepoints (Figure 15B). Images shown are representative of two movies.

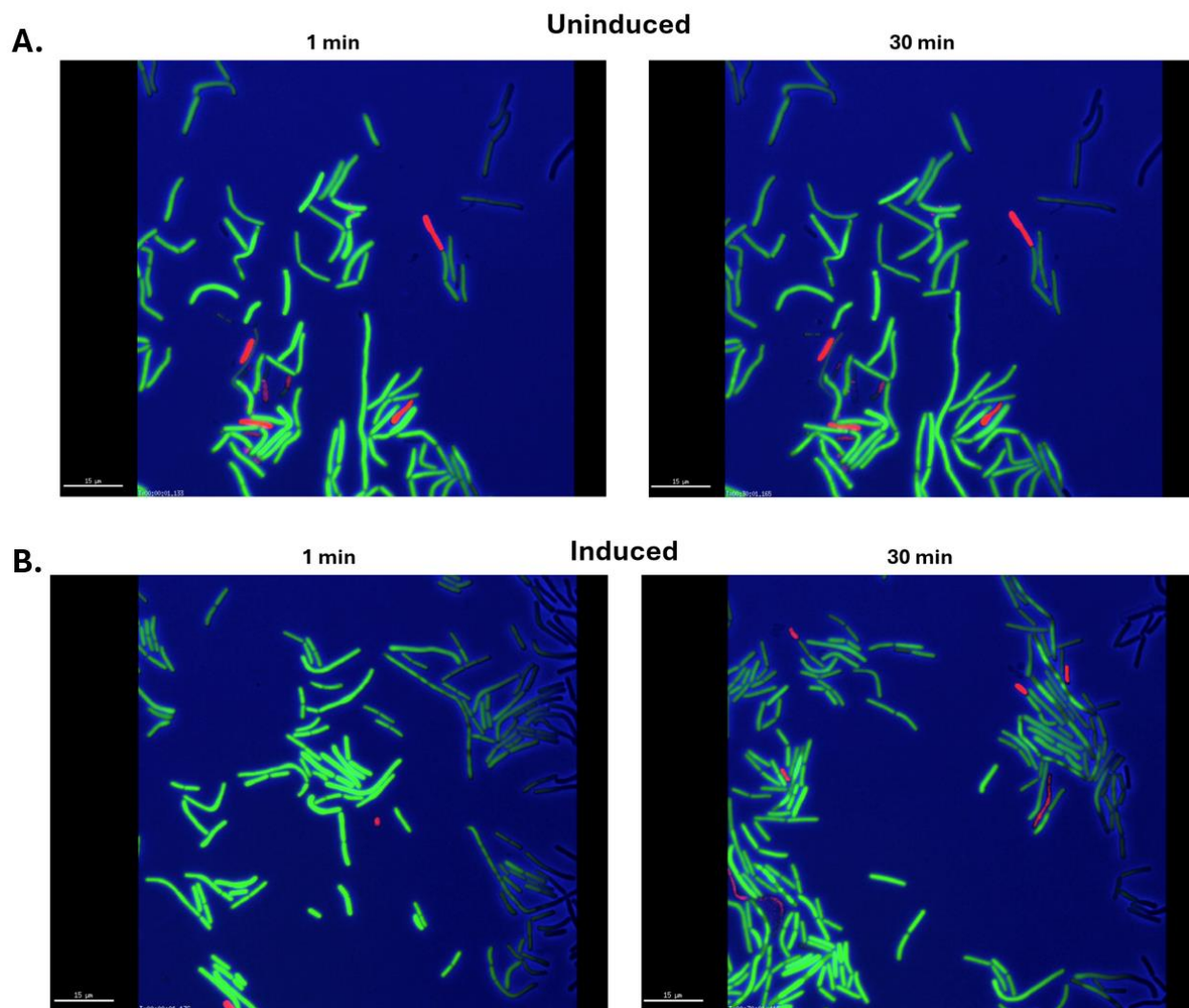


Figure 15. Live Dead Cell Imaging of HN13 expressing TpeE-FAST. Cultures containing pNF1 were imaged every minute for 30 minutes using the SYTO 9 and propidium iodide stains. Live cells will appear green, whereas dead cells will appear red. **(A)** Cultures that were uninduced (will not express high levels of TpeE-FAST) had no qualitative differences between timepoint 1 and 30. **(B)** Cultures that were induced with lactose had no qualitative difference between each timepoint as well. Two movies were conducted for each.

Growth of Strain 13 with TpeE-FAST

Due to inconclusive results, Strain 13 was used to confirm fluorescent results. The growth of Strain 13 cultures containing TpeE-FAST with and without the toxin were measured during induction. As expected from previous growth curves, Strain 13 exhibited a normal growth rate with a healthy bacterial yield (Figure 16). However, both cultures that contained the TpeE-FAST, although similar to each other, still exhibited slower growth rates but on average have a higher bacterial yield than HN13 cultures previously tested (Figure 10 & 16). This suggested that Strain 13 may be able to handle the expression of TpeE-FAST more so than HN13.

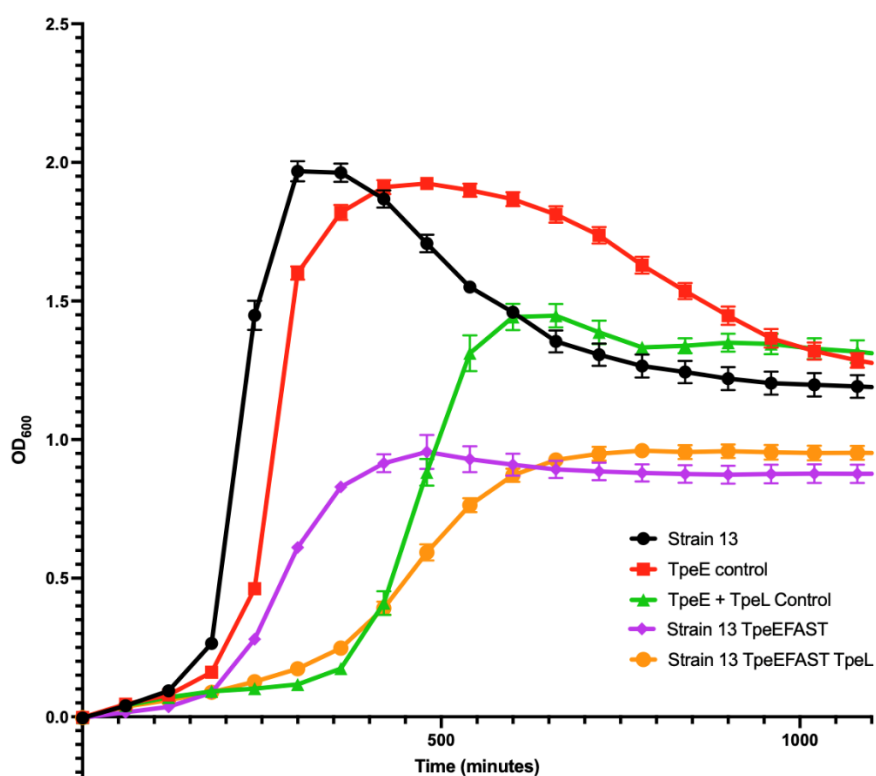


Figure 16. Expression of *tpeE-FAST* in *C. perfringens* Strain 13 negatively affects its growth rate. Strain 13 (control) in black; TpeE alone in red; TpeE + TpeL in green; TpeE-FAST + TpeL in purple; and TpeE-FAST + TpeL in orange. Each strain was induced with lactose (20mM). Measurements were taken every 3 minutes for 24 hours. Mean and SEM were calculated from 6 replicates for each timepoint.

Secretion of TpeL: Strain 13 with TpeE-FAST

Strain 13 cultures containing TpeE-FAST and TpeL-His6 were tested for secretion via western blotting as described previously. Along with the TpeE-FAST and TpeL cultures, a wildtype culture containing TpeE and TpeL-His6 was used as a control (Figure 17). For the TpeE-FAST and TpeL cultures 1.1 and 1.2, TpeL-His6 was detected in both the whole-cell lysate and supernatant at ~200kD, suggesting that attaching the FAST to TpeE does not inhibit the secretion of TpeL in Strain 13 (Figure 17). Comparative densitometry was conducted to determine secretion efficiency. This showed that on average Strain 13 TpeE-FAST cultures could secrete at a higher efficiency than HN13 cultures (Figure 12).

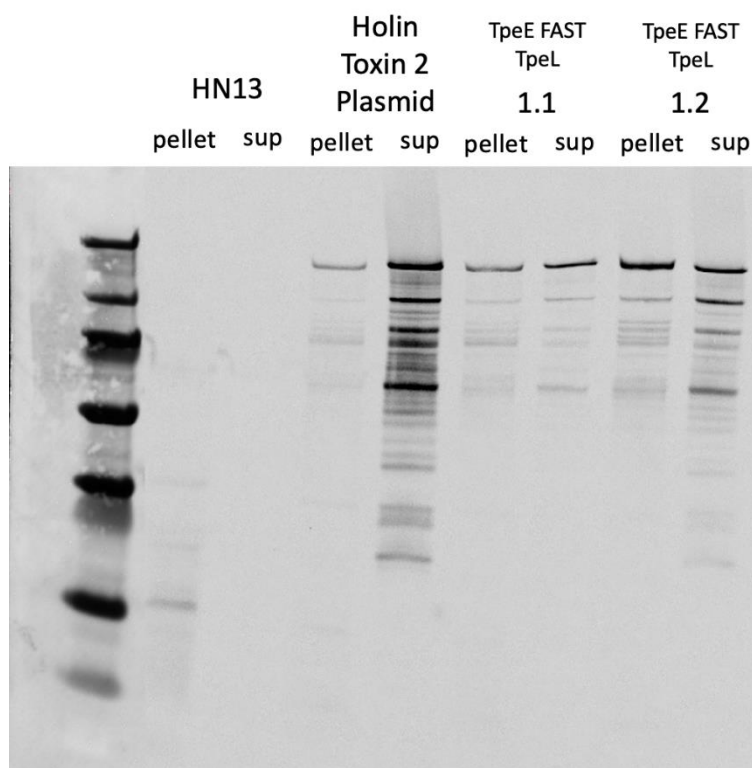


Figure 17. Western blot showing detection of His6-tagged TpeL. TpeL-His6 was detected in the whole-cell extract and supernatant for cultures 1.1 and 1.2, suggesting that the FAST fusion does not inhibit TpeL secretion in Strain 13. Cultures were grown for 5-6 hours and induced with 20mM lactose for the first 2 hours.

Fluorescence Microscopy of Strain 13 with TpeE-FAST

To test the hinge-like motion depicted in our secretion model, Strain13 cultures containing TpeE-FAST were imaged with either a membrane permeable dye (Coral) or an impermeable dye (AmberNP). Unfortunately, for both TpeE-FAST alone and TpeE-FAST toxin cultures, there was no observed change in fluorescence for either the coral or amberNP dye, suggesting that strain 13 did not express the FAST tag (Figure 18 & 19). These results were replicated several times with various concentrations of lactose. A fluorescence microscopy was conducted on a mixed sample of TpeE-FAST and WT TpeE to examine expression. The cells expressing TpeE-FAST were undetectable in a mixed culture (Figure 20).

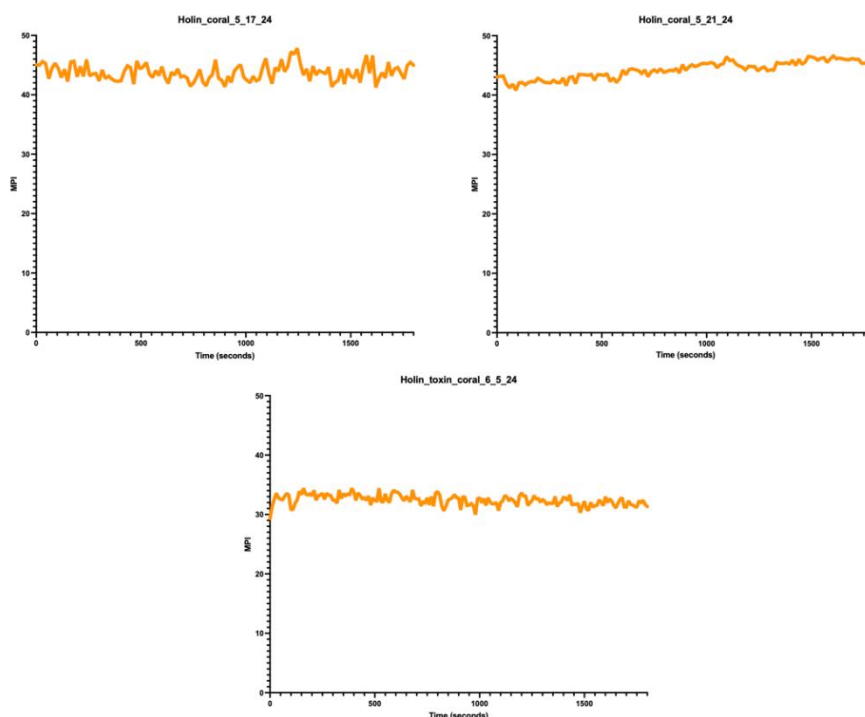


Figure 18. Fluorescence of TpeE-FAST using coral dye. Cells were imaged every 30 seconds to create a 1-hour movie. Excitation: 516nm light for 0.5 seconds every frame; Emission: 600nm. For both Holin alone and Holin Toxin cultures, mean pixel intensity did not increase overtime. With further analysis of each movie taken, it was determined that strain 13 was not expressing the FAST tag.

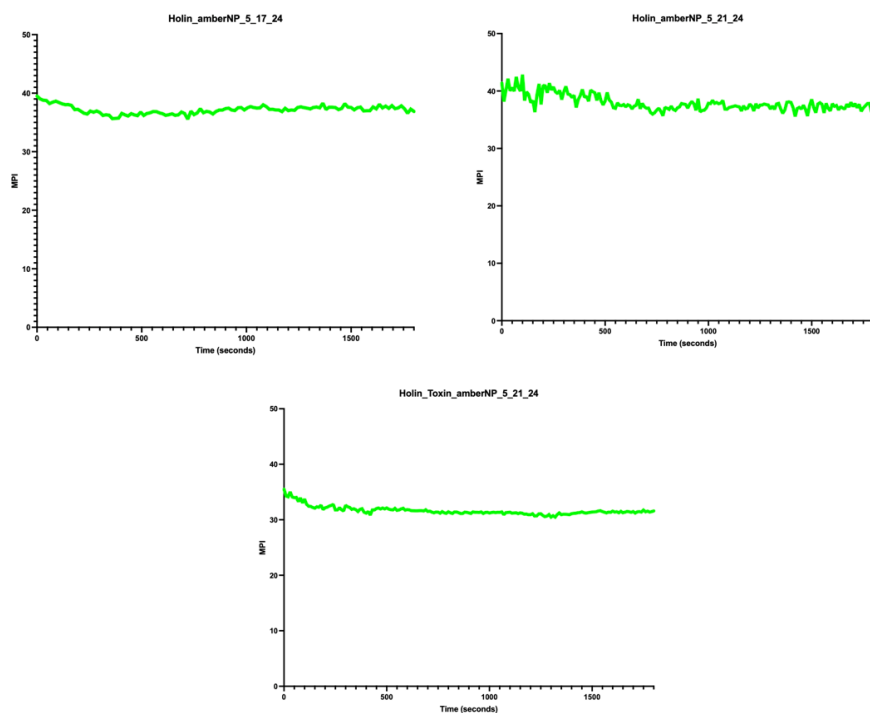


Figure 19. Fluorescence of TpeE-FAST using amberNP dye. Cells were imaged every 30 seconds to create a 1-hour movie. Excitation: 505nm light for 1 second every frame; Emission: 559nm. For both Holin alone and Holin Toxin cultures, mean pixel intensity did not increase overtime. With further analysis of each movie taken, it was determined that strain 13 was not expressing the FAST tag.

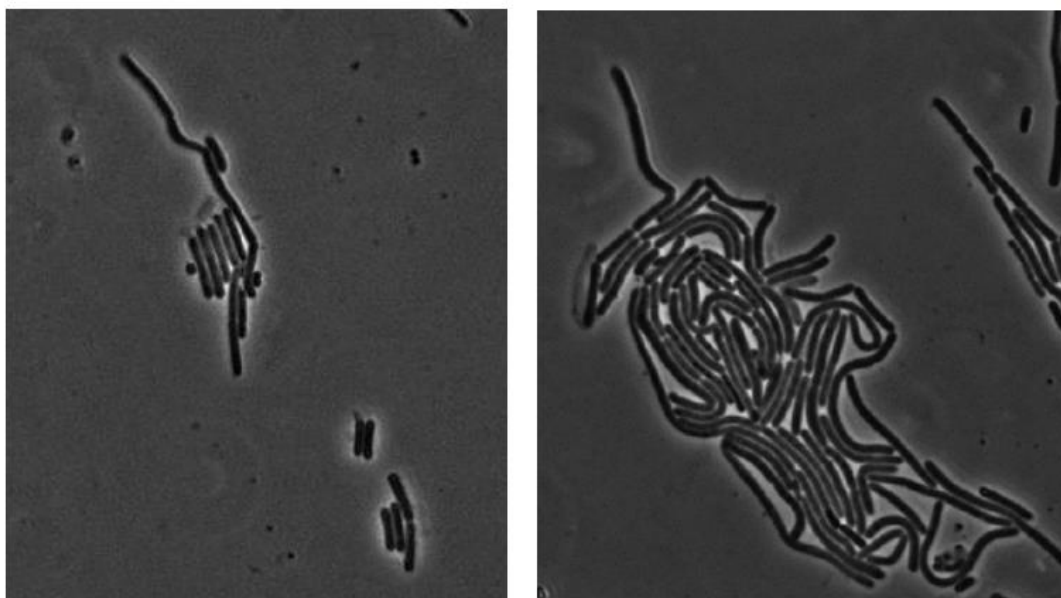


Figure 20. Fluorescent imaging conducted on a mixed culture of TpeE-FAST and TpeE WT. Cells expressing TpeE-FAST are indistinguishable from cells with no FAST tag. This suggests that Strain 13 TpeE-FAST cultures were not expressing the fast tag.

Lysine Specific Biotinylation of Surface Proteins: Results

In this experiment, HN13, a holin only culture, toxin only culture, and a holin toxin culture were used to determine if the methods for cell-surface biotinylation were replicable in *C. perfringens*. After using the amine reactive biotinylating agent, cell-surface proteins with exposed lysine residues were labelled, separated, and visualized. For each sample, cell-surface biotinylated proteins were successfully detected using streptavidin (Figure 21). Intriguingly, for samples containing the toxin, detection of a large protein (~250kD) was consistently labeled which was later confirmed to be TpeL, using mass spectrometry and visualization using anti-His₆ antibodies (Figure 21).

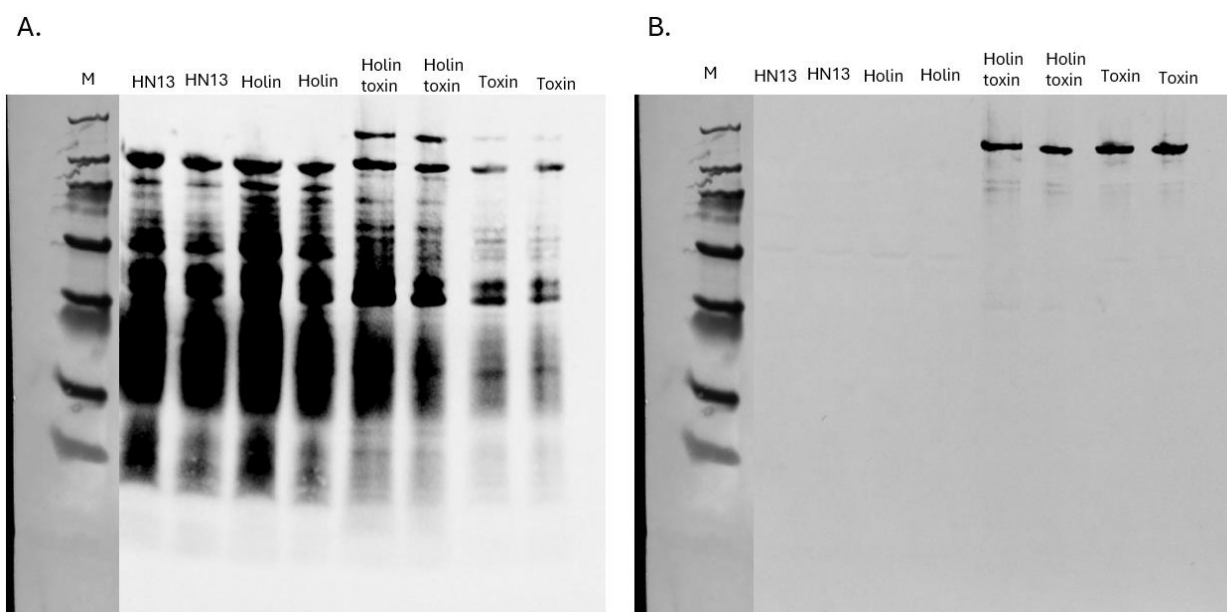


Figure 21. (A) Western blot showing the detection of biotinylated proteins within the whole-cell extract using the lysine reactive biotinylating reagent. For each of the samples, biotinylated cell-surface proteins were successfully detected. Unexpectedly, TpeL-His₆ was biotinylated and detected, **(B)** which was confirmed via probing for a His₆ tag and mass spectrometry. Proteins were visualized using fluorescently labelled streptavidin.

Growth of TpeE Cys Mutants

The expression of all 4 mutants (S3C, N65C, N60C, and K59C) had a negative effect on the growth rate of HN13 when compared to the expression of TpeE WT (Figure 22). However,

the overall bacterial yield was similar across all cultures (Figure 22). For holin-toxin cultures, the expression of mutant TpeE still had a negative effect on the growth rate of HN13 but behaved similarly to the expression of TpeE-TpeL two plasmid control (Figure 23).

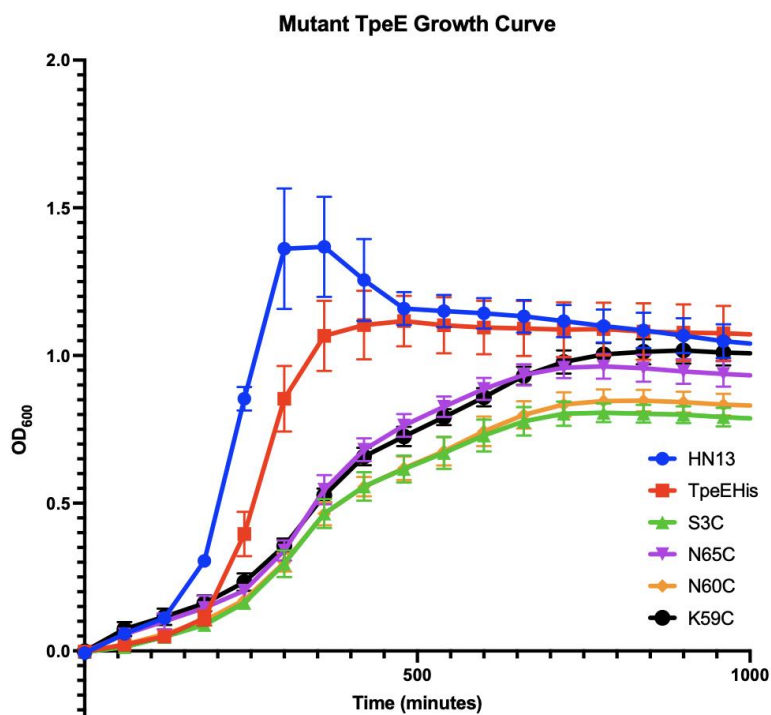


Figure 22. Growth of HN13 cultures expressing mutant TpeE in the absence of the toxin: HN13 (Blue), TpeE-His (Red), S3C (Green), N65C (Purple), N60C (Orange), and K59C (Black). This depicts that expression of mutant TpeE has a negative effect on the growth rate of HN13. Cultures were induced with 20mM lactose with a starting dilution of 1:100. OD₆₀₀ was measured every 3 minutes. This graph is representative of 3 replicate curves.

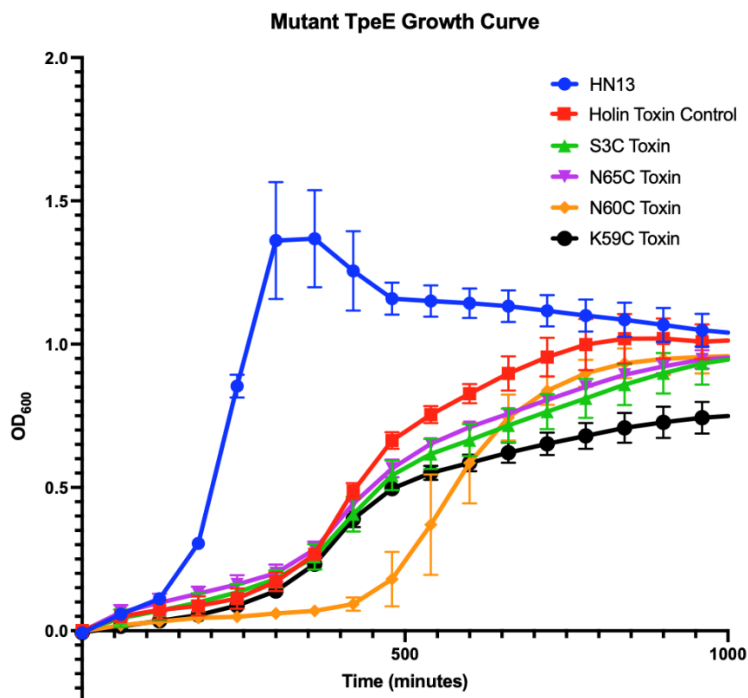


Figure 23. Growth of HN13 cultures expressing the mutant TpeE in the presence of TpeL: HN13 (Blue), Holin Toxin (Red), S3C Toxin (Red), N65C Toxin (Purple), N60C Toxin (Orange), and K59C Toxin (Black). This shows that expression of the mutant TpeE in the presence of the toxin has a negative effect on the growth rate of HN13. OD₆₀₀ was measured every 3 minutes. This graph is representative of 3 replicates.

Secretion: TpeE Mutants

In this experiment, cysteine residues were substituted in the N-terminus and C-terminus of TpeE and subsequently expressed in *C. perfringens*. Cultures containing mutant TpeE and TpeL-His6 were tested for secretion via western blotting as described previously. Alongside the mutant cultures, a holin toxin culture was ran as a control for TpeL-His6 secretion. For the control, TpeL-His6 was detected in both the whole-cell lysate and the supernatant (Figure 24). For the mutant TpeE and TpeL cultures, TpeL-His6 was detected in both the whole-cell lysate and supernatant at ~200kD, suggesting that mutant TpeE can facilitate secretion of TpeL (Figure 24 and 25).

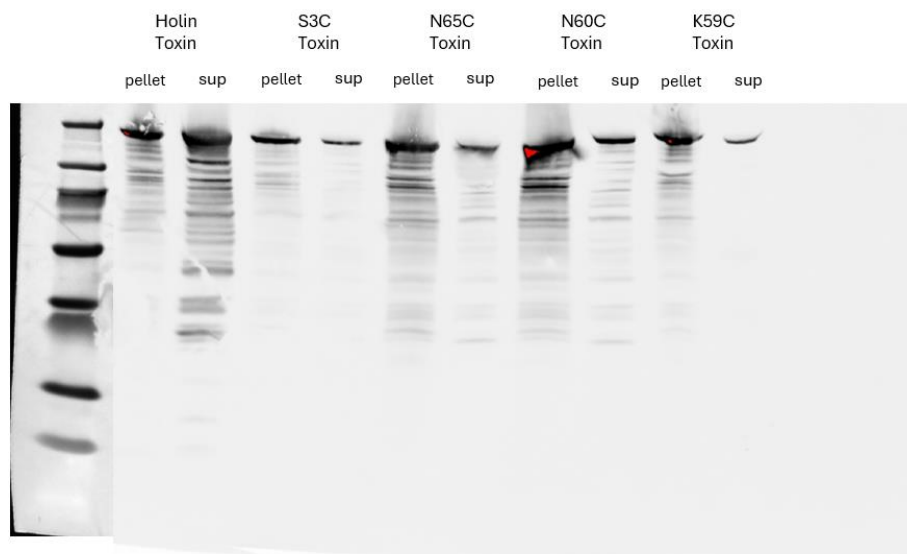


Figure 24. Western blot showing detection of His6-tagged TpeL. For each culture containing mutant TpeE and TpeL-His6, TpeL was detected in both the whole-cell lysates and supernatants, suggesting that mutant TpeE was able to facilitate secretion of TpeL. Cultures were grown for 5-6 hours and induced with 20mM lactose for the first 2 hours.

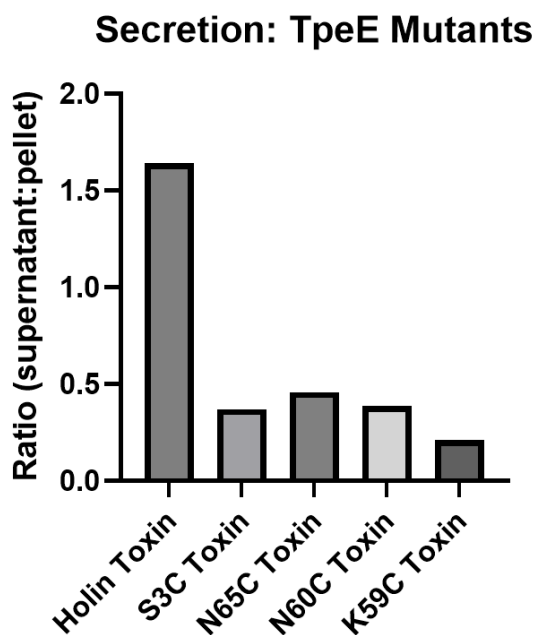


Figure 25. Cys mutant TpeE Secretion Densitometry. This graph depicts the secretion efficiency of Holin Toxin WT, S3C Toxin, N65C Toxin, N60C Toxin, and K59C Toxin in HN13. Secretion efficiency was calculated by mapping out the mean pixel intensity for both the supernatant and whole-cell pellet fractions, calculating the area underneath intensity peaks, and comparing supernatant:pellet. This suggests that the mutations effect secretion efficiency but do not completely inhibit secretion of TpeL.

TpeE Mutants: Biotinylation

In this experiment, mutant TpeE with and without the toxin were expressed and subjected to cell-surface biotinylation using a sulfhydryl reactive biotin reagent to test the hinge-like motion of TpeE. After biotinylation, cell-surface proteins with exposed cysteine residues were labeled, separated, and visualized. For each sample, cell-surface proteins were successfully labeled and visualized (Figure 26). However, for samples containing mutant TpeE, there was no detection of biotinylated TpeE in the presence or absence of the toxin (Figure 26). This experiment was conducted several times with increasing durations of induction to try and visualize TpeE, but each attempt failed. Membrane fractions were separated following biotinylation and visualized using the same method, yielding similar results (Figure 27).

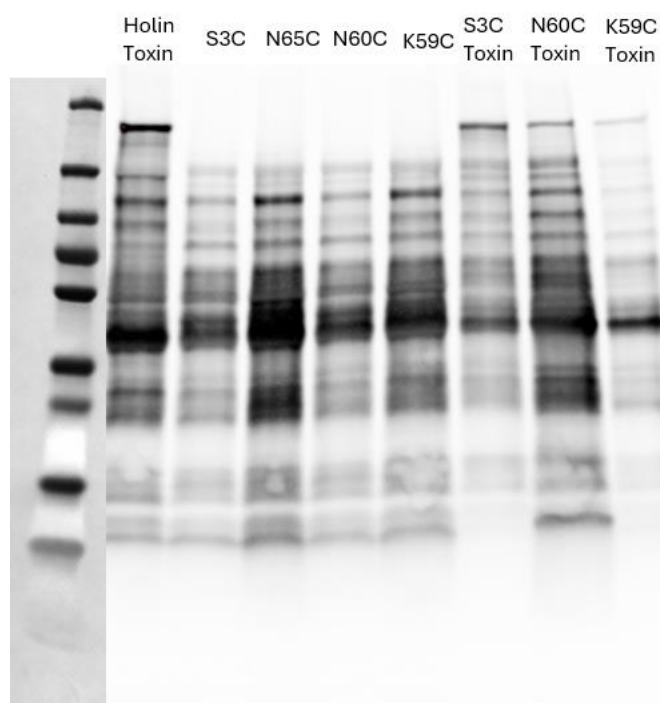


Figure 26. Western blot showing the detection of biotinylated proteins within whole-cell extracts using the cysteine reactive biotinylating reagent. For each of the samples, biotinylated cell-surface proteins were successfully detected including TpeL-His6. However, mutant TpeE was unable to be visualized. Proteins were visualized using streptavidin.

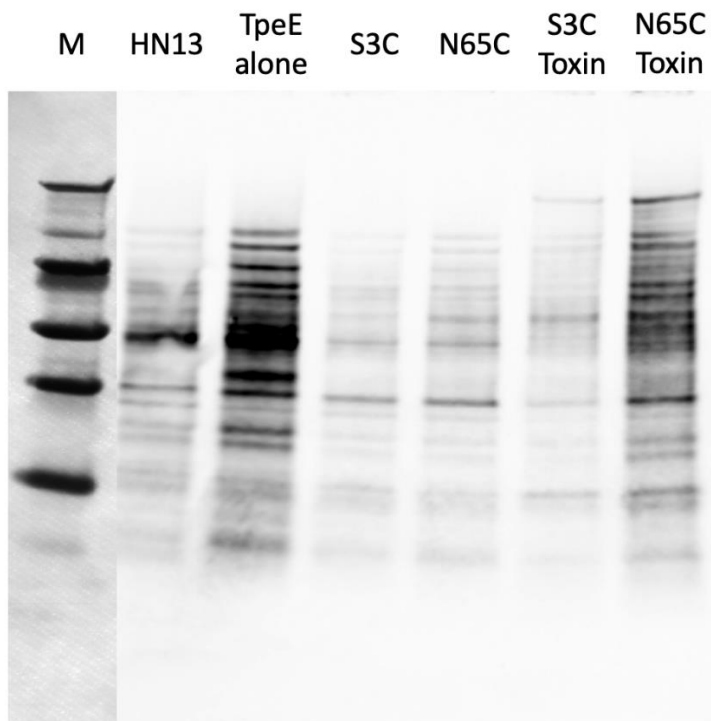


Figure 27. Western blot depicting the detection of cell-surface biotinylated proteins with membrane fractions of TpeE mutants, using a cysteine reactive biotinylating reagent. In each sample, proteins were successfully biotinylated and visualized, including TpeL on holin-toxin cultures. However, it cannot be determined if mutant TpeE is being biotinylated in either the presence or absence of the toxin.

Discussion:

It was hypothesized that TpeE may follow a similar secretion method as the proposed pore-forming Tat-secretion model [13]. This proposed model for TpeE-dependent secretion stated that in the presence of the toxin, the holin will oligomerize and flip its amphipathic helix into the cell-membrane to form a pore that will facilitate secretion (Figure 6) [13]. This model was later reviewed based on recent developments on the Tat-secretion model, which similar aspects of the previous secretion model [37]. In this study, the ability of the amphipathic helix in TpeE to flip into the cell-membrane was tested using both FAST fluorescence and biotinylation technology.

For FAST fluorescence, a FAST tag was fused to the C-terminus of TpeE and exposed to a set of permeable (Coral) and impermeable (AmberNP) dye. In theory, if the amphipathic helix flips into the cell-membrane in the presence of the toxin, then, in a TpeE-FAST TpeL culture, the FAST will be exposed to the outside of the cell where it binds to both the Coral and AmberNP dye. Whereas in a holin-alone culture, the amphipathic helix should not flip, leaving the FAST within the cytoplasm where it will bind to only the Coral dye.).

Unfortunately, cultures expressing the TpeE-FAST fusion experienced a decrease in growth rate and overall bacterial yield when compared to HN13 and a TpeE WT culture (Figure 10). This suggests that the FAST tag may affect the stability of TpeE as it is inserted into the membrane, forming aggregates within the cell-membrane. Fluorescent live-dead and proton motive force stains were used to determine if the membrane integrity was compromised during expression, but induced and uninduced cultures behaved similarly. It is still unclear as to what the reasoning is for the decrease in overall growth, however it is thought that conclusive results could be derived if only comparing cultures expressing the FAST tag.

After determination of growth defects, the ability of the holin-FAST fusion to secrete the toxin was investigated using western blotting and densitometry. Anti-His₆ western blots detected TpeL-His₆ (~200 kD) for all TpeE-FAST cultures in both the whole-cell extract and supernatant fractions, suggesting that the FAST fusion does not inhibit secretion of the toxin (Figure 11). However, analysis by densitometry revealed a decrease in secretion efficiency when compared to the WT holin-toxin cultures (Figure 12). This suggests that the FAST affects the function of the holin but does not inhibit it. Since the FAST tag was not inhibiting secretion of TpeL, fluorescence imaging was conducted.

For the Coral dye, the MPI increased over time for both the holin alone and holin toxin culture throughout a 1-hour movie (Figure 13). This result is expected as the coral dye should pass through the cell-membrane and bind to all available FAST tags within the cytoplasm as well as any FAST exposed to the outside of the cell. For the AmberNP dye, the holin-alone culture results were as expected, having little to no fluorescent signal throughout 1-hour movie (Figure 14). However, for the holin-toxin culture, the MPI was slightly higher than the signal of the holin-alone culture, but no change in fluorescent signal over time was observed (Figure 14). This was not expected since it was believed that the MPI would increase as more holin and toxin would be produced. Although, there may be a mechanism that regulates the amount of toxin that gets secreted, affecting the rate at which the amphipathic helix will flip and expose the FAST tag.

Results on the growth and secretion efficiency of TpeE-FAST cultures were replicated using Strain 13. Each culture expressing the FAST tag experienced a slower growth rate when compared to Strain 13 and a TpeE WT culture (Figure 16). However, higher OD levels were detected in Strain 13 TpeE-FAST cultures when compared to HN13 expressing the FAST fusion (Figure 10 & 16). According to anti-His₆ western blots, TpeL-His₆ was detected in both whole-cell extracts and supernatants for each TpeE-FAST culture at a higher efficiency than HN13 cultures (Figure 12 & 17). This suggested that Strain 13 could handle the TpeE-FAST fusion more than HN13.

Unfortunately, fluorescence results were not replicated in Strain 13. For both Coral and AmberNP, the MPI did not increase for either the holin-alone or the holin-toxin culture (Figure 18 & 19). With further analysis of a mixed culture of TpeE-FAST and TpeE WT, it was found that the Strain 13 TpeE-FAST culture did not express the FAST tag (Figure 20). Strain 13 may

have modified the FAST fusion, which may also be a reasoning as to why Strain 13 was more stable during expression.

Since there was a possibility of the two-plasmid system causing adverse effects on expression and growth of the holin-toxin cultures, a one plasmid system was investigated. After multiple attempts, there were no clones isolated that possessed the correct sequence for both *tpeE*-FAST and *tpeL*. However, it is suggested that a one plasmid system may be beneficial as that is closer to the natural system and would limit the amount of antibiotic stress placed on the organism during expression.

Fluorescence results using HN13 suggested that the amphipathic helix may not flip in the presence of the toxin or *C. perfringens* may have a way to regulate the amount of toxin that gets secreted at one time. As an alternative to FAST Fluorescence, biotinylation technology was pursued.

Cell-surface biotinylation was conducted using a lysine specific biotinylating reagent to label all surface exposed lysine residues in membrane associated proteins in *C. perfringens*. This was done to confirm if cell-surface biotinylation was replicable in *C. perfringens* and could be applied to TpeE-dependent secretion of TpeL. Cell-surface proteins were in fact labeled with the amine specific reagent and visualized via western blotting using fluorescently labelled streptavidin (Figure 21). In addition to cell-surface proteins, a ~200 kD protein was consistently being labeled in holin-toxin cultures, which was later confirmed to be TpeL-His₆ through anti-His₆ western blots and mass spectrometry (Figure 21). This is consistent between holin-toxin and toxin-alone cultures, suggesting that TpeL can exit the cell-membrane at lower levels in absence of the holin (Figure 21). Due to large levels of labeling utilizing a lysine specific reagent, a

cysteine specific biotinylating reagent was used as a more targeted approach to studying the mechanism behind holin-mediated secretion.

Since TpeE has no native cysteine residues, amino acids in the N- and C-terminus were substituted for cysteine. Substitutions were made as conservatively as possible to ensure that the holin could fold and function properly, however selection was incredibly limited. Four substitutions in TpeE were made: S3C, K59C, N60C, and N65C. The goal behind this experiment was to visualize and later detect, through mass spectroscopy, differences in labeling for C-terminal mutations in the presence or absence of the toxin.

The ability for mutated TpeE to secrete the toxin was examined through detection of TpeL-His₆ in anti-His₆ western blots. TpeL-His₆ was detected in the whole-cell extracts and supernatants for each mutant (Figure 24). This suggests that the cysteine substitutions have not affected the holins ability to fold, insert in the membrane, and secrete the toxin.

Unfortunately, visualization of Cys-biotin labeled TpeE in whole-cell extracts was not possible in either the positive control (S3C) or experimental treatments (K59C, N60C, and N65C), due to a substantial amount of background noise from proteins of similar size (Figure 26). Membrane fractions were prepped after biotinylation, yielding similar results (Figure 27). Due to the inability to visualize biotinylated S3C TpeE, it is unclear whether it would be possible to visualize one biotin molecule for every holin present in any of the experimental samples. Varying levels of inducing agent concentrations, induction times, and biotinylation times were attempted to visualize biotinylated TpeE, but these attempts ultimately failed. Even if proper visualization of biotinylated TpeE were to occur, it was unclear whether detection of biotinylated residues would be possible since the identification of TpeL through mass spectrometry showed no detection of biotinylated residues. However, an interesting result worth investigating was the

consistent cell-surface labeling and visualization of TpeL in toxin alone cultures (Figure 21). This was also present in membrane fractions of mutant holin-toxin cultures, suggesting that TpeL will get secreted and may reassociate with cell-membrane (Figure 27).

Due to the inconclusive nature of the biotinylation results as well as the fluorescence results, it is suggested that TpeE-dependent secretion may not follow the proposed pore-forming model of Tat-secretion. However, it is important to highlight a critical flaw within the design of the experiments used to test this mechanism. This model states that a pore must be formed around the toxin to facilitate secretion. It is not well understood if the formation of this pore would be loose enough around the toxin to cause the cell-membrane to become compromised enough to allow small molecules from the environment to leak through it. The design of this experiment did not take this into account as the utilization of small molecules, such as fluorescent dyes and biotinylating reagents, were critical in this study and may have affected the results.

Several more recent studies have found evidence that Tat-secretion may follow a membrane destabilization secretion model [82]. This model switches that focus to the importance of the transmembrane helix length of TatA [83, 84]. It states that the estimated length of the TatA transmembrane helix (22.5 Å) is too short for the for the average lipid length of cell-membrane of *E. coli* (37.5 Å) [83]. In Chapter III, this model will be studied using TpeE-dependent secretion in *C. perfringens* as a model.

Chapter III

TpeE-Dependent Secretion of TpeL: Membrane Destabilization Model

Abstract

The Clostridia are anaerobic Gram-positive pathogens which cause numerous lethal diseases in humans and animals. All Clostridial pathogens secrete toxins as an essential aspect of their pathogenesis. One family of toxins are the large clostridial cytotoxins (LCT), which include TpeL from *C. perfringens* and TcdA/B from *C. difficile*. All LCTs lack a signal peptide for Sec-dependent secretion. However, the pathogenicity locus encoding each toxin gene also encodes a phage holin-like protein, TpeE for *C. perfringens*. Each toxin has been shown to be dependent on their cognate holin for secretion. Specifically, TpeE shares a similar membrane topology with the TatA protein, a key component of the Twin-Arginine Transport (Tat) secretion system while other holins are similar to the phage lambda holin. Our main hypothesis is that TpeE represents a novel and ubiquitous class of secretion proteins with features from both Tat and holin-like protein secretion systems. Recent publications on the Tat secretion system in *E. coli* suggests that the transmembrane helix of TatA plays more of a role in translocation than the amphipathic helix. This is due to the length of the transmembrane helix (TMH) of TatA being too short compared to the average lipid length in the cytoplasmic membrane, causing destabilization when recruited which facilitates translocation of the target protein. Due to previous results in our lab and recent findings for the Tat secretion system, we have developed a new model for TpeE-dependent secretion in which TpeL inserts into the cytoplasmic membrane signaling the oligomerization of TpeE which will destabilize the membrane and facilitate secretion. Several insertions and deletions in the TMH of TpeE were made to test this model via western blotting. Preliminarily, insertions in the TMH of TpeE seems to have a negative effect on their secretion efficiency without the detection of premature lysis, whereas the deletions seem to increase the likelihood of the cells to prematurely lysis before sample collection. These preliminary results support what is

currently understood in the membrane destabilization model. Molecular dynamics will be performed to help simulate what this mechanism may look like in *C. perfringens*.

Introduction:

As previously discussed, *C. perfringens* is the causative agent of both food poisoning and gas gangrene [85, 86]. Its ability to secrete approximately 20 toxins is key to its pathogenesis [87]. The large clostridial toxins (LCTs) are an example of one protein family that this organism can secrete [13]. As previously stated in Chapter II, each of these toxins have been associated with virulence in multiple hosts [70-72]. To do so, LCTs will shut down cell signaling, eventually leading to cell death, through the glycosylation of Rho family GTPases [70]. A common characteristic across these toxin is that they all lack a signal peptide required for translocation via the Sec- and Tat-secretion systems [13]. However, present in its pathogenicity locus is a cognate holin shown to be required in secretion of some of the LCTs [13]. These cognate holins come in two membrane topologies: a topology similar to the phage lambda holin (TcsE and TcdE) and a membrane topology similar to TatA, a key protein in the translocation process of the Tat-secretion system (Figure 2). Due to this similarity, it was hypothesized that TpeE-dependent secretion may represent a novel secretion system that shares aspects of Tat- and holin-dependent secretion [13].

The Tat-secretion system has two supported models: a pore-forming model and membrane destabilization model, the latter being most recently supported [75]. The membrane destabilization model will be the focus of this chapter. The theory behind this model focuses more on the length of the transmembrane helix than on the orientation of the amphipathic helix. Studies have shown that the transmembrane length of TatA, calculated to be 22.5 Å, is too short for the average lipid length in the cell-membrane of *E. coli*, calculated to be 37.5 Å (Figure 28) [83]. During recruitment, this length discrepancy may cause a hydrophobic mismatch of lipids,

resulting in a destabilized region large enough to facilitate translocation of the target protein [83, 84, 88].

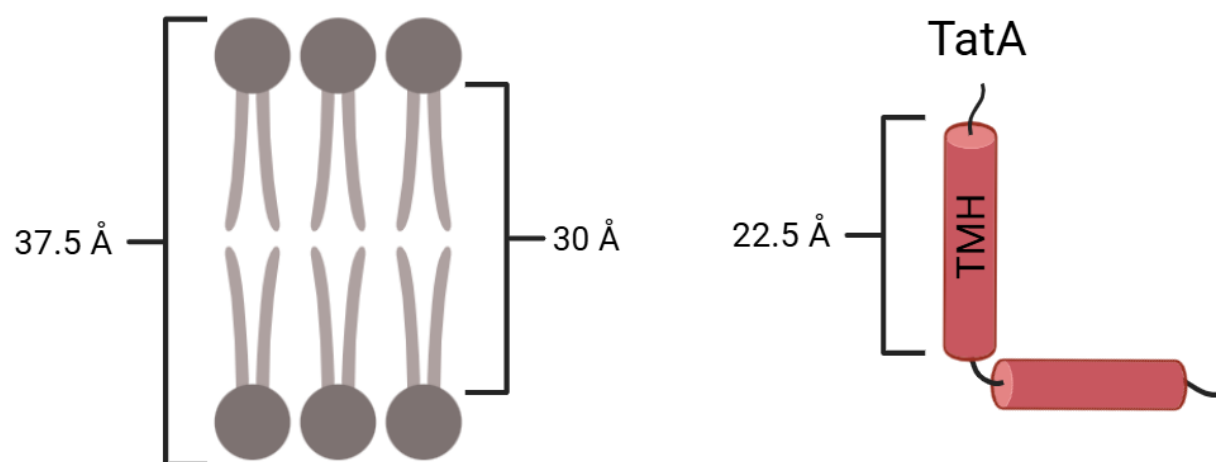


Figure 28. Illustration of calculated length of the transmembrane helix domain in TatA for *E. coli* compared to the average lipid length of the cell-membrane of *E. coli* [83].

Mutant TatA of various lengths and their ability to translocate target proteins have been studied to further characterize this secretion model [83, 88]. They found that shortening lengthening of the transmembrane helix led to a defect in translocation as well as overall cell health [83, 84, 88]. Molecular dynamics simulations, conducted by Mehner-Breitfeld et al, helped visualize these defects (Figure 29) [84]. Shortening the transmembrane helix led to an increase in membrane thinning when compared to the wild-type [84]. Whereas lengthening the transmembrane helix led to an increase in membrane stability when compared to the wild-type [84].

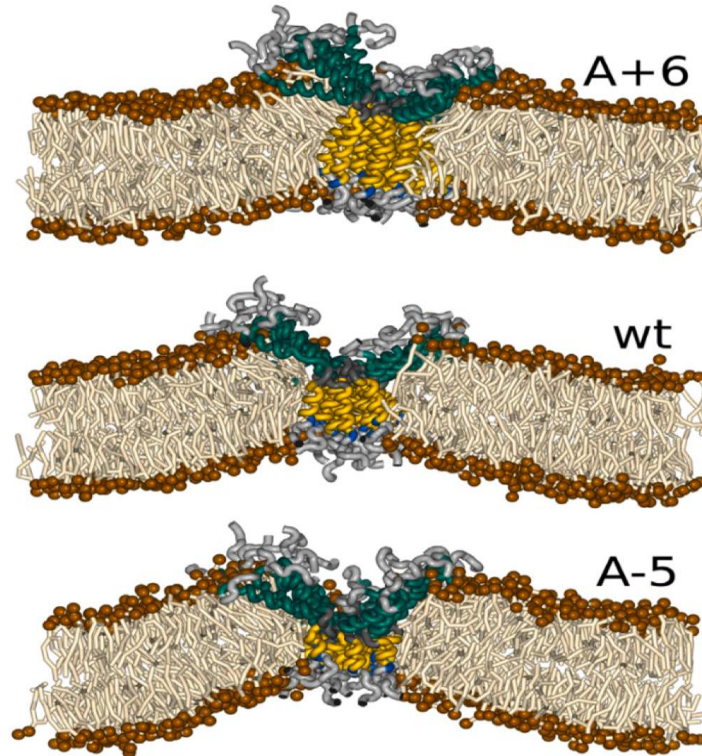


Figure 29. Molecular dynamics simulations, conducted by Mehner-Breitfeld et al, depicting the insertion and recruitment of wild-type (Middle), +6 insertion mutant (Top), and -5 deletion mutant (Bottom) transmembrane subunits of TatA. The -5-deletion mutant experienced far greater membrane destabilization than the wild-type. However, a +6-insertion mutant experienced far greater membrane stability when compared to the wild-type [84].

Due to the recent support for the membrane destabilization model and the inconclusive results of Chapter II, the secretion model for TpeE-dependent secretion of TpeL was reevaluated according to the membrane destabilization model. This new secretion model states that in the presence of the toxin, the holin oligomerize, forming a destabilized region in the cell-membrane large enough to facilitate secretion of TpeL (Figure 30).

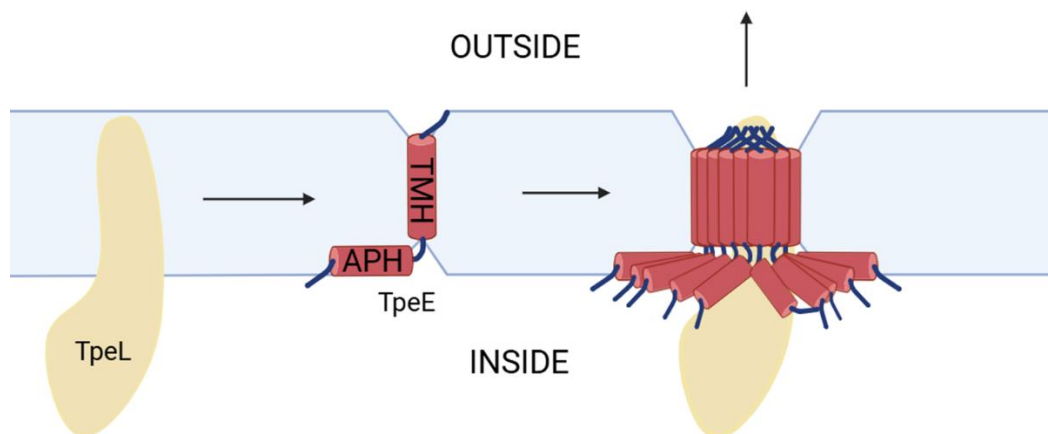


Figure 30. New secretion model for TpeE-dependent secretion of TpeL, according to a recently published membrane destabilization model for Tat-secretion. This states that in the absence of the toxin, the holin will not oligomerize, forming a small, destabilized pocket in the cell-membrane. However, in the presence of the toxin, the holin will oligomerize around the toxin, forming a large, destabilized region within the cell-membrane which will facilitate secretion.

To ensure that this phenomenon occurs in *C. perfringens*, the estimated length of the transmembrane helix of TpeE will need to be compared to the average lipid length of the cell-membrane in *C. perfringens*. Unfortunately, information on the solved structure of TpeE and the lipidomics of *C. perfringens* are not well studied and so estimation of the average lengths may not be entirely representative. The *C. perfringens* membrane consists primarily of 3 lipid types: phosphatidylethanolamine (PE), alanyl-phosphatidylglycerol (ala-PG), and cardiolipin [43]. According to what is known about these lipid types, the primary molecular species for both PE and ala-PG was 14:0, 14:0 which attributes to 26.5% and 33.6%, respectively [43]. Molecular species that are also present in large percentages are 12:0,14:0; 14:0,16:0; and 16:0,16:0 which attribute to 19%, 22.4%, and 17.6% within the PE and 18.7%, 26.3%, and 15.2% within the ala-PG, respectively [43]. A rough estimation of average membrane width in *C. perfringens* based on average carbon-carbon bond lengths, average phosphate group length, and estimated lipid percentages led to an average length of 34.2 Å.

To estimate the length of TpeE, homology modeling using AlphaFold3 and Robetta was applied. A validated model of TpeE led to the estimated transmembrane helix length of 21.3 Å, calculated using PyMol (Figure 44). This estimated length for TpeE is slightly shorter than the calculated lipid length of *C. perfringens* which is consistent with the membrane-destabilization model. If accurate, this would strongly suggest that TpeE-dependent secretion could be facilitated by hydrophobic mismatches within the cell-membrane caused by the recruitment/oligomerization of TpeE.

To test this model, TpeE will be subjected to insertions and deletions of amino acids that will manipulate the length of the transmembrane helix. The overall growth and secretion efficiency of cultures expressing these mutants will be compared to TpeE WT cultures to determine any effect. It is hypothesized that shorter TpeE mutants will demonstrate higher levels premature cell-lysis (detected via visualization of biotinylated *C. perfringens* protein, BCP), and longer TpeE mutants will demonstrate a lower secretion efficiency or inhibit secretion entirely. Molecular dynamics will eventually be performed to simulate visualize this mechanism.

Methods:

Bacterial Strains and Culture Conditions

The bacterial strains and plasmids used in these experiments are listed in Table 1. *C. perfringens* strain HN13 was cultured in PGY medium (3% proteose #3 peptone, 2% glucose, 1% yeast extract, and 0.1% sodium thioglycolate) at 37°C, anaerobically. DH10B *E. coli* strain was grown in Luria-Bertani (LB) broth (1% salt and tryptone and 0.5% yeast extract) at 37°C shaken at 300rpm. For HN13 cultures containing pKRAH-erm, Erythromycin (30µg/µL) was added to PGY or TY media that were used for HN13 cultures containing pKRAH-erm, whereas

for cultures with pKRAH1, 20 μ g/ μ L of chloramphenicol was used. For DH10B cultures containing pBad30, ampicillin (100 μ g/mL) was added to LB media, whereas for cultures containing the pCRBluntII TOPO vector, kanamycin (100 μ g/ μ L) was added to LB media.

Cloning of Mutant TpeE into HN13

Insertions and deletions were made in the N-terminus of the transmembrane helix of TpeE to minimize any effects they may have on the interactions/stability within the cytoplasmic membrane. The region chosen for mutation was based on the predicted membrane topology of TpeE (Figure 31). Mutations were performed via overlapping PCR using a chromosomal prep of *C. perfringens* Type C JGS 1495 strain as a DNA template. Primer sets for sequential insertions are ONF 22:23, 24:25, 26:27, 28:29, and 30:31, respectively. Primer sets for sequential deletions are ONF 32:33, 34:35, 36:37, 38:39, and 40:41, respectively. ONF 21 and 42 were used to flank the 5' and 3' end of *tpeE*. PCR products were then ligated to pCRBluntII TOPO via blunt-end ligation and electroporated into *E. coli* DH10B. Plasmid preps were then cut by 5' PstI and 3' BamHI sites, ligated to pKRAH-erm which were then electroporated into *C. perfringens* HN13. Sequences were checked in pCRBluntII TOPO using the M13 forward and reverse primer set.

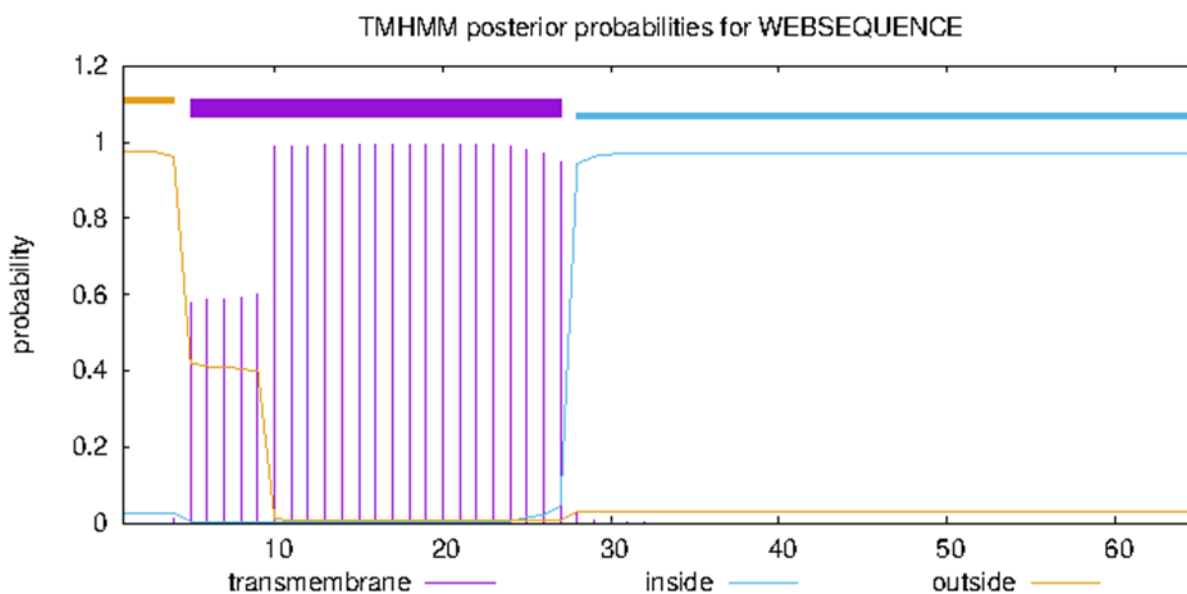


Figure 31. Membrane topology of TpeE. This graph depicts the probability of amino acids found extracellularly (outside), within a transmembrane helix (TMH), or within the cytoplasm (inside) where 0 is unlikely and 1 is highly likely. The first 3 amino acids have ~1 probability of being located outside the cell. However, amino acids 4-9 have ~0.6 probability of being within a TMH which suggests that they may also be located on the outside of the cells. The approximate size of the TMH of TpeE is most likely 15 amino acids starting from the 10th position and ending at the 25th position with probabilities ~1. Insertions and deletions were made around the N-terminus of the TMH of TpeE around positions 12 and 13.

Table 3. List of primers used in the membrane destabilization experiments.

Name	Description	Sequence
ONF21	Forward primer specific to the intergenic region upstream of <i>tpeE</i>	5'- CTGCAGCTAGACAGCACGTAAACCAA TAAAAATAGAGC -3'
ONF22	Forward: specific to the N-terminus of the transmembrane helix, adds 1 Leu	5'- GGCTACTCAACTTGGAGCTTTTGCTTTA CTATTTTCCTACTTG -3'
ONF23	Reverse: specific to the N-terminus of the transmembrane helix, adds 1 Leu	5'- GCAAAAGCTCCAAGTTGAGTAGCCATA ATTTTAAACAGTTCTG -3'
ONF24	Forward: specific to the N-terminus of the transmembrane helix, adds 2 Leu	5'- GGCTACTCAACTTCTTGGAGCTTTTGCT TTACTATTTTCCTACTTG -3'
ONF25	Reverse: specific to the N-terminus of the transmembrane helix, adds 2 Leu	5'- GCAAAAGCTCCAAGAAGTTGAGTAGCC ATAATTTTAAACAGTTCTG -3'
ONF26	Forward: specific to the N-terminus of the transmembrane helix, adds 3 Leu	5'- GGCTACTCAACTTCTTCTTGGAGCTTTT GCTTTACTATTTTCCTACTTG -3'
ONF27	Reverse: specific to the N-terminus of the transmembrane helix, adds 3 Leu	5'- GCAAAAGCTCCAAGAAGAAGTTGAGTA GCCATAATTTTAAACAGTTCTG -3'
ONF28	Forward: specific to the N-terminus of the transmembrane helix, adds 4 Leu	5'- GGCTACTCAACTTCTTCTTGGAGCT TTTGCTTTACTATTTTCCTACTTG -3'
ONF29	Reverse: specific to the N-terminus of the transmembrane helix, adds 4 Leu	5'- GCAAAAGCTCCAAGAAGAAGAAGTTGA GTAGCCATAATTTTAAACAGTTCTG -3'
ONF30	Forward: specific to the N-terminus of the transmembrane helix, adds 5 Leu	5'- GGCTACTCAACTTCTTCTTCTTGGGA GCTTTTGCTTTACTATTTTCCTACTTG -3'

ONF31	Reverse: specific to the N-terminus of the transmembrane helix, adds 5 Leu	5'- GCAAAAGCTCCAAGAAGAAGAAG TTGAGTAGCCATAATTTTAAACAGTTCT G -3'
ONF32	Forward: specific to the N-terminus of the transmembrane helix, deletes Gln	5'- TATGGCTACTGGAGCTTTTGCTTTACTAT TTTCCTACTTG -3'
ONF33	Reverse: specific to the N-terminus of the transmembrane helix, deletes Gln	5'- GCAAAAGCTCCAGTAGCCATAATTTTAA ACAGTTCTGAAT -3'
ONF34	Forward: specific to the N-terminus of the transmembrane helix, deletes Gln-Glu	5'- AATTATGGCTACTGCTTTTGCTTTACTAT TTTCCTACTTGTTATTTTATG -3'
ONF35	Reverse: specific to the N-terminus of the transmembrane helix, deletes Gln-Glu	5'- AGTAAAGCAAAGCAGTAGCCATAATTT TAAACAGTTCTG -3'
ONF36	Forward: specific to the N-terminus of the transmembrane helix, deletes Gln-Glu-Ala	5'- TAAAATTATGGCTACTTTTGCTTTACTAT TTTCCTACTTGTTATTTTATG -3'
ONF37	Reverse: specific to the N-terminus of the transmembrane helix, deletes Gln-Glu-Ala	5'- AGGAAAATAGTAAAGCAAAGTAGCCA TAATTTTAAACAGTTCTGAATCC -3'
ONF38	Forward: specific to the N-terminus of the transmembrane helix, deletes Gln-Glu-Ala-Phe	5'- GTTTAAAATTATGGCTACTGCTTTACTAT TTTCCTACTTGTTATTTTATG -3'
ONF39	Reverse: specific to the N-terminus of the transmembrane helix, deletes Gln-Glu-Ala-Phe	5'- TAGGAAAATAGTAAAGCAGTAGCCATAA TTTTAAACAGTTCTGAATCCAC -3'
ONF40	Forward: specific to the N-terminus of the transmembrane helix, deletes Gln-Glu-Ala-Phe-Ala	5'- CTGTTTAAAATTATGGCTACTTTACTATT TTCCTACTTG -3'
ONF41	Reverse: specific to the N-terminus of the transmembrane helix, deletes Gln-Glu-Ala-Phe-Ala	5'- CAAGTAGGAAAATAGTAAAGTAGCCATA ATTTTAAACAGTTCTGAATCCAC -3'
ONF42	Reverse: Downstream region of tpeE	5'- GTCGACCCTTTCAAATTTTATTCTTCTTA ACCCTCCTTTAGTATTTTATATAC -3'

Table 4. List of plasmids used in these experiments.

Name	Description	Sequence
------	-------------	----------

pKRAH1	Lactose-inducible vector	cm ^r
pKRAH-erm	Lactose-inducible vector	erm ^r
pCRBluntIITOPO	Cloning vector	kan ^r
pNF 11	<i>tpeE(-1)</i> -CRBluntIITOPO	kan ^r
pNF 12	<i>tpeE(-2)</i> -CRBluntIITOPO	kan ^r
pNF 13	<i>tpeE(-3)</i> -CRBluntIITOPO	kan ^r
pNF 14	<i>tpeE(-4)</i> -CRBluntIITOPO	kan ^r
pNF 15	<i>tpeE(-5)</i> -CRBluntIITOPO	kan ^r
pNF 16	<i>tpeE(+1)</i> -CRBluntIITOPO	kan ^r
pNF 17	<i>tpeE(+2)</i> -CRBluntIITOPO	kan ^r
pNF 18	<i>tpeE(+3)</i> -CRBluntIITOPO	kan ^r
pNF 19	<i>tpeE(+4)</i> -CRBluntIITOPO	kan ^r
pNF 20	<i>tpeE(+5)</i> -CRBluntIITOPO	kan ^r
pNF 21	<i>tpeE(-1)</i> -pKRAH	erm ^r
pNF 22	<i>tpeE(-2)</i> -pKRAH	erm ^r
pNF 23	<i>tpeE(-3)</i> -pKRAH	erm ^r
pNF 24	<i>tpeE(-4)</i> -pKRAH	erm ^r
pNF 25	<i>tpeE(-5)</i> -pKRAH	erm ^r
pNF 26	<i>tpeE(+1)</i> -pKRAH	erm ^r
pNF 27	<i>tpeE(+2)</i> -pKRAH	erm ^r
pNF 28	<i>tpeE(+3)</i> -pKRAH	erm ^r
pNF 29	<i>tpeE(+4)</i> -pKRAH	erm ^r
pNF 30	<i>tpeE(+5)</i> -pKRAH	erm ^r
pNF 31	<i>tpeE-His</i> -pKRAH	erm ^r
pAS45	<i>tpeL-His</i> -pKRAH1	cm ²

Growth Curves

Growth curves were conducted for each mutant created to ensure its overall health during expression of both the holin and the toxin. Anaerobically, each mutant was cultured in 1ml of PGY media overnight at 37°C. Overnight cultures were diluted (1:100) using 2 ml of PGY media, containing a 20 mM lactose concentration. This was then aliquoted into a 96 well plate, 6 wells per culture. The optical density 600 (OD) of each well was taken every 3 minutes for 24 hours. The average OD for each timepoint was graphed in Prism 9 (GraphPad) to visualize and calculate the growth rate and bacterial yield.

TpeL Secretion

Secretion was determined by conducting western blots using anti-His₆ antibodies to detect and measure the amount of TpeL-His₆ secreted. *C. perfringens* cultures were incubated anaerobically in PGY media overnight at 37°C. The overnight cultures were diluted (1:50) in 5mls of PGY and grown at 37°C. The cultures were induced with lactose (20 mM) every hour for 5-6 hours and then centrifuged to separate the pellet and the supernatant (3,500 rpm for 5 minutes). The supernatant fractions for each were filtered and concentrated using trichloroacetic acid precipitation and washed with acetone. The pellet fractions were collected by resuspending the pellet in Dulbecco's phosphate-buffer saline and lysed through a series of bead beating steps using zircon beads. The fractions were then suspended in 4x SDS-PAGE buffer with 100 mM dithiothreitol and heated at 95°C for 15 minutes. Proteins were separated via SDS-PAGE and immunoblotted with anti-His₆ antibodies. After separation, proteins were transferred to a polyvinylidene membrane and blocked for 5 minutes with 20mls of Every Blot Blocking Buffer (BioRad). The primary antibody was added to the membrane and incubated at room temperature for 1 hour or kept overnight in a 4°C fridge. The membranes were washed 5 times for 5 minutes with Tris-buffered saline-1% Tween 20 (TBS-T). The secondary antibody was diluted in 20 ml of Every Blot Blocking Buffer, added to the membrane, and incubated for 1 hour in the dark at room temperature. The membrane was washed with TBS-T 6 times for 5 minutes and then submerged in methanol and dried for imaging. The membrane was imaged with the StainFree and Starbright filters on the Bio-Rad ChemiDoc MP imaging system. Densitometry was conducted using ImageJ by creating a region of interest around each band to graph the pixel intensities. The area underneath the peaks in the graph corresponds to the amount of TpeL secreted.

Homology Modeling of TpeE

Homology modeling of TpeE was conducted using both AlphaFold3 server and Robetta modeling system. Five models from each system were created using the amino acid sequence of TpeE in a *C. perfringens* Type C strain. Models were energy minimized, using the Maestro energy minimization tool, and subjected to validation tests, such as Verify3D, ProSA, and the Swiss model assessment. The model that most consistently had the best scores was chosen.

Results:

Growth of HN13 During Expression of Shortened TpeE

When compared to TpeE WT, the expression of TpeE with a shortened transmembrane helix in the absence of the toxin had a negative effect on the growth rate of HN13, except for TpeE -4 (Figure 32). However, expression showed no effect on the overall bacterial yield of the cultures (Figure 32). In the presence of the toxin, the expression of the deletions had a drastic effect on the growth rate and bacterial yield of HN13 (Figure 33).

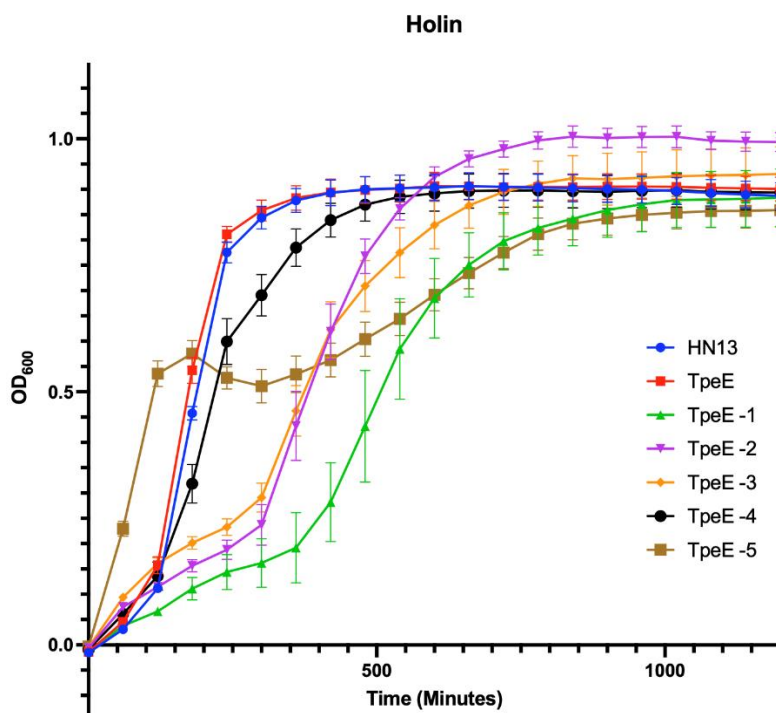


Figure 32. Growth of HN13 during the expression of mutant TpeE with deletions in the transmembrane helix in the absence of the toxin: HN13 (Blue), TpeE (Red), TpeE -1 (Green), TpeE -2 (Purple), TpeE-3 (Orange), TpeE -4 (Black), and TpeE -5 (Brown). This shows that the expression of all mutants, except TpeE-4, has a negative effect on the growth rate of HN13. However, overall bacterial yields were similar.

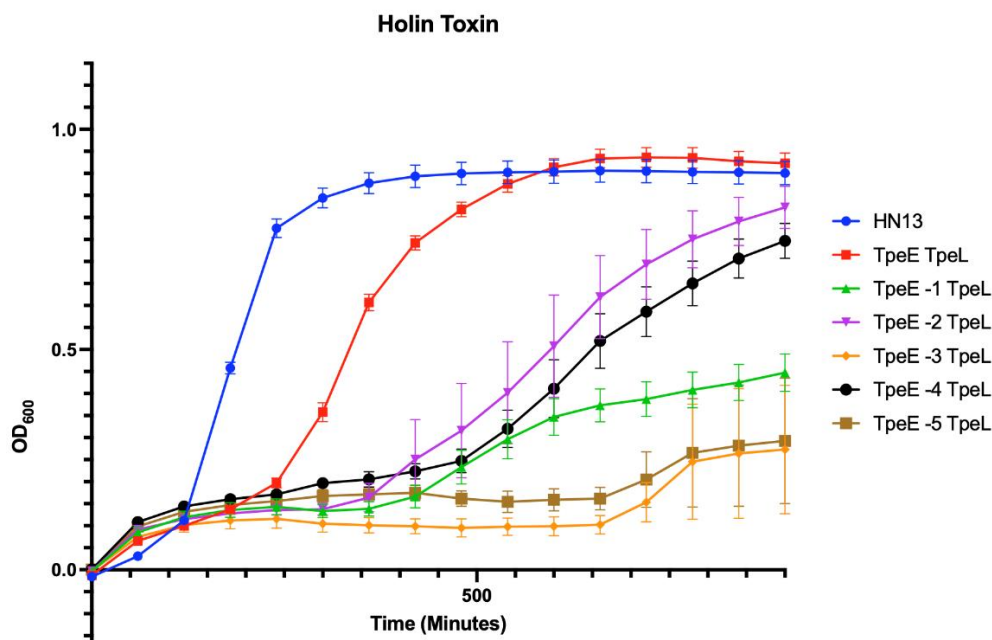


Figure 33. Growth of HN13 during the expression of mutant TpeE with deletions in the transmembrane helix in the presence of the toxin: HN13 (Blue), TpeE-TpeL (Red), TpeE -1 TpeL (Green), TpeE -2 TpeL (Purple), TpeE -3 TpeL (Orange), TpeE -4 TpeL (Black), TpeE -5 TpeL (Brown). This shows that the expression of TpeE with a shortened transmembrane helix in the presence of the toxin has a drastic effect on the growth rate of HN13. OD₆₀₀ was measured every 3 minutes.

Expression of mutant TpeE with a longer transmembrane helix had a negative effect on the growth rate of HN13 when compared to expression of TpeE WT (Figure 34). Bacterial yield across all insertions remained similar (Figure 34). During expression of the insertions alongside the toxin, mutant cultures behave similarly to the TpeE-TpeL control, although still having a negative effect on the growth rate of HN13 (Figure 35).

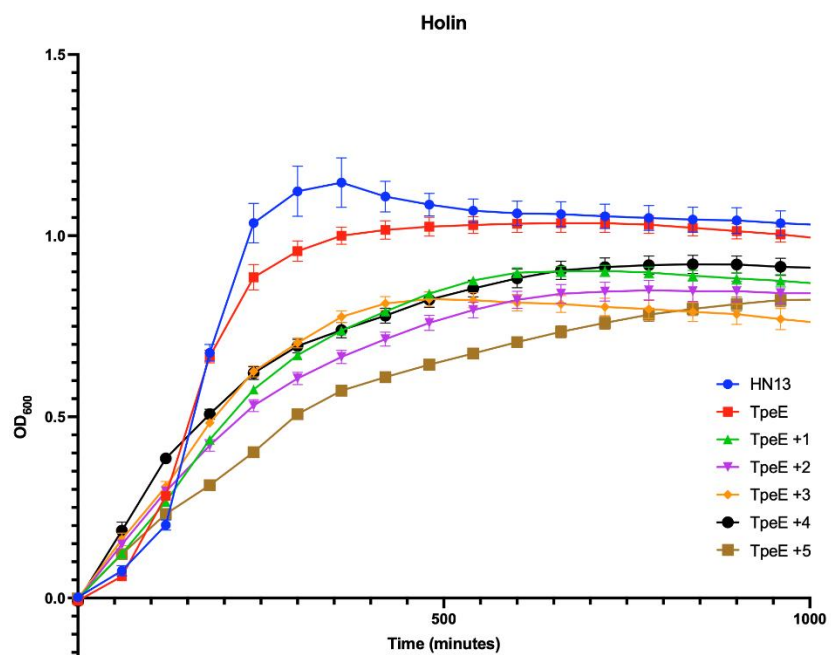


Figure 34. Growth of HN13 during the expression of lengthened TpeE in the absence of the toxin: HN13 (Blue), TpeE (Red), TpeE +1 (Green), TpeE +2 (Purple), TpeE +3 (Orange), TpeE +4 (Black), TpeE +5 (Brown). This shows that the expression of lengthened TpeE in the absence of the toxin has a negative effect on the growth rate of HN13. OD₆₀₀ was measured every 3 minutes.

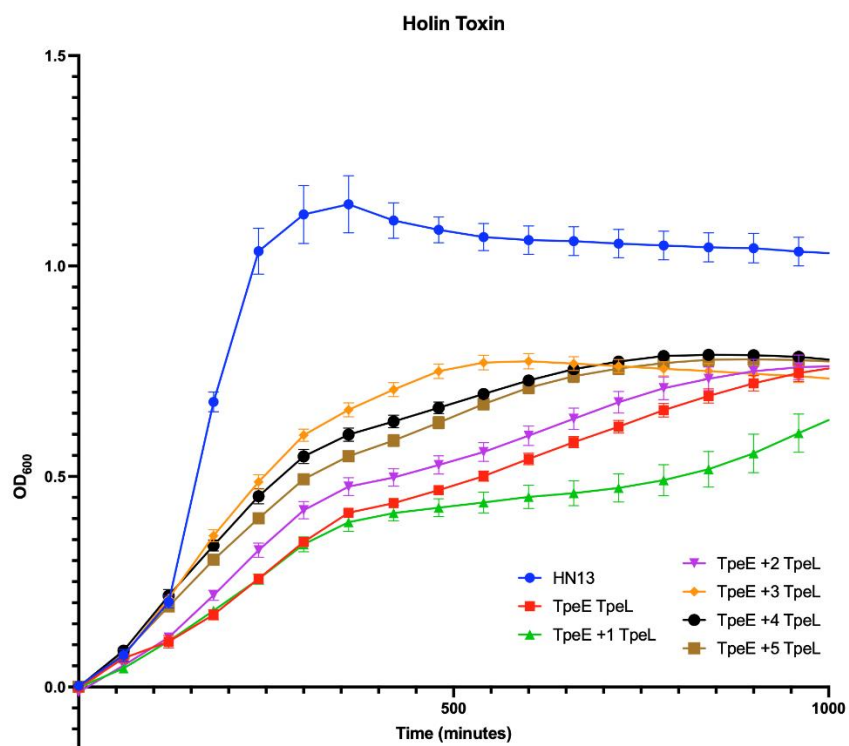


Figure 35. Growth of HN13 during expression of lengthened TpeE in the presence of the toxin: HN13 (Blue), TpeE-TpeL (Red), TpeE +1 TpeL (Green), TpeE +2 TpeL (Purple), TpeE +3 TpeL (Orange), TpeE +4 TpeL (Black), TpeE +5 TpeL (Brown).

+4 TpeL (Black), TpeE +5 TpeL (Brown). This shows that the expression of lengthened TpeE in the presence of the toxin has a negative effect on the growth rate of HN13 but behaves similarly to the TpeE-TpeL control. OD₆₀₀ was taken every 3 minutes for 24hrs.

Homology Model: TpeE

Five models each from Alphafold 3 and Robetta were constructed using the amino acid sequence of TpeE from *C. perfringens* Type C JGS 1495. Each model was subjected to energy minimization through the pre-processing tool in Maestro. Afterwards, structural analysis of these models was conducted using Verify3D, ProSA, and Swiss model assessment. Results for each are depicted below.

For Alphafold 3, all models failed the Verify3D test with average scores less than 0.2. For ProSA which determines if the structure is similar to solved structures, scores for each model are as follows -1.39, -1.35, -1.37, -1.44, and -1.43 for model 1, 2, 3, 4, and 5, respectively (Figure 36). These scores all fall within a range of all solved NMR structures. For the Swiss assessment, model 1 was 100% Ramachandran favored with 0 bad bonds, 4 bad angles, and a QMean score of 0.76 (Figure 37). Models 2, 3, 4, and 5 were 100% Ramachandran favored with 0 bad bonds, 3 bad angles, and QMean scores of 0.75, 0.76, 0.75, and 0.76, respectively (Figure 38-41).

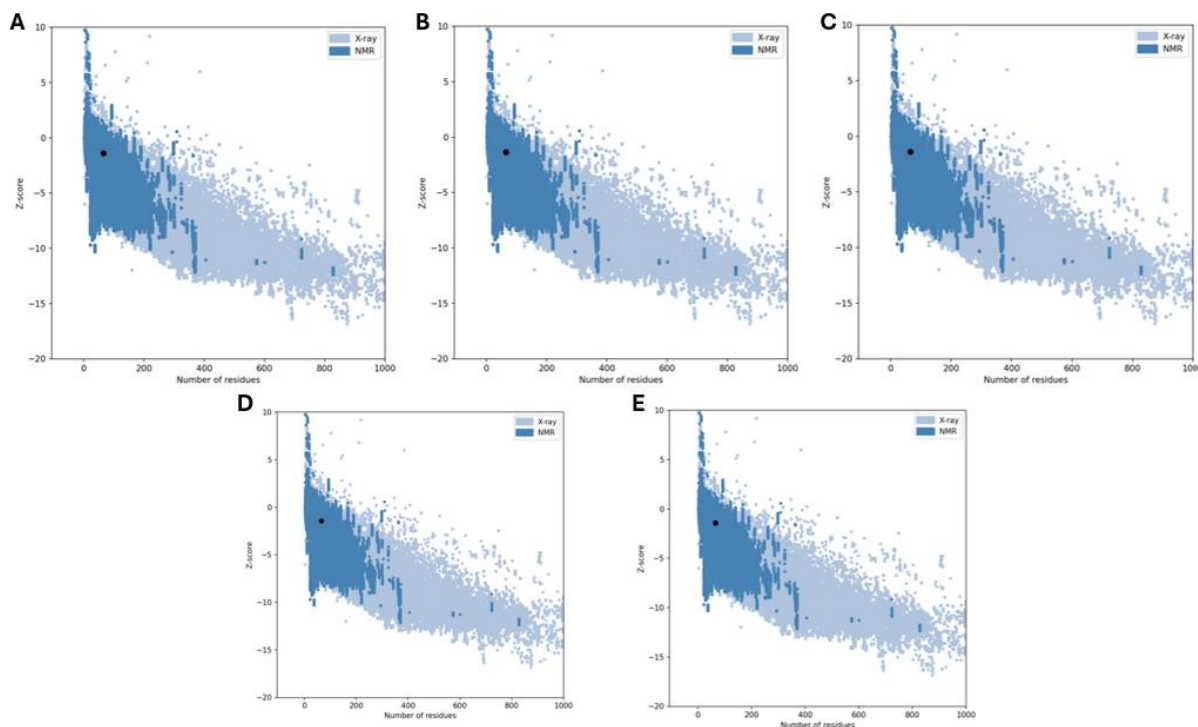


Figure 36. Test results from the structural validation test ProSA to determine the similarity of predicted TpeE model from AlphaFold3 to solved protein structures. **(A)** Model 1 resulted in a score of -1.39. **(B)** Model 2 resulted in a score of -1.35. **(C)** Model 3 resulted in a score of -1.37. **(D)** Model 4 resulted in a score of -1.44. **(E)** Model 5 resulted in a score of -1.41. These scores indicate that each model falls within the range of solved NMR structures.

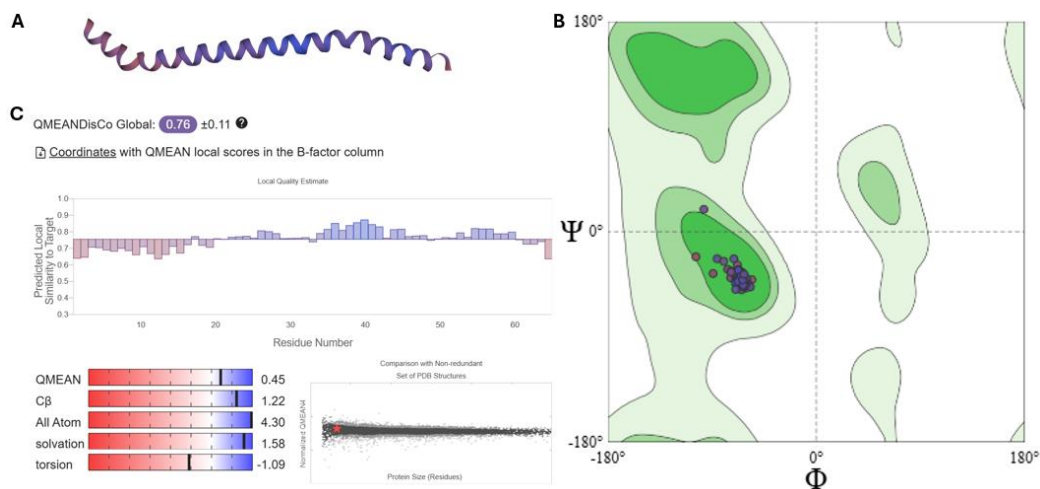


Figure 37. Predicted model 1 for TpeE using AlphaFold 3. **(A)** Visualization of model, **(B)** Ramachandran plot depicting no major outliers, and **(C)** QMEANDisCo global score of 0.76.

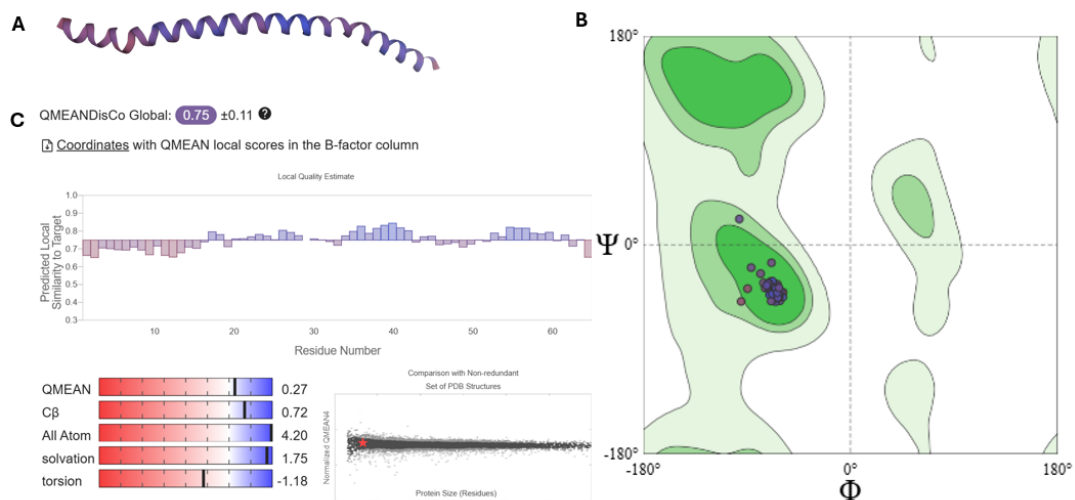


Figure 38. Predicted model 2 for TpeE using AlphaFold 3. (A) Visualization of model, (B) Ramachandran plot depicting no major outliers, and (C) QMEANDisCo global score of 0.75.

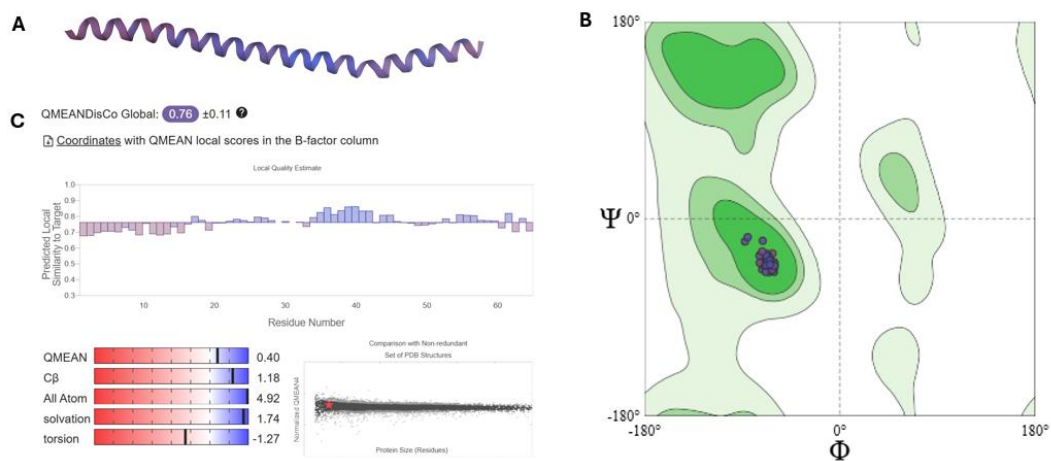


Figure 39. Predicted model 3 for TpeE using AlphaFold 3. (A) Visualization of model, (B) Ramachandran plot depicting no major outliers, and (C) QMEANDisCo global score of 0.76.

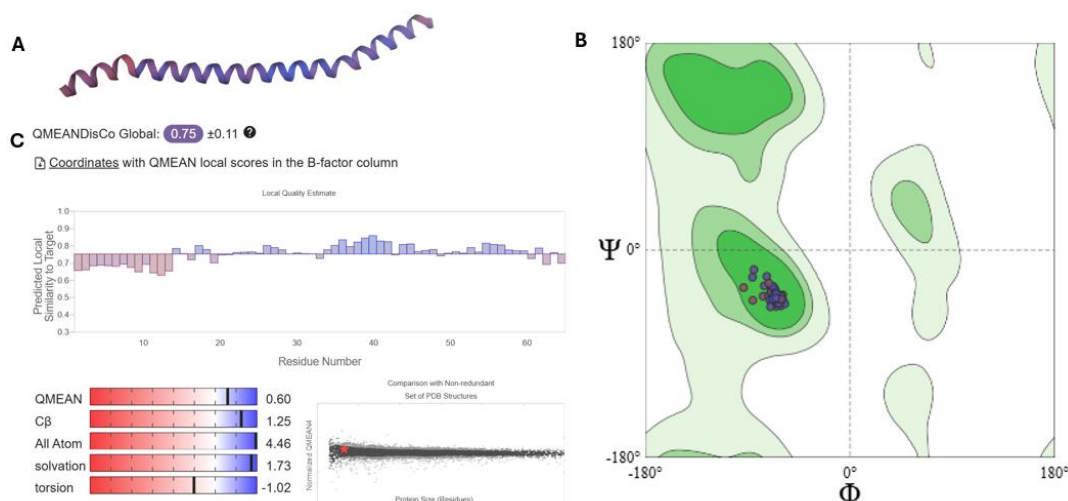


Figure 40. Predicted model 4 for TpeE using AlphaFold 3. (A) Visualization of model, (B) Ramachandran plot depicting no major outliers, and (C) QMEANDisCo global score of 0.75.

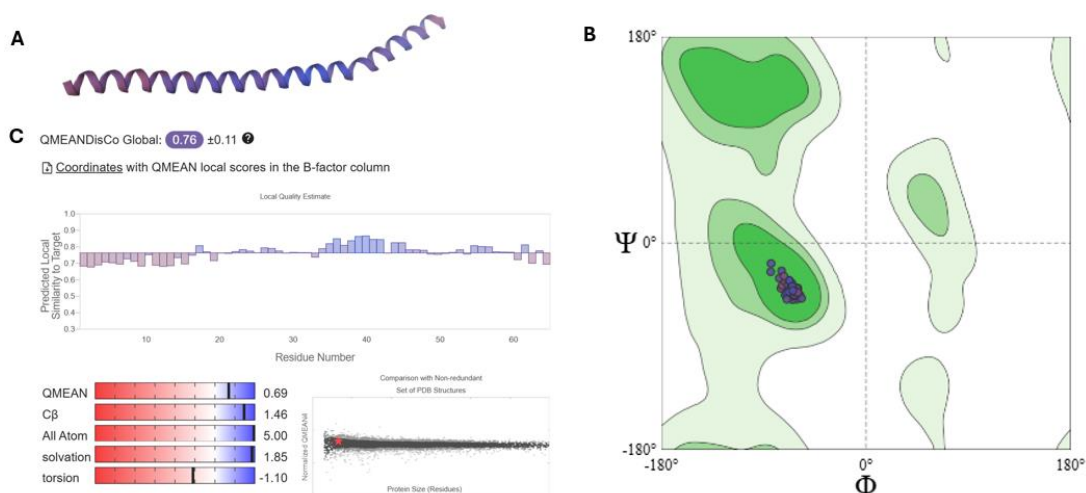


Figure 41. Predicted model 5 for TpeE using AlphaFold 3. (A) Visualization of model, (B) Ramachandran plot depicting no major outliers, and (C) QMEANDisCo global score of 0.76.

For Robetta, all models failed the Verify3D with average scores less than 0.2. For ProSA, the results are as follows -1.39, -1.39, -1.43, -1.4, and -1.37 for models 1, 2, 3, 4, and 5, respectively (Figure 42). For the Swiss model assessment, all models were 100% Ramachandran favored with 0 bad bonds. Models 1 and 3 had 2 bad angles and QMean scores of 0.79 and 0.76, respectively (Figure 43 and 45). Models 2 and 5 had only 1 bad angle with QMean scores of

0.79 and 0.78, respectively (Figure 44 and 47). Model 4 had 3 bad bonds with a QMean score of 0.78 (Figure 46).

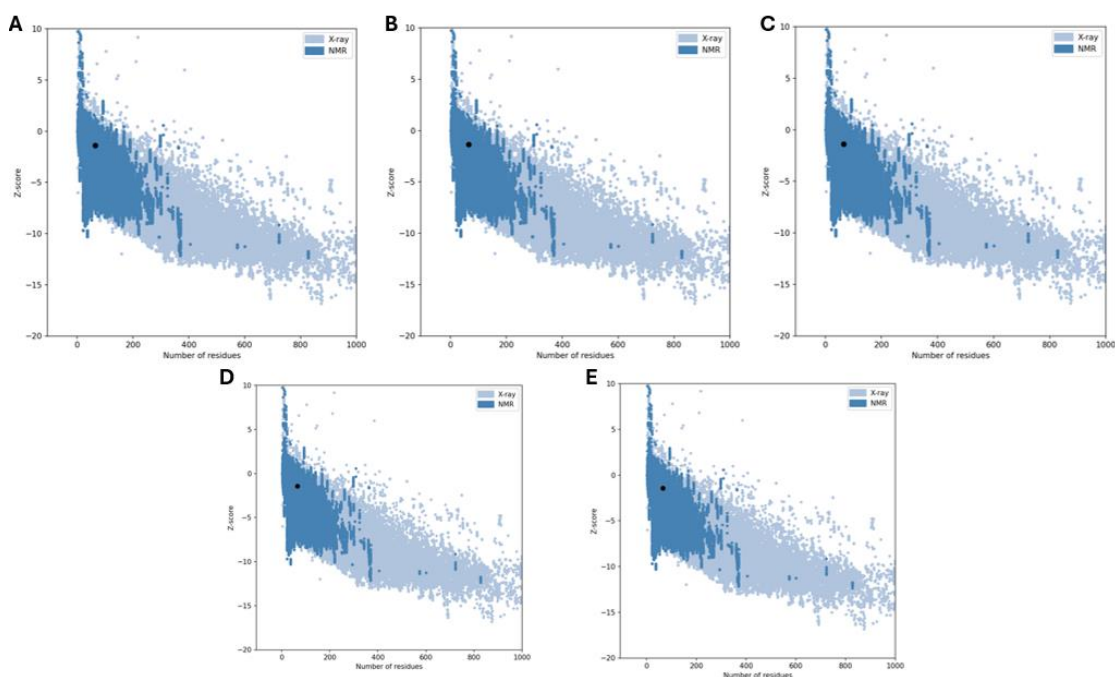


Figure 42. Test results from the structural validation test ProSA to determine the similarity of predicted TpeE model from Robetta to solved protein structures. **(A)** Model 1 resulted in a score of -1.39. **(B)** Model 2 resulted in a score of -1.39. **(C)** Model 3 resulted in a score of -1.43. **(D)** Model 4 resulted in a score of -1.4. **(E)** Model 5 resulted in a score of -1.37. These scores indicate that each model falls within the range of solved NMR structures.

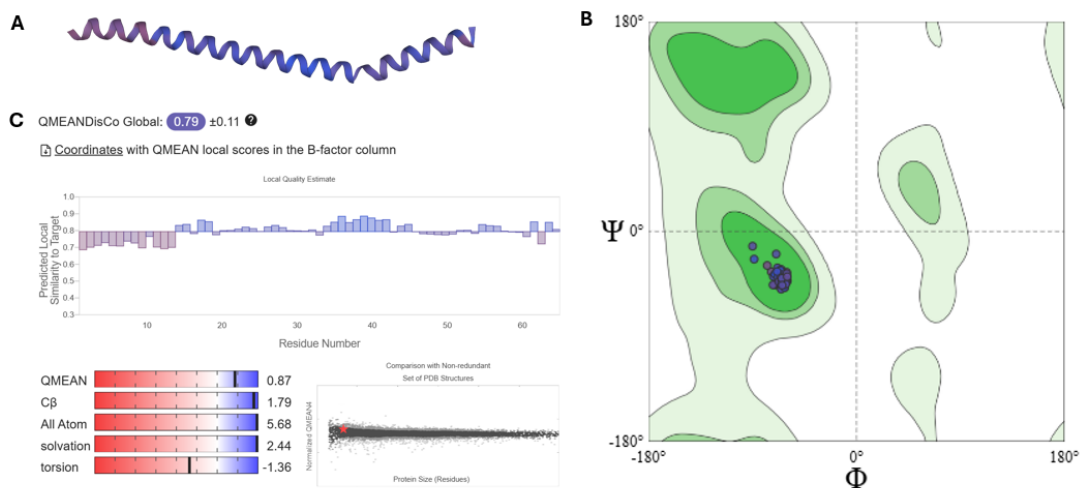


Figure 43. Predicted model 1 for TpeE using Robetta. **(A)** Visualization of model, **(B)** Ramachandran plot depicting no major outliers, and **(C)** QMEANDisCo global score of 0.79.

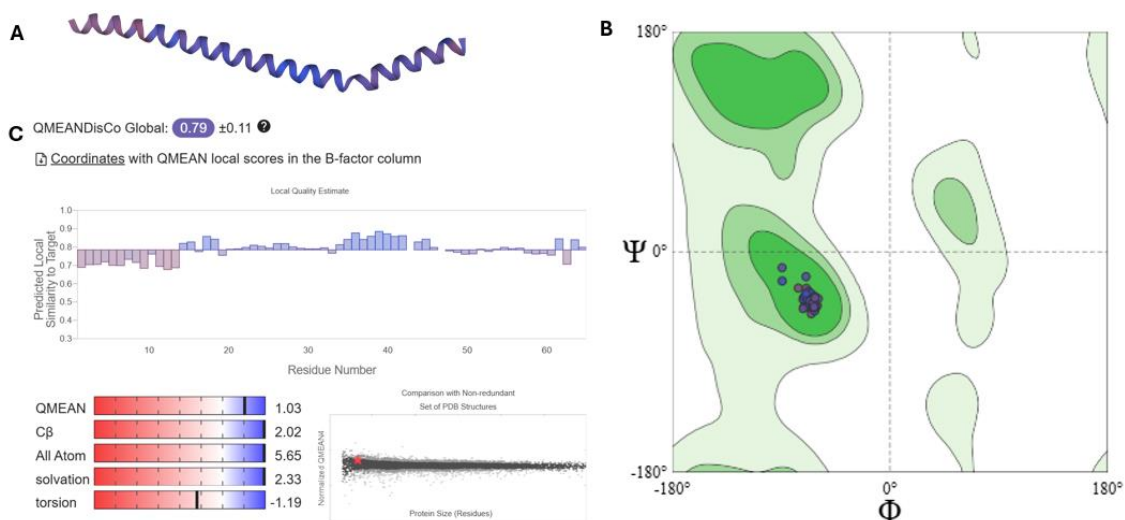


Figure 44. Predicted model 2 for TpeE using Robetta. (A) Visualization of model, (B) Ramachandran plot depicting no major outliers, and (C) QMEANDisCo global score of 0.79.

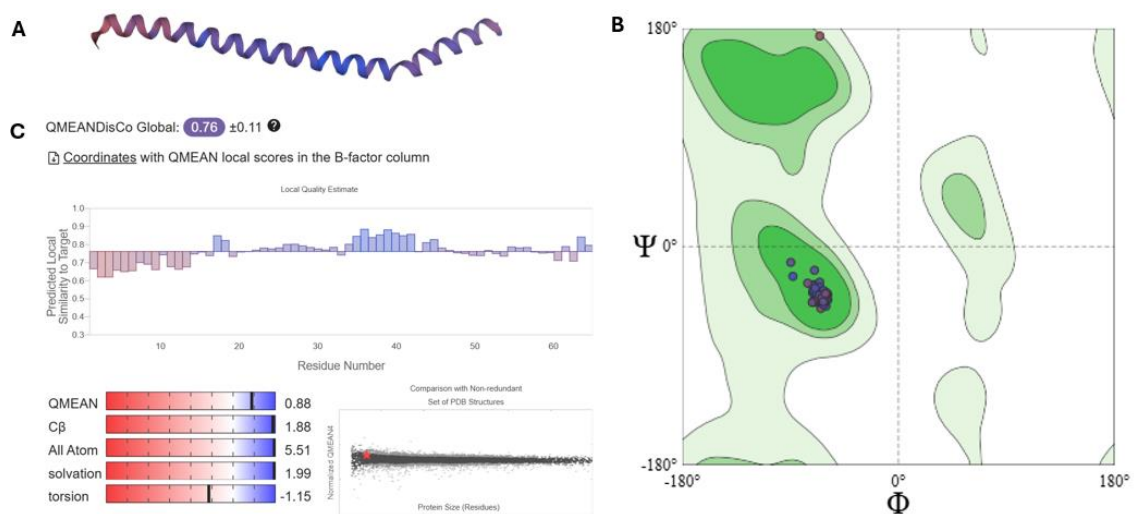


Figure 45. Predicted model 3 for TpeE using Robetta. (A) Visualization of model, (B) Ramachandran plot depicting no major outliers, and (C) QMEANDisCo global score of 0.76.

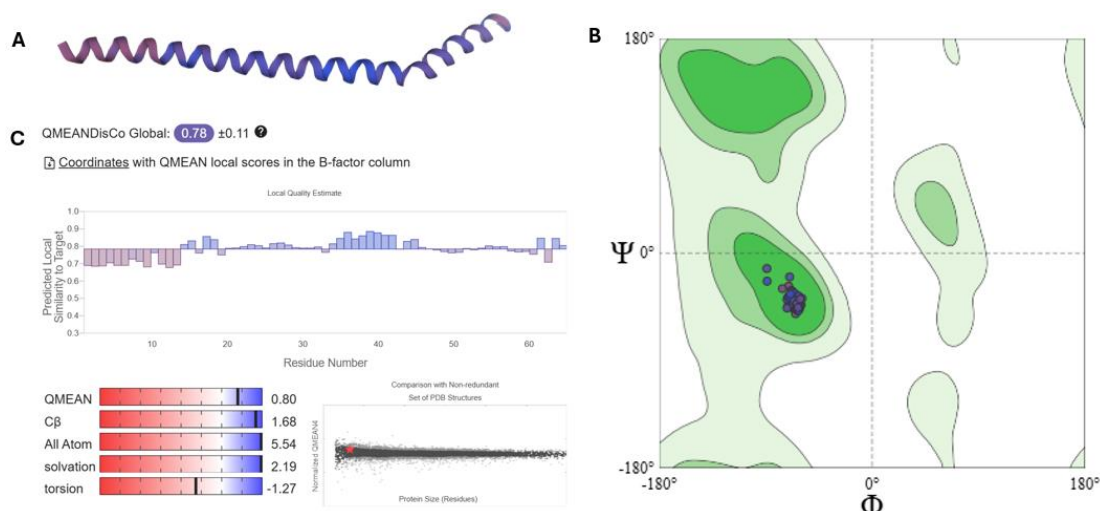


Figure 46. Predicted model 4 for TpeE using Robetta. (A) Visualization of model, (B) Ramachandran plot depicting no major outliers, and (C) QMEANDisCo global score of 0.78.

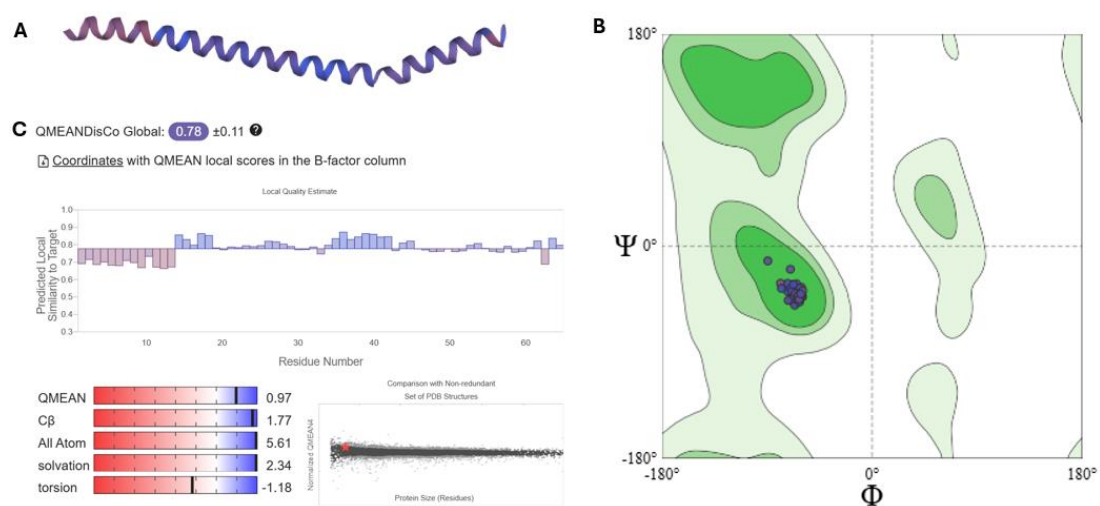


Figure 47. Predicted model 5 for TpeE using Robetta. (A) Visualization of model, (B) Ramachandran plot depicting no major outliers, and (C) QMEANDisCo global score of 0.78.

Keeping these results in mind, the Robetta model 2 was chosen to be the best representation of TpeE as it was scoring the highest consistently for each test.

Preliminary Secretion: TpeE Mutants

For shortened TpeE mutants, higher levels of TpeL-His₆ (~200 kD) were detected in the supernatant fractions when compared to the TpeE-TpeL control, qualitatively (Figure 48A, 49).

This trend was present in all samples except TpeE -4 TpeL (Figure 48A). A common

characteristic amongst all deletion samples, except TpeE -4 TpeL, was the detection of premature lysis via BCP (~25kd) (Figure 48B).

For lengthened TpeE mutants, lower levels of TpeL-His₆ (~200 kD) were detected between whole-cell extracts and supernatants (Figure 50A, 51). Although, the TpeE-TpeL control showed no presence of TpeL-His₆ within the supernatant fraction (Figure 50A). Contrary to the shortened mutants, the lengthened mutants showed no evidence of premature lysis (no detection of BCP) throughout induction (Figure 50B).

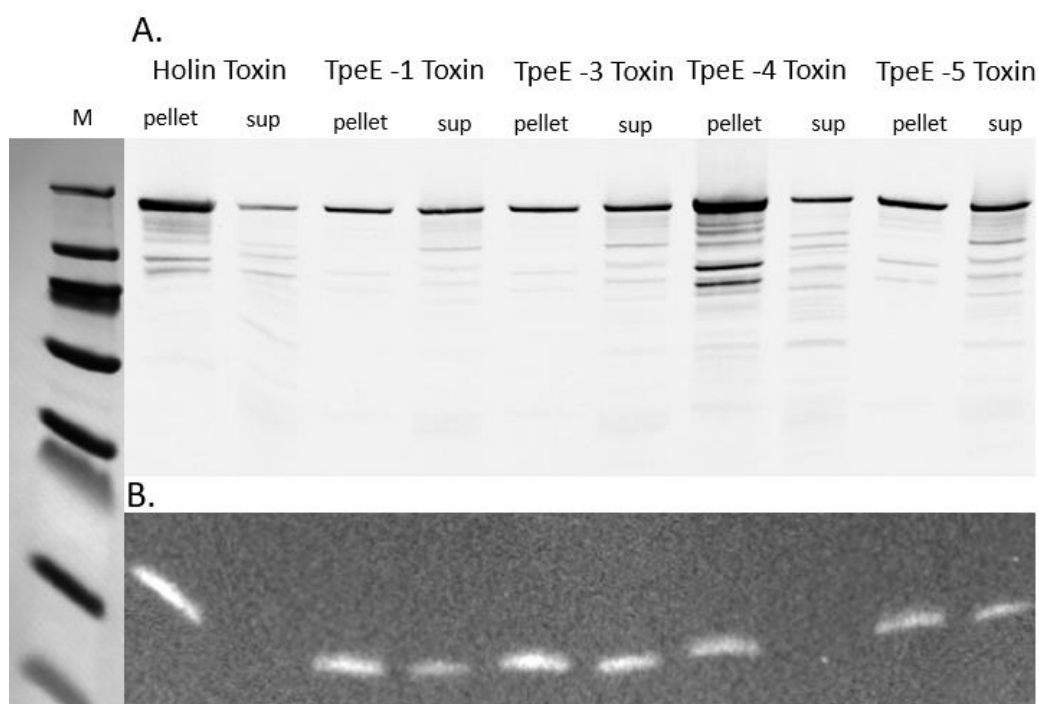


Figure 48. Western blot showing the detection of TpeL-His₆ in the whole-cell extracts and supernatants of shortened TpeE cultures. **(A.)** Detection of TpeL-His₆ was present in all supernatants of shortened TpeE mutants. **(B.)** However, increased levels of lysis (detection of BCP) in the supernatants were detected in all samples except TpeE -4 Toxin. This suggests that secretion of TpeL-His₆ by shortened TpeE may be due to premature lysis before sample collection.

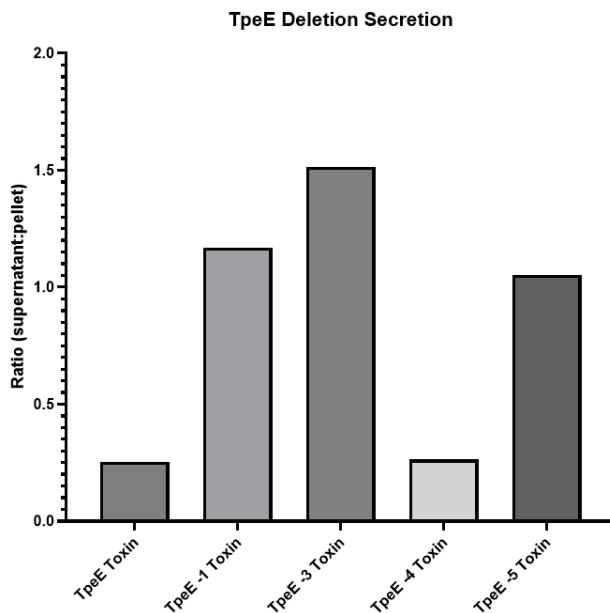


Figure 49. Shortened Mutant TpeE Secretion Densitometry. This graph depicts the secretion efficiency of TpeE Toxin WT (HN13), TpeE (-1) Toxin (HN13), TpeE (-3) Toxin (HN13), TpeE (-4) Toxin (HN13), and TpeE (-5) Toxin (HN13). Secretion efficiency was calculated by mapping out the mean pixel intensity for both the supernatant and whole-cell pellet fractions, calculating the area underneath intensity peaks, and comparing supernatant:pellet. This suggests that deleting amino acids in the TMH of TpeE may effect the secretion efficiency of TpeE. This was conducted only once.

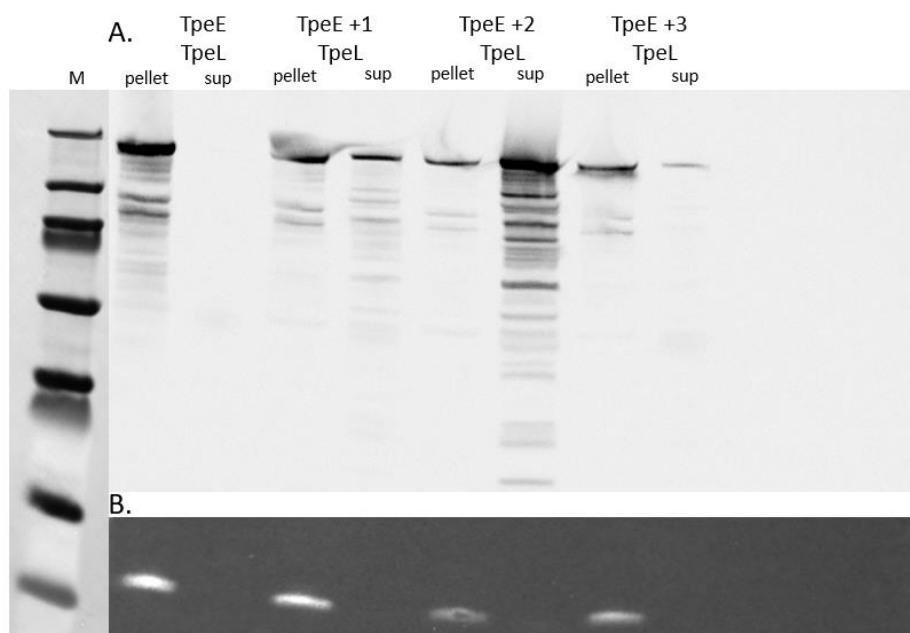


Figure 50. Anti-His₆ western blot detecting TpeL-His₆ in the whole cell-extracts and supernatants of lengthened TpeE cultures. **(A.)** Unfortunately, there was no TpeL-His₆ present in the supernatant of the TpeE-TpeL control culture, suggesting that there may have been an issue with the TCA

precipitation of that sample. Qualitatively, lower levels of TpeL-His₆ were detected in the TpeE +1 and +3 insertions, suggesting that lengthening the transmembrane helix may lower the secretion efficiency of TpeE. However, it is important to note that TpeE +2 did not experience this. **(B.)** There was no lysis detected in the supernatants of lengthened TpeE samples (through detection of BCP), which suggests that longer transmembrane helix may stabilize the cell-membrane.

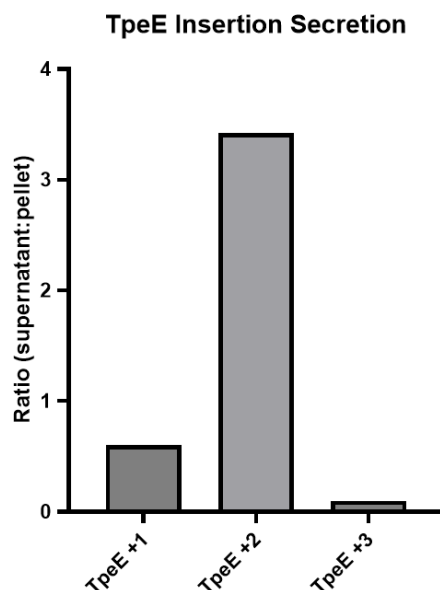


Figure 51. Lengthened Mutant TpeE Secretion Densitometry. This graph depicts the secretion efficiency of TpeE (+1) Toxin (HN13), TpeE (+2) Toxin (HN13), TpeE (+3) Toxin (HN13). Secretion efficiency was calculated by mapping out the mean pixel intensity for both the supernatant and whole-cell pellet fractions, calculating the area underneath intensity peaks, and comparing supernatant:pellet. This suggests that inserting amino acids in the TMH of TpeE may effect the secretion efficiency of TpeE. This was conducted only once.

Discussion

The goal of this chapter was to find evidence that the proposed membrane-destabilization model could be applied to TpeE-dependent secretion of TpeL in *C. perfringens*. This model would suggest that, in the presence of the toxin, the holin will oligomerize, causing hydrophobic mismatches within the lipid bilayer, which will destabilize the membrane and facilitate secretion (Figure 30). According to rough estimations of the transmembrane helix length of TpeE (21.3 Å) and the average lipid length in *C. perfringens* (34.2 Å), it is believed that TpeE may cause membrane destabilization during oligomerization in the presence of the toxin.

According to preliminary secretion results, shorter TpeE mutants led to a negative effect on growth rate and bacterial yield, a qualitative change in secretion efficiency, and an increase in premature cell-lysis (Figure 32,33, 48B). This was consistent with our model and the proposed Tat-secretion model since it suggests that if the transmembrane is too short, then there will be far greater destabilization in the cell-membrane, leading to an overwhelming amount of stress on the cell [83, 84, 88]. As for longer TpeE mutants, expression led to a negative effect on growth rate, a qualitative change in secretion efficiency with no detection of premature cell lysis (Figure 34, 35, 49B). This is also consistent with the proposed model since it also suggests that longer transmembrane helices will help stabilize the membrane, preventing destabilization, as well as lowering secretion efficiency [83, 84, 88]. Although, these results are preliminary and require more replication to provide any conclusive results.

Along with optimization and replication of the secretion results, it is crucial that other confounding variables are investigated. These variables would include overall membrane stability along with the expression and localization of TpeE mutants. This could be examined by tagging TpeE mutants with a His₆ tag and visualize membrane and cytoplasmic fractions via anti-His₆ western blots [13]. Membrane stability could be determined by measuring membrane leakiness via fluorescence microscopy using a proton motive force stain [89]. It would also be beneficial to create and compare cultures expressing mutant TpeE that incorporate full-turn modifications instead of deleting/inserting single amino acids. This could be used as an alternative as it will help conserve protein-protein interaction during the secretion process. By doing so, these could provide useful information on the underlying factors caused by the manipulation of the transmembrane helix length.

It is also recommended to continue with developing a molecular dynamics simulation of TpeE-dependent secretion using the information presented previously. The visualization of this model could provide more insight into the dynamics of this mechanism as well as lead to the development of new experiments and a more defined secretion model.

Identifying the relationship between TpeE and TpeL and the mechanism behind its secretion will not only provide a deeper understanding on LCTs but will also provide insight in defining the elusive Tat-secretion model.

Chapter IV

Conclusions

Clostridial pathogens are Gram-positive, anaerobic, spore-forming organisms responsible for various diseases in both humans and animals. More specifically, *C. perfringens* is known for causing both gas gangrene and food poisoning worldwide [7, 90, 91]. Much like other clostridial pathogens, *C. perfringens* is able to cause disease primarily through the secretion of various toxins, ~20, that vary between strains, called toxinotypes [1, 92, 93]. The identification of these toxinotypes during treatment has been incredibly useful for both humans and animals and has been continually updated throughout several years [7].

One family of proteins secreted by clostridial pathogens is the large clostridial toxins (LCTs) [13, 94]. This family includes glycosylating toxins that will bind to and inactivate GTPases, interfering with host cell signaling and eventually lead to cell death via apoptosis [13, 95, 96]. More specifically, TpeL, commonly associated with *C. perfringens*, glycosylates Rac and Ras proteins, GTPases crucial during cell-signaling [13, 97]. A common characteristic shared amongst all LCTs is that they all lack a signal peptide required for general translocation via Sec- or Tat-secretion [13]. To facilitate secretion, it has been shown that LCTs require a holin-like protein that functions differently for each system [58]. A recent publication on the secretion of TpeL has supported this claim however the exact mechanism has yet to be determined [13]. The goal of this thesis was to help characterize the mechanism of the holin-mediated secretion of TpeL.

It was hypothesized that TpeE may mediate the secretion of TpeL following a similar mechanism for Tat-secretion, since TpeE shares a similar membrane topology to TatA [13]. Tat-secretion has two models currently being proposed: Pore-forming and Membrane destabilization. The focus of Chapter II was testing the pore-forming model of Tat-secretion using Tpe-dependent secretion as a model.

The pore-forming model for TpeE-dependent secretion states that, in the presence of the toxin (TpeL), TpeE will oligomerize with the amphipathic helix flipping inside the membrane to establish a pore that will facilitate secretion. FAST fluorescence and Biotinylation technology were used to test if the amphipathic helix does in fact change in orientation in the presence of TpeL. The theory behind the FAST fluorescence experiment was that if TpeE was tagged on the C-terminus with a FAST tag and exposed to a set of permeable (Coral) and impermeable (AmberNP) dyes, then we could determine a difference in mean pixel intensity (MPI) for the impermeable dye in the presence of the toxin. Unfortunately, this experiment ended with inconclusive results. The Coral dye reacted as expected, with the MPI increasing over time for both a holin-alone and a holin-toxin culture (Figure 15). Whereas the AmberNP reacted as expected for a holin-alone culture but increased only slightly in overall fluorescence for a holin-toxin culture with no increase over time (Figure 16). Due to this, biotinylation technology was used to indirectly visualize and test any change in orientation of the amphipathic helix suggested by the pore-forming model.

The idea behind using biotinylation was that if non-native amino acids were substituted in the C-terminus of TpeE and exposed to a specific biotinylation reagent, then differences in biotin labeling would be detected between a holin-alone and a holin-toxin culture. Unfortunately, labeling of TpeE with any biotinylation agent could not be detected, even within a S3C positive control (Figure 26). Membrane fractions were isolated after labeling and visualized as well, yielding the same results (Figure 27). However, TpeL was unexpectedly being labeled with both a lysine specific and cysteine specific biotinylation reagent which suggests that the toxin may reassociate with the cell membrane following secretion. These results were confirmed through anti-His₆ western blotting and mass spectrometry (Figure 22).

It may be beneficial to repeat such experiments using a one plasmid system, as subjecting holin-toxin cultures to two antibiotics may be too stressful on its growth while expressing the toxin. As a more direct approach to testing the flipping of the amphipathic helix of TpeE, it may be beneficial to further analyze the structure of TpeE and predict a region where the flipping may occur. This region could then be subjected to substitutions with stiff amino acids, such as proline, that could immobilize the holin, inhibiting secretion of the toxin [98]. This may give more definitive results if proper controls are considered like membrane insertion and stability of the mutated holin, expression of the holin, and growth of the culture.

Due to inconclusive results with the pore-forming model, a membrane-destabilization model was tested using TpeE as model as well. The membrane-destabilization model switches the focus from the amphipathic helix to the length of the transmembrane helix. The idea is that the transmembrane helix of TatA is too short compared to the average lipid length of the membrane in *E. coli* [83, 84, 88]. This causes a hydrophobic mismatch, destabilizing the membrane during recruitment to facilitate translocation [83, 84, 88]. To test this with TpeE, amino acids were sequentially inserted and deleted which will manipulate the length of the transmembrane helix, affecting its ability to secrete TpeL.

Preliminary results have shown that longer transmembrane helices have a lower secretion efficiency when compared to wild-type holin-toxin controls (Figure 37). Whereas results from shortened transmembrane helices have higher secretion efficiency (Figure 36). However, the incorporation of shortened transmembrane helices has led to an increase in the detection of premature lysis (Figure 36). It is suggested to continue performing comparative western blotting between the wild-type and mutant holins to achieve statistically significant results. To ensure that the results aren't due to other confounding variables, it is crucial to determine if the ability

of the holin to insert into the membrane hasn't been compromised. This could be done by conducting comparative western blotting between membrane fractions of the wild-type and mutant holins.

The continuation of this project could lead to a deeper understanding of the relationship between TpeE and TpeL as well as the mechanism behind the Tat-secretion system.

Acknowledgements

First, I would like to acknowledge my family and friends who have provided a never-ending resource of support. Their belief in me has pushed me through the many challenges I faced throughout my journey here.

I am incredibly grateful to my committee members, Dr. Florian Schubot and Dr. David Popham, for their scientific insight and suggestions which helped improve my project.

Most importantly, I would like to thank my research advisor, Dr. Stephen Melville, for his constant support both inside and outside the lab. His mentorship was crucial to my development as a scientist. I am deeply grateful for his patience and support throughout my project.

References

1. Kiu, R. and L.J. Hall, *An update on the human and animal enteric pathogen Clostridium perfringens*. *Emerg Microbes Infect*, 2018. **7**(1): p. 141.
2. Chen, J. and B.A. McClane, *Characterization of Clostridium perfringens TpeL toxin gene carriage, production, cytotoxic contributions, and trypsin sensitivity*. *Infect Immun*, 2015. **83**(6): p. 2369-81.
3. Prevention, T.C.f.D.C.a. *About C. perfringens food poisoning*. 2024 April 3, 2024 [cited 2025 April 4]; Available from: <https://www.cdc.gov/clostridium-perfringens/about/index.html>.
4. Annamaraju, P.Y.P. *Clostridium perfringens Infection*. 2023 August 8, 2023 [cited 2025 April 4]; Available from: <https://www.ncbi.nlm.nih.gov/books/NBK559049/>.
5. Uzal, F.A., et al., *Towards an understanding of the role of Clostridium perfringens toxins in human and animal disease*. *Future Microbiol*, 2014. **9**(3): p. 361-77.
6. Mehdizadeh Gohari, I., et al., *Pathogenicity and virulence of Clostridium perfringens*. *Virulence*, 2021. **12**(1): p. 723-753.
7. Rood, J.I., et al., *Expansion of the Clostridium perfringens toxin-based typing scheme*. *Anaerobe*, 2018. **53**: p. 5-10.
8. Uzal, F.A., et al., *Clostridium Perfringens Toxins Involved in Mammalian Veterinary Diseases*. *Open Toxinology J*, 2010. **2**: p. 24-42.
9. Navarro, M.A., B.A. McClane, and F.A. Uzal, *Mechanisms of Action and Cell Death Associated with Clostridium perfringens Toxins*. *Toxins (Basel)*, 2018. **10**(5).
10. Freedman, J.C., A. Shrestha, and B.A. McClane, *Clostridium perfringens Enterotoxin: Action, Genetics, and Translational Applications*. *Toxins (Basel)*, 2016. **8**(3).
11. Sakurai, J., et al., *Clostridium perfringens iota-toxin: structure and function*. *Toxins (Basel)*, 2009. **1**(2): p. 208-28.
12. Anne, J., A. Economou, and K. Bernaerts, *Protein Secretion in Gram-Positive Bacteria: From Multiple Pathways to Biotechnology*. *Curr Top Microbiol Immunol*, 2017. **404**: p. 267-308.
13. Saadat, A. and S.B. Melville, *Holin-Dependent Secretion of the Large Clostridial Toxin TpeL by Clostridium perfringens*. *J Bacteriol*, 2021. **203**(8).
14. Popoff, M.R. and P. Bouvet, *Clostridial toxins*. *Future Microbiol*, 2009. **4**(8): p. 1021-64.
15. Tweten, R.K., *Clostridium perfringens beta toxin and Clostridium septicum alpha toxin: their mechanisms and possible role in pathogenesis*. *Vet Microbiol*, 2001. **82**(1): p. 1-9.
16. Tsirigotaki, A., et al., *Protein export through the bacterial Sec pathway*. *Nat Rev Microbiol*, 2017. **15**(1): p. 21-36.
17. Natale, P., T. Bruser, and A.J. Driessen, *Sec- and Tat-mediated protein secretion across the bacterial cytoplasmic membrane--distinct translocases and mechanisms*. *Biochim Biophys Acta*, 2008. **1778**(9): p. 1735-56.
18. McDonough, J.A., et al., *Identification of functional Tat signal sequences in Mycobacterium tuberculosis proteins*. *J Bacteriol*, 2008. **190**(19): p. 6428-38.
19. den Blaauwen, T. and A.J. Driessen, *Sec-dependent preprotein translocation in bacteria*. *Arch Microbiol*, 1996. **165**(1): p. 1-8.
20. Berks, B.C., T. Palmer, and F. Sargent, *Protein targeting by the bacterial twin-arginine translocation (Tat) pathway*. *Curr Opin Microbiol*, 2005. **8**(2): p. 174-81.
21. Lee, P.A., D. Tullman-Ercek, and G. Georgiou, *The bacterial twin-arginine translocation pathway*. *Annu Rev Microbiol*, 2006. **60**: p. 373-95.
22. Goosens, V.J. and J.M. van Dijl, *Twin-Arginine Protein Translocation*. *Curr Top Microbiol Immunol*, 2017. **404**: p. 69-94.

23. Muller, M., *Twin-arginine-specific protein export in Escherichia coli*. Res Microbiol, 2005. **156**(2): p. 131-6.
24. Kleiner-Grote, G.R.M., J.M. Risse, and K. Friehs, *Secretion of recombinant proteins from E. coli*. Eng Life Sci, 2018. **18**(8): p. 532-550.
25. Frain, K.M., C. Robinson, and J.M. van Dijl, *Transport of Folded Proteins by the Tat System*. Protein J, 2019. **38**(4): p. 377-388.
26. Gimenez, M.R., et al., *Genome wide identification and experimental validation of Pseudomonas aeruginosa Tat substrates*. Sci Rep, 2018. **8**(1): p. 11950.
27. Lavander, M., et al., *The twin arginine translocation system is essential for virulence of Yersinia pseudotuberculosis*. Infect Immun, 2006. **74**(3): p. 1768-76.
28. Juhas, M., D.W. Crook, and D.W. Hood, *Type IV secretion systems: tools of bacterial horizontal gene transfer and virulence*. Cell Microbiol, 2008. **10**(12): p. 2377-86.
29. Grohmann, E., et al., *Type IV secretion in Gram-negative and Gram-positive bacteria*. Mol Microbiol, 2018. **107**(4): p. 455-471.
30. Ke, Y., et al., *Type IV secretion system of Brucella spp. and its effectors*. Front Cell Infect Microbiol, 2015. **5**: p. 72.
31. Costa, T.R.D., et al., *Type IV secretion systems: Advances in structure, function, and activation*. Mol Microbiol, 2021. **115**(3): p. 436-452.
32. Goessweiner-Mohr, N., et al., *Conjugative type IV secretion systems in Gram-positive bacteria*. Plasmid, 2013. **70**(3): p. 289-302.
33. Bowman, L. and T. Palmer, *The Type VII Secretion System of Staphylococcus*. Annu Rev Microbiol, 2021. **75**: p. 471-494.
34. Rivera-Calzada, A., et al., *Type VII secretion systems: structure, functions and transport models*. Nat Rev Microbiol, 2021. **19**(9): p. 567-584.
35. Kengmo Tchoupa, A., et al., *The type VII secretion system protects Staphylococcus aureus against antimicrobial host fatty acids*. Sci Rep, 2020. **10**(1): p. 14838.
36. Ates, L.S., E.N.G. Houben, and W. Bitter, *Type VII Secretion: A Highly Versatile Secretion System*. Microbiol Spectr, 2016. **4**(1).
37. Bruser, T. and D. Mehner-Breitfeld, *Occurrence and potential mechanism of holin-mediated non-lytic protein translocation in bacteria*. Microb Cell, 2022. **9**(10): p. 159-173.
38. Young, R., *Bacteriophage lysis: mechanism and regulation*. Microbiol Rev, 1992. **56**(3): p. 430-81.
39. Vidor, C.J., et al., *A Highly Specific Holin-Mediated Mechanism Facilitates the Secretion of Lethal Toxin TcsL in Paenibacillus sordellii*. Toxins (Basel), 2022. **14**(2).
40. DiBenedetto, N.V., et al., *The TcdE holin drives toxin secretion and virulence in Clostridioides difficile*. bioRxiv, 2023.
41. Guan, Z. and H. Goldfine, *Lipid diversity in clostridia*. Biochim Biophys Acta Mol Cell Biol Lipids, 2021. **1866**(9): p. 158966.
42. Roy, H. and M. Ibba, *RNA-dependent lipid remodeling by bacterial multiple peptide resistance factors*. Proc Natl Acad Sci U S A, 2008. **105**(12): p. 4667-72.
43. Johnston, N.C., J.K. Baker, and H. Goldfine, *Phospholipids of Clostridium perfringens: a reexamination*. FEMS Microbiol Lett, 2004. **233**(1): p. 65-8.
44. Moss, C.W. and V.J. Lewis, *Characterization of clostridia by gas chromatography. I. Differentiation of species by cellular fatty acids*. Appl Microbiol, 1967. **15**(2): p. 390-7.
45. Carter, G.P., et al., *Defining the Roles of TcdA and TcdB in Localized Gastrointestinal Disease, Systemic Organ Damage, and the Host Response during Clostridium difficile Infections*. mBio, 2015. **6**(3): p. e00551.

46. Cohen, A.L., et al., *Toxic shock associated with Clostridium sordellii and Clostridium perfringens after medical and spontaneous abortion*. Obstet Gynecol, 2007. **110**(5): p. 1027-33.
47. Centers for Disease, C. and Prevention, *Clostridium sordellii toxic shock syndrome after medical abortion with mifepristone and intravaginal misoprostol--United States and Canada, 2001-2005*. MMWR Morb Mortal Wkly Rep, 2005. **54**(29): p. 724.
48. Carter, G.P., et al., *TcsL is an essential virulence factor in Clostridium sordellii ATCC 9714*. Infect Immun, 2011. **79**(3): p. 1025-32.
49. Gu, C., et al., *Characterization of Virulent netB(+)/tpeL(+)Clostridium perfringens Strains from Necrotic Enteritis-Affected Broiler Chicken Farms*. Avian Dis, 2019. **63**(3): p. 461-467.
50. Park, M. and F. Rafii, *The prevalence of plasmid-coded cpe enterotoxin, beta(2) toxin, tpeL toxin, and tetracycline resistance in Clostridium perfringens strains isolated from different sources*. Anaerobe, 2019. **56**: p. 124-129.
51. Coursodon, C.F., et al., *TpeL-producing strains of Clostridium perfringens type A are highly virulent for broiler chicks*. Anaerobe, 2012. **18**(1): p. 117-21.
52. Schirmer, J. and K. Aktories, *Large clostridial cytotoxins: cellular biology of Rho/Ras-glucosylating toxins*. Biochim Biophys Acta, 2004. **1673**(1-2): p. 66-74.
53. Jank, T. and K. Aktories, *Structure and mode of action of clostridial glucosylating toxins: the ABCD model*. Trends Microbiol, 2008. **16**(5): p. 222-9.
54. Voth, D.E. and J.D. Ballard, *Clostridium difficile toxins: mechanism of action and role in disease*. Clin Microbiol Rev, 2005. **18**(2): p. 247-63.
55. Guttenberg, G., et al., *Molecular characteristics of Clostridium perfringens TpeL toxin and consequences of mono-O-GlcNAcylation of Ras in living cells*. J Biol Chem, 2012. **287**(30): p. 24929-40.
56. Lu, S., et al., *CDD/SPARCLE: the conserved domain database in 2020*. Nucleic Acids Res, 2020. **48**(D1): p. D265-D268.
57. Reddy, B.L. and M.H. Saier, Jr., *Topological and phylogenetic analyses of bacterial holin families and superfamilies*. Biochim Biophys Acta, 2013. **1828**(11): p. 2654-71.
58. Saier, M.H., Jr. and B.L. Reddy, *Holins in bacteria, eukaryotes, and archaea: multifunctional xenologues with potential biotechnological and biomedical applications*. J Bacteriol, 2015. **197**(1): p. 7-17.
59. Anthony, T., et al., *Functional analysis of a putative holin-like peptide-coding gene in the genome of Bacillus licheniformis AnBa9*. Arch Microbiol, 2010. **192**(1): p. 51-6.
60. Aunpad, R. and W. Panbangred, *Evidence for two putative holin-like peptides encoding genes of Bacillus pumilus strain WAPB4*. Curr Microbiol, 2012. **64**(4): p. 343-8.
61. Czepiel, J., et al., *Clostridium difficile infection: review*. Eur J Clin Microbiol Infect Dis, 2019. **38**(7): p. 1211-1221.
62. Rao, A.K., et al., *Clinical Guidelines for Diagnosis and Treatment of Botulism, 2021*. MMWR Recomm Rep, 2021. **70**(2): p. 1-30.
63. Rhinesmith, E. and L. Fu, *Tetanus Disease, Treatment, Management*. Pediatr Rev, 2018. **39**(8): p. 430-432.
64. Cirillo, L., et al., *Clostridium septicum infection complicating Hemolytic-Uremic Syndrome: a case report and review of the literature*. J Nephrol, 2024. **37**(1): p. 181-186.
65. Aronoff, D.M., *Clostridium novyi, sordellii, and tetani: mechanisms of disease*. Anaerobe, 2013. **24**: p. 98-101.
66. Takehara, M., et al., *Cellular Entry of Clostridium perfringens Iota-Toxin and Clostridium botulinum C2 Toxin*. Toxins (Basel), 2017. **9**(8).

67. Kuehne, S.A., et al., *The role of toxin A and toxin B in Clostridium difficile infection*. Nature, 2010. **467**(7316): p. 711-3.
68. Dong, M., G. Masuyer, and P. Stenmark, *Botulinum and Tetanus Neurotoxins*. Annu Rev Biochem, 2019. **88**: p. 811-837.
69. Flores-Diaz, M. and A. Alape-Giron, *Role of Clostridium perfringens phospholipase C in the pathogenesis of gas gangrene*. Toxicon, 2003. **42**(8): p. 979-86.
70. Orrell, K.E. and R.A. Melnyk, *Large Clostridial Toxins: Mechanisms and Roles in Disease*. Microbiol Mol Biol Rev, 2021. **85**(3): p. e0006421.
71. Li, X., et al., *Paeniclostridium sordellii hemorrhagic toxin targets TMPRSS2 to induce colonic epithelial lesions*. Nat Commun, 2022. **13**(1): p. 4331.
72. Tian, S., et al., *Genome-Wide CRISPR Screen Identifies Semaphorin 6A and 6B as Receptors for Paeniclostridium sordellii Toxin TcsL*. Cell Host Microbe, 2020. **27**(5): p. 782-792 e7.
73. Schweitzer, T., H. Genth, and A. Pich, *Clostridium novyi's Alpha-Toxin Changes Proteome and Phosphoproteome of HEp-2 Cells*. Int J Mol Sci, 2022. **23**(17).
74. Govind, R. and B. Dupuy, *Secretion of Clostridium difficile toxins A and B requires the holin-like protein TcdE*. PLoS Pathog, 2012. **8**(6): p. e1002727.
75. Frain, K.M., J.M. van Dijl, and C. Robinson, *The Twin-Arginine Pathway for Protein Secretion*. EcoSal Plus, 2019. **8**(2).
76. Cline, K., *Mechanistic Aspects of Folded Protein Transport by the Twin Arginine Translocase (Tat)*. J Biol Chem, 2015. **290**(27): p. 16530-8.
77. Frobel, J., P. Rose, and M. Muller, *Twin-arginine-dependent translocation of folded proteins*. Philos Trans R Soc Lond B Biol Sci, 2012. **367**(1592): p. 1029-46.
78. *The Fluorescence-Activating and Absorption-Shifting Tag*. Available from: <https://www.the-twinkle-factory.com/the-science-behind-fast-and-splitfast/>.
79. Stylianidou, S., et al., *SuperSegger: robust image segmentation, analysis and lineage tracking of bacterial cells*. Mol Microbiol, 2016. **102**(4): p. 690-700.
80. Scientific, T. *Biotinylation*. Available from: <https://www.thermofisher.com/us/en/home/life-science/protein-biology/protein-biology-learning-center/protein-biology-resource-library/pierce-protein-methods/biotinylation.html>.
81. Bonn, F., S. Maass, and J.M. van Dijl, *Enrichment of Cell Surface-Associated Proteins in Gram-Positive Bacteria by Biotinylation or Trypsin Shaving for Mass Spectrometry Analysis*. Methods Mol Biol, 2018. **1841**: p. 35-43.
82. Asher, A.H. and S.M. Theg, *Electrochromic shift supports the membrane destabilization model of Tat-mediated transport and shows ion leakage during Sec transport*. Proc Natl Acad Sci U S A, 2021. **118**(12).
83. Hao, B., W. Zhou, and S.M. Theg, *Hydrophobic mismatch is a key factor in protein transport across lipid bilayer membranes via the Tat pathway*. J Biol Chem, 2022. **298**(7): p. 101991.
84. Mehner-Breitfeld, D., et al., *TatA and TatB generate a hydrophobic mismatch important for the function and assembly of the Tat translocon in Escherichia coli*. J Biol Chem, 2022. **298**(9): p. 102236.
85. Buboltz, J.B. and H.M. Murphy-Lavoie, *Gas Gangrene*, in *StatPearls*. 2025: Treasure Island (FL).
86. Bintsis, T., *Foodborne pathogens*. AIMS Microbiol, 2017. **3**(3): p. 529-563.
87. Grenda, T., et al., *Clostridium perfringens-Opportunistic Foodborne Pathogen, Its Diversity and Epidemiological Significance*. Pathogens, 2023. **12**(6).
88. Hou, B., et al., *The TatA component of the twin-arginine translocation system locally weakens the cytoplasmic membrane of Escherichia coli upon protein substrate binding*. J Biol Chem, 2018. **293**(20): p. 7592-7605.

89. Stratford, J.P., et al., *Electrically induced bacterial membrane-potential dynamics correspond to cellular proliferation capacity*. Proc Natl Acad Sci U S A, 2019. **116**(19): p. 9552-9557.
90. Valeriani, R.G., et al., *Gas gangrene-associated gliding motility is regulated by the Clostridium perfringens CpAL/VirSR system*. Anaerobe, 2020. **66**: p. 102287.
91. Ghoneim, N.H. and D.A. Hamza, *Epidemiological studies on Clostridium perfringens food poisoning in retail foods*. Rev Sci Tech, 2017. **36**(3): p. 1025-1032.
92. Hassan, K.A., et al., *Genomic analyses of Clostridium perfringens isolates from five toxinotypes*. Res Microbiol, 2015. **166**(4): p. 255-63.
93. Anwar, Z., S.B. Regan, and J. Linden, *Enrichment and Detection of Clostridium perfringens Toxinotypes in Retail Food Samples*. J Vis Exp, 2019(152).
94. Chandrasekaran, R. and D.B. Lacy, *The role of toxins in Clostridium difficile infection*. FEMS Microbiol Rev, 2017. **41**(6): p. 723-750.
95. Petersen, L., et al., *The Essential Role of Rac1 Glucosylation in Clostridioides difficile Toxin B-Induced Arrest of G1-S Transition*. Front Microbiol, 2022. **13**: p. 846215.
96. Just, I. and R. Gerhard, *Large clostridial cytotoxins*. Rev Physiol Biochem Pharmacol, 2004. **152**: p. 23-47.
97. Nagahama, M., et al., *Clostridium perfringens TpeL glycosylates the Rac and Ras subfamily proteins*. Infect Immun, 2011. **79**(2): p. 905-10.
98. Cordes, F.S., J.N. Bright, and M.S. Sansom, *Proline-induced distortions of transmembrane helices*. J Mol Biol, 2002. **323**(5): p. 951-60.